Health and Medical Research Fund

Research Dissemination Reports

醫療衞生研究基金

研究成果報告

Advanced Technology 失進科技

Clinical Trials 臨床試驗

Primary Healthcare and Preventive Medicine 基層醫療與預防醫學

Non-communicable Diseases 非傳染病

Musculoskeletal Conditions 肌肉骨骼疾病





3

22

25

28

29

EDITOR-IN-CHIEF

Martin CS Wong 黃至生

SENIOR EDITORS

LW Chu 朱亮榮 Michael G Irwin Bonnie CH Kwan 關清霞 Eric CH Lai 賴俊雄 KY Leung 梁國賢 Anthony CF Ng 吳志輝 Regina WS Sit 薛詠珊

EDITORS

Ivy HY Chan 陳巧兒 KS Chan 陳健生 Sherry KW Chan 陳詰燁 Jason PY Cheung 鍾培言 Kelvin KL Chong 莊金隆 James CH Chow 周重行 WS Chow 周榮新 Jacqueline PW Chung 鍾佩樺 Adrian CH Fung 馮智衡 Brian SH Ho 何思灝 Ellis KL Hon 韓錦倫 Junjie Huang 黃俊杰 WK Hung 熊維嘉 WC Kwok 郭宏駿 Ho Lam 林 KO Lam 林嘉安 Rex PK Lam 林沛堅 PY Lau 婁培友 Danny WH Lee 李偉雄 WK Leung 梁惠強 Kenneth KW Li 李啟煌 Janice YC Lo 羅懿之 Herbert HF Loong 龍浩鋒 Rashid Lui 雷諾信 James KH Luk 陸嘉熙 David Christopher Lung 龍振邦 Henry KF Mak 麥嘉豐 Billy WL Ng 吳濰龍 Martin W Pak 白 Jeremy YC Teoh 張源津 KY Tse 謝嘉瑜 Harry HX Wang 王皓翔 Andus WK Wong 黃永權 Kenneth KY Wong 黃格元 Hao Xue 薜 浩 Jason CS Yam 任卓昇 TK Yau 游子覺 Kelvin KH Yiu 姚啟恒

EPIDEMIOLOGY ADVISERS

Edmond SK Ma 馬紹強 Shelly LA Tse 謝立亞 Esther YT Yu 余懿德 Hunter KL Yuen 袁國禮

Claire C Zhong 鍾陳雯

STATISTICAL ADVISERS

Marc KC Chong 莊家俊 Eddy KF Lam 林國輝 Carlos KH Wong 黃競浩

HONORARY ADVISERS

David VK Chao 周偉強 Paul BS Lai 賴寶山

Health and Medical Research Fund

Research Dissemination Reports

Editorial

ADVANCED TECHNOLOGY

Machine learning models for estimating risks of hepatic complications in patients with nonalcoholic fatty liver disease: risk stratification and treatment recommendation (abridged secondary publication)

TCF Yip, GLH Wong, VWS Wong, HLY Chan, YK Tse, PC Yuen, OX Tan

Genetic markers for primary open-angle glaucoma using next-generation 9 sequencing: abridged secondary publication

LJ Chen, JC Yam, NC Chan, C Huang, M Zhang, B Gong, Z Yang, CP Pang, CC Tham

Mate-pair low-pass genome sequencing for prenatal diagnosis of fetuses with ultrasound anomalies: abridged secondary publication Z Dong, TY Leung, IFM Lo, YKY Kwok

Molecular stratification of gliomas using next-generation sequencing: 18 abridged secondary publication

AKY Chan, DTM Chan, JYT Chan, H Chen, NYF Chung, QJQ Huang, JSH Kwan, KKW Li, WC Li, EM Liu, XZ Liu, HHF Loong, TM Malta, Y Mao, HK Ng, H Noushmehr, MFM Poon, WS Poon, ZF Shi, WW Wang, ZY Zhang

Magnetic resonance imaging—based machine learning to detect mild cognitive impairment associated with Alzheimer's disease: abridged secondary publication

H Ko, VCT Mok, L Shi, J Abrigo, BYK Lam, ATC Lee

Design, modelling, evaluation, and optimisation of intensive care unit network in Hong Kong: abridged secondary publication *EWM Wong, G Joynt, K Chan*

2,111 ,, 01,8, 4,0,1,0,1, 6,,0,1

CLINICAL TRIALS

Effectiveness and safety of time-lapse imaging for in vitro fertilisation: abridged secondary publication

DYL Chan, TC Li, JPW Chung, TL Lee, CC Wang

High-flow nasal cannula therapy for children and adolescents with obstructive sleep apnoea: abridged secondary publication

KCC Chan, KL Kwok, AM Li

ADVISORY BOARD		
nam Arulkumaran United Kingdom	Diagnostic accuracy of gingival bleeding on brushing, salivary activated MMP-8, and a self-reported questionnaire in early detection of periodontitis: abridged secondary publication	32
Peter Cameron Australia	LJ Jin, G Pelekos, DKL Ho, M Tonetti	
el KY Chan Australia	Dance injury and prevention strategies in recreational dancers: abridged secondary publication AYL Wong, PSH Yung, D Samartzis, DKC Chan, B Surgenor, C Hiller, C Chan,	36
Christiani Inited States	V Schoeb, D Harbutt	
rew Coats Australia	NON-COMMUNICABLE DISEASES	
Fee, Jr ted States	Prostate Health Index for risk stratification before magnetic resonance imaging: abridged secondary publication PKF Chiu, WCW Chu, CMC Cho, YCJ Teoh, CF Ng	38
chael Kidd Australia	MUSCULOSKELETAL CONDITIONS	
Kleinman Jnited States	Relationships among whole-body sagittal alignment, musculoskeletal parameters, body balance, and health-related quality of life in Hong Kong	41
Leeder Australia	Chinese adults: abridged secondary publication GCW Man, Z Hu, WCW Chu, SW Law, WH Cheung, LCM Lau, PSH Yung,	
Sheyu Li PR China	JCY Cheng Registry for congenital upper limb anomalies in Prince of Wales Hospital,	4
g Luo R China	Hong Kong: abridged secondary publication WH Cheung, PC Ho, WL Tse, MCK Mak, JJSC Koo, JWC Ting, WW Chau,	10
awlinson Australia	RMY Wong	
an Samet	Author index & Disclaimer	48
iang Shi PR China		
ghong Xu PR China		
amataka Japan		
mer Yang Canada		
n-hong Yoo public of Korea		
ming Zhang PR China		
f the Editorial Board e available online at		

Cathy Tao 陶潔瑩

ASSISTANT MANAGING EDITOR

Warren Chan 陳俊華

Editorial

Dissemination reports are concise informative reports of health-related research supported by the Health and Medical Research Fund administered by the Health Bureau. In this edition, we present 13 dissemination reports of projects related to advanced technology, clinical trials, primary and preventive medicine, healthcare noncommunicable diseases, and musculoskeletal conditions. In particular, research findings of three projects may provide insights to enhance clinical practices and help inform health policy formulation in Hong Kong.

Nonalcoholic fatty liver disease (NAFLD) is a global health problem that affects around 30% of the world's population. NAFLD is highly associated with type 2 diabetes (T2D), and both are well-established risk factors for development of cirrhosis and subsequent hepatocellular carcinoma. As patients with NAFLD are commonly managed in primary care or endocrine clinics, Yip et al¹ developed a deep learning model using routinely collected clinical, laboratory, and medication data from nearly 27 000 patients with NAFLD; such data were validated in approximately 385000 patients with T2D. The model with the best calibration and discriminatory power had an area under the timedependent receiver operating characteristic curve of 0.865 in the validation cohort. Such models could be useful to facilitate clinicians to accurately predict and stratify patients with T2D regarding their risks of liver-related complications for management and follow-up.

In recent years, next-generation sequencing, including low-pass genome sequencing, has emerged as a powerful tool in prenatal genetic analysis, offering superior detection resolution and enhanced

sensitivity for identifying mosaicism, compared to chromosomal microarray analysis (CMA). Dong et al² compared an in-house low-pass mate-pair genome sequencing approach with CMA in a prospective cohort of 400 fetuses with ultrasound abnormalities to evaluate detection performance. Compared to CMA, the low-pass mate-pair approach resulted in an increased diagnostic yield and was able to identify additional cryptic and mosaic copy number variants, as well as to reclassify 60% of variants of uncertain significance identified by CMA. The study showed that low-pass mate-pair genome sequencing can serve as an alternative method for classifying fetal ultrasound abnormalities.

Prostate cancer is the second most common cancer in men globally and its incidence is rising, especially in Hong Kong. Multiparametric magnetic resonance imaging (MRI) can improve detection of prostate cancer and can guide targeted biopsies and reduce unnecessary ones. However, access to MRI is limited in the public healthcare setting, and it is important to focus resources on patients at higher risk. Chiu et al³ conducted a study aimed at optimising allocation of MRI resources based on risk stratification using the blood Prostate Health Index (PHI) in a cohort of 159 Chinese men with clinical suspicion of prostate cancer. The study found that the use of MRI and PHI improved risk stratification for men with elevated prostate-specific antigen levels. Selectively avoiding MRI in men with lower PHI scores can save costs and reduce unnecessary biopsies, while ensuring timely diagnosis of clinically significant prostate cancer. Risk stratification based on PHI can optimise allocation of MRI resources and improve the efficiency of prostate cancer screening and early detection.

Supplement editors

Dr Anne Fung Head

Research and Data Analytics Office Health Bureau

References

- 1. Yip TCF, Wong GLH, Wong VWS, et al. Machine learning models for estimating risks of hepatic complications in patients with nonalcoholic fatty liver disease: risk stratification and treatment recommendation (abridged secondary publication). Hong Kong Med J 2025;31(Suppl 7):S4-8.
- $2. \quad \mathsf{Dong}\,\mathsf{Z}, \mathsf{Leung}\,\mathsf{TY}, \mathsf{Lo}\,\mathsf{IFM}, \mathsf{Kwok}\,\mathsf{YKY}.\,\mathsf{Mate-pair}\,\mathsf{low-pass}$

Dr Richard A Collins Senior Scientific Reviewer Research and Data Analytics Office Health Bureau

PAGIL.

- genome sequencing for prenatal diagnosis of fetuses with ultrasound anomalies: abridged secondary publication. Hong Kong Med J 2025;31(Suppl 7):S13-7.
- Chiu PKF, Chu WCW, Cho CMC, Teoh YCJ, Ng CF. Prostate Health Index for risk stratification before magnetic resonance imaging: abridged secondary publication. Hong Kong Med J 2025;31(Suppl 7):S38-40.

Machine learning models for estimating risks of hepatic complications in patients with nonalcoholic fatty liver disease: risk stratification and treatment recommendation (abridged secondary publication)

TCF Yip *, GLH Wong †, VWS Wong, HLY Chan, YK Tse, PC Yuen, QX Tan

KEY MESSAGES

- 1. A deep learning model incorporating domain adaptation techniques was developed using clinical, laboratory, and medication data to predict liver-related complications in patients with nonalcoholic fatty liver disease (NAFLD).
- 2. The deep learning model demonstrated accuracy in both a development cohort of patients with NAFLD and an independent validation cohort of patients with type 2 diabetes and probable NAFLD.
- 3. The deep learning model can guide referrals, further assessments, and intervention recommendations in patients with type 2 diabetes at risk of NAFLD.

Hong Kong Med J 2025;31(Suppl 7):S4-8

HMRF project number: 05190057

- ¹ TCF Yip, ¹ GLH Wong, ¹ VWS Wong, ² HLY Chan, ¹ YK Tse, ³ PC Yuen, ⁴ QX Tan
- Department of Medicine and Therapeutics, The Chinese University of Hong Kong, Hong Kong SAR, China
- ² Department of Internal Medicine, Union Hospital, Hong Kong SAR, China
- ³ Department of Computer Science, Hong Kong Baptist University, Hong Kong SAR, China
- Department of Computer Science and Engineering, The Chinese University of Hong Kong, Hong Kong SAR, China
- * Principal applicant: tcfyip@cuhk.edu.hk
- † Corresponding author: wonglaihung@cuhk.edu.hk

Introduction

Nonalcoholic fatty liver disease (NAFLD), also known as metabolic dysfunction-associated steatotic liver disease, affects approximately 30% of the population worldwide. Cirrhosis remains the most important risk factor for long-term liver-related complications including hepatic decompensation and hepatocellular carcinoma (HCC) in patients with NAFLD.1 NAFLD is closely related to type 2 diabetes mellitus (T2DM), which itself is a risk factor for HCC. Given that patients with NAFLD are commonly managed in primary care or endocrine clinics, it is important to stratify patients according to their risk of liver-related complications to enable timely referral, intervention, and HCC surveillance.^{2,3} This study aimed to develop a model for stratifying patients with T2DM who are at risk of NAFLD using deep learning for clinical, laboratory, and medication data.

Methods

The International Classification of Diseases, Ninth Revision, Clinical Modification was used for coding diagnoses and procedures.⁴ Consecutive patients with a diagnosis of fatty liver were included in the development cohort, whereas consecutive patients with T2DM were included in the validation cohort.

Baseline was defined as the earliest date of diagnosis. Patients were excluded if they were aged <18 years, had incomplete demographic data, lacked hepatitis B surface antigen test results, were infected with hepatitis B, C, and/or D, were infected with HIV, had excessive alcohol use or alcohol-related liver disease, had other coexisting autoimmune or metabolic liver diseases, developed liver-related complications within 6 months of baseline, or had <6 months of follow-up. Duplicate cases were excluded from the validation cohort to ensure independence.

The NAFLD ridge score of ≥0.44 was indicative of at risk for NAFLD. Patients not at risk of NAFLD or with type 1 diabetes were excluded. Patients were followed up until the diagnosis of liver-related complications, death, last follow-up (31 July 2021), or 15 years of follow-up, whichever occurred first. The primary endpoint was liver-related events including ascites, spontaneous bacterial peritonitis, variceal bleeding, hepatic encephalopathy, hepatorenal syndrome, HCC, liver transplantation, and liver-related mortality. Baseline laboratory parameters including liver and renal biochemistries, lipid profile, complete blood picture, and blood glucose were collected, as were other relevant diagnoses, procedures, concomitant drugs, and laboratory parameters.

Five domain adaptation models were examined, including adversarial discriminative domain adaptation (ADDA), conditional domain adversarial networks (CDAN), confidence-regularised self-training (CRST), unsupervised domain adaptation by backpropagation (DANN), and maximum classifier discrepancy (MCD) for unsupervised domain adaptation. A total of 39 features including patients' demographics, medication use, comorbidities, and laboratory tests was included. Missing data were imputed using an autoencoder. Feature importance was determined using the permutation method.

The cumulative incidence function of liverrelated events, with adjustment for the competing risk of non-liver-related causes, was estimated using Gray's method. The discriminatory performance of the models was assessed using the area under the receiver operating characteristic curve (AUROC) with competing risk. Model calibration was assessed using calibration curves. The optimal single cut-off was determined using Youden's index. The performances of existing scores including the Fibrosis-4 index and NAFLD outcomes score were analysed using established cut-offs.5 The timedependent sensitivity, specificity, and positive and negative predictive values of the optimal cut-offs of the five models were reported. All statistical tests were two-sided. A P value of <0.05 was considered statistically significant.

Results

In total, 26993 patients with NAFLD (mean age, 56.3 years; 46.1% male; 0.6% with cirrhosis) in the development cohort and 411 395 patients with T2DM (mean age, 61.8 years; 50.7% male; 0.4% with cirrhosis) in the validation cohort were included in the analysis (Table).

Respectively in the development and validation cohorts, 281 (1.0%) and 5984 (1.5%) patients developed liver-related events at a median follow-up of 1.9 (range, 1.4-10.3) years and 11.1 (range, 7.4-15.0) years; the respective 15-year cumulative incidences of liver-related events were 3.0% (95% confidence interval [CI]=2.6%-3.4%) and 1.9% (95% CI=1.8%-1.9%).

In the development cohort, the MCD and CRST models had better sensitivity, with a 15-year AUROC of 0.898 and 0.886, respectively, whereas the 15-year AUROCs of the ADDA, CDAN, and DANN models were 0.844, 0.830, and 0.840, respectively (Fig 1). All five domain adaptation models outperformed the Fibrosis-4 index and NAFLD outcomes score. All five models demonstrated reasonable calibration, with slight risk overestimation among high-risk patients. The MCD model performed best in calibration. At the optimal cut-off of 0.197, the MCD model achieved 82.3% (95% CI=80.3%-84.3%) sensitivity,

81.9% (95% CI=81.3%-82.5%) specificity, 12.2% (95% CI=12.1%-12.4%) positive predictive value, and 99.3% (95% CI=99.2%-99.4%) negative predictive value.

Among the 411 395 patients with T2DM in the validation cohort, 26993 were randomly selected to fine-tune the model hyperparameters through domain adaptation algorithms. The remaining 384402 patients were used for validation. The AUROCs for sensitivity of MCD, CRST, ADDA, CDAN, and DANN were 0.865, 0.858, 0.855, 0.849, and 0.843, respectively (Fig 1). All five domain adaptation models outperformed the Fibrosis-4 index and NAFLD outcomes score. The MCD model achieved the highest discriminatory power in both cohorts. All five models had good calibration, with subtle risk overestimation among high-risk patients. The MCD model performed best in calibration. Using the optimal cut-off, the MCD model achieved 68.7% (95% CI=68.2%-69.1%) sensitivity, 84.8% (95% CI=84.7%-84.8%) specificity, 7.9% (95% CI=7.9%-7.9%) positive predictive value, and 99.3% (95% CI=99.3%-99.3%) negative predictive value.

The 10 most important features in the MCD model were age, alanine aminotransferase, diabetes, gamma-glutamyl transferase, cirrhosis, aspartate aminotransferase, creatinine, use of thiazide diuretics, platelets, and use of sulphonylureas (Fig 2). Age, cirrhosis, diabetes, gamma-glutamyl transferase, and creatinine were selected by all five models.

Discussion

incidence Although the of liver-related complications was lower in patients with NAFLD than in those with chronic viral hepatitis, the high prevalence of NAFLD was due to a substantial total number of patients at risk of liver-related complications. Identifying patients with NAFLD at risk of developing liver-related complications may facilitate timely referrals and interventions. In clinical practice, patients with NAFLD are managed in primary care or endocrine clinics. Clinicians need to identify those who would benefit from referral to secondary care. Experts have suggested various care pathways for risk stratification and management of such patients. These pathways recommend screening for NAFLD with advanced fibrosis in at-risk patients including those with T2DM. The Fibrosis-4 index, an extensively validated serum fibrosis score, is used as a screening tool to exclude advanced fibrosis in primary care and endocrine clinics.3 However, its lower AUROC indicates less accuracy in detecting advanced fibrosis in patients with T2DM. We therefore developed deep learning models to predict the risk of developing liver-related complications in patients with NAFLD. Through domain adaptation,

TABLE. Baseline characteristics of patients in the development and validation cohorts.

Characteristic	Development cohort (n=26 993)*	Validation cohort (n=411 395)*	P value
Age, y	56.3±13.5	61.8±12.4	<0.00
Male sex	12 432 (46.1)	208 589 (50.7)	< 0.00
Cirrhosis	172 (0.6)	1723 (0.4)	< 0.00
Diabetes mellitus	11 906 (44.1)	411 395 (100)	< 0.00
Hypertension	17 733 (65.7)	195 977 (47.6)	< 0.00
Dyslipidaemia	22 547 (83.5)	172 963 (42.0)	< 0.00
Renal replacement therapy	198 (0.7)	1207 (0.3)	<0.00
Alanine aminotransferase, U/L	44 (27-69)	23 (16-33)	<0.00
Missing	0	0	
Aspartate aminotransferase, U/L	32 (23-47)	22 (17-31)	<0.00
Missing	42.9	56.2	
Fibrosis-4 index	1.1 (0.7-1.7)	1.2 (0.8-1.9)	< 0.00
Missing	43.9	56.2	
Albumin, g/L	41.7±4.7	40.6±5.0	< 0.00
Missing	0	9.7	
Total bilirubin, µmol/L	. 12.1±8.4	11.9±9.8	< 0.00
Missing	0	0.1	
Haemoglobin, g/dL	13.7±1.8	13.5±1.8	< 0.00
Missing	54.8	0	
White blood cells, ×109/L	7.8±2.6	8.7±3.8	<0.00
Missing	54.8	0	
Platelets, ×109/L	255.7±74.4	250.2±76.9	< 0.00
Missing	3.6	0.1	
Gamma-glutamyl transferase, U/L	57 (34-107)	50 (26-119)	<0.00
Missing	41.1	86.4	
Alpha-fetoprotein, μg/L	2.9 (2.0-4.0)	2.4 (1.7-3.5)	<0.00
Missing	26.2	74.5	
Creatinine, µmol/L	73 (61.3-87.4)	81 (67-97)	< 0.00
Missing	0.2	0	
International normalised ratio	1.0±0.2	1.0±0.3	<0.00
Missing	29.6	23.8	
Triglycerides, mmol/L		2.0±1.9	< 0.00
Missing	2.0	0	
Total cholesterol, mmol/L	4.9±1.1	5.1±1.2	<0.00
Missing	2.0	0	
High-density lipoprotein cholesterol, mmol/L	1.2±0.3	1.2±0.3	<0.00
Missing	2.2	0	

Data are presented as mean±standard deviation, No. (%) of participants, or % of participants.

TABLE. (cont'd)

Characteristic	Development cohort (n=26 993)*	Validation cohort (n=411 395)*	P value
Low-density lipoprotein cholesterol, mmol/L	2.8±1.0	3.0±1.0	<0.001
Missing	2.3	0.1	
Haemoglobin A1c, %	6.7±1.4	8.0±2.0	< 0.001
Missing	14.0	0	
Fasting glucose, mmol/L	6.5±2.1	8.5±3.1	< 0.00
Missing	1.9	1.1	
Follow-up duration, y	1.9 (1.4-10.3)	11.1 (7.4-15.0)	< 0.00
Medication			
Angiotensin- converting enzyme inhibitor/ angiotensin receptor blocker	10 932 (40.5)	72 769 (17.7)	<0.00
Aspirin	4629 (17.1)	67 798 (16.5)	< 0.00
Beta blocker	10 296 (38.1)	113 874 (27.7)	<0.00
Calcium channel blocker	13 845 (51.3)	100 313 (24.4)	<0.00
Thiazide diuretics	3545 (13.1)	41 334 (10.0)	<0.00
Lipid-lowering agents	11 890 (44.0)	72 783 (17.7)	<0.00
Statin	10 983 (40.7)	56 086 (13.6)	<0.00
Other lipid- lowering agents	2343 (8.7)	22 548 (5.5)	<0.00
Oral hypoglycaemic agents	9390 (34.8)	199 067 (48.4)	<0.00
Metformin	8908 (33.0)	121 459 (29.5)	< 0.00
Sulphonylureas	5946 (22.0)	135 122 (32.8)	<0.00
Dipeptidyl peptidase 4 inhibitor	1066 (3.9)	995 (0.2)	<0.00
Sodium-glucose co-transporter-2 inhibitor	235 (0.9)	21 (0.0)	<0.00
Thiazolidinedione	924 (3.4)	603 (0.1)	<0.00
Glucagon-like peptide-1 receptor agonist	38 (0.1)	15 (0.0)	<0.00
Others	329 (1.2)	2945 (0.7)	<0.00
Insulin	1995 (7.4)	18 404 (4.5)	<0.00

the MCD model demonstrated accuracy in both the development cohort of patients with NAFLD and the validation cohort of patients with T2DM at risk of NAFLD. The MCD model may be a useful alternative for identifying high-risk individuals with T2DM who require referral.

Our study had several limitations. First,

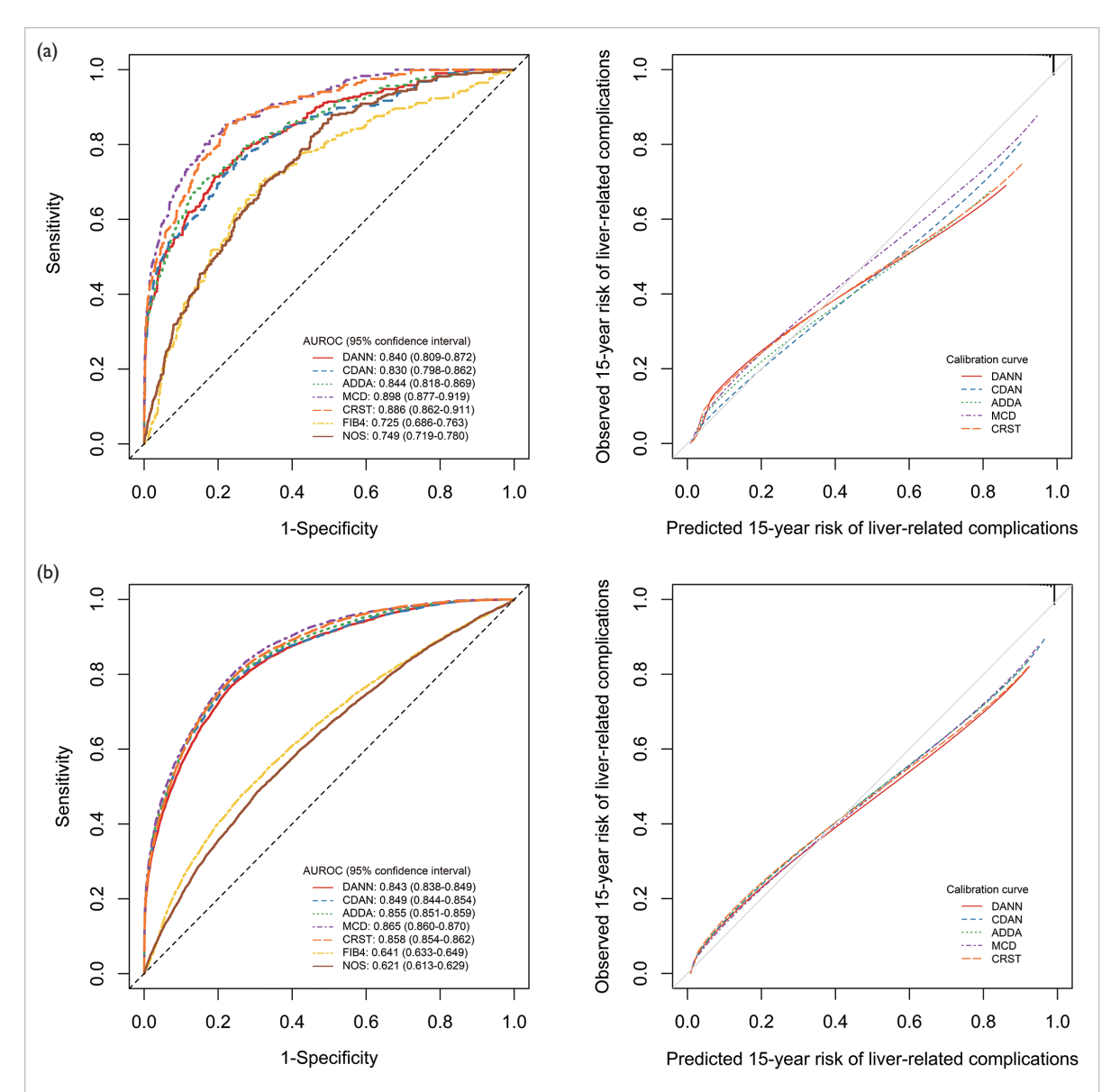


FIG 1. Area under the receiver operating characteristic curves (AUROCs) and calibration curves for predicting liver-related events within 15 years in patients with nonalcoholic fatty liver disease (NAFLD) in the (a) development and (b) validation cohorts. Abbreviations: ADDA=adversarial discriminative domain adaptation, CDAN=conditional domain adversarial networks, CRST=confidence-regularised self-training, DANN=domain adaptation by back-propagation, FIB4=fibrosis-4 index, MCD=maximum classifier discrepancy, and NOS=NAFLD outcomes score

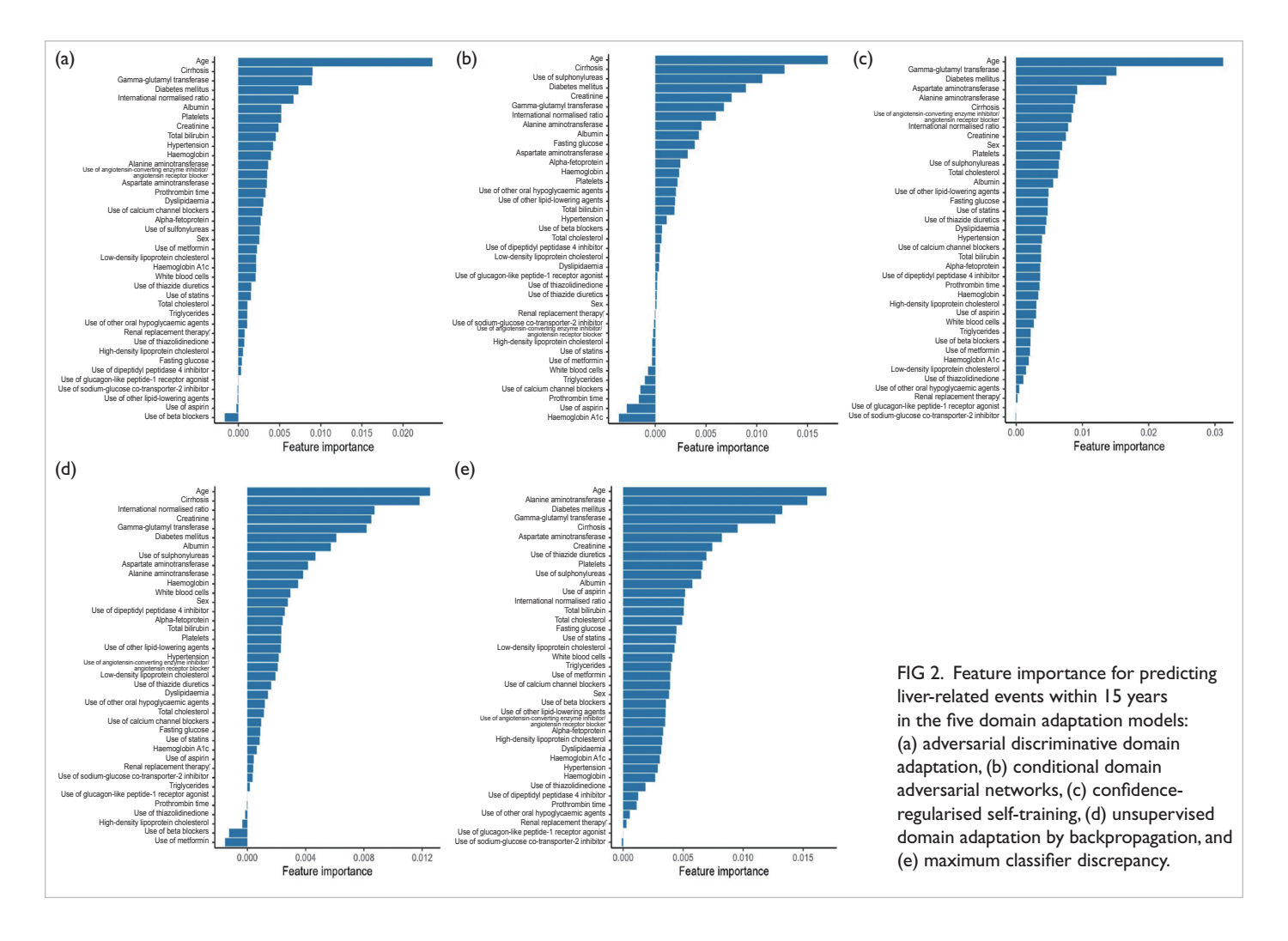
substantial proportions of laboratory data were missing. The imputation autoencoder was incorporated into the model architecture to minimise bias due to missing data. Second, there was no external validation of the model. Future validation studies should assess the model's generalisability in other populations of patients at risk of NAFLD. Nonetheless, our study had important strengths. In particular, our cohorts included a broader range of patients including those with multiple comorbidities, who are often excluded from other trials. Our findings are therefore more applicable to routine clinical practice. Additionally, we implemented strict exclusion criteria to minimise bias.

Conclusion

We developed and validated a deep learning model based on clinical, laboratory, and medication data to predict liver-related complications in patients with NAFLD and in patients with T2DM and probable NAFLD.

Funding

This study was supported by the Health and Medical Research Fund, Health Bureau, Hong Kong SAR Government (#05190107). The full report is available from the Health and Medical Research Fund website (https://rfs2.healthbureau.gov.hk).



Disclosure

The results of this research have been previously published in:

- 1. Zhang X, Yip TC, Tse YK, et al. Trends in risk factor control and treatment among patients with non-alcoholic fatty liver disease and type 2 diabetes between 2000 and 2020: a territory-wide study. Aliment Pharmacol Ther 2023;57:1103-16.
- 2. Yip TC, Hui WY, Ho WW, et al. Laboratory parameter-based model for predicting hepatic complications in non-alcoholic fatty liver disease: a territory-wide cohort study. Gut 2023;72(Suppl 1):A146-A148.
- 3. Yip TC, Yam TF, Lai MS, et al. A laboratory parameter-based risk score for predicting liver-related complications in patients with non-alcoholic fatty liver disease. Hepatol Int 2023;17(Supp 1):S47-48.
- 4. Lin H, Yip TC, Zhang X, et al. Age and the relative importance of liver-related deaths in nonalcoholic fatty liver disease. Hepatology 2023;77:573-84.
- 5. Yip TC, Li G, Wong GL, Tse YK, Wong VW. Accuracy of administrative coding for nonalcoholic fatty liver disease and related hepatic complications: a single-center validation study. Hepatology

2021;74(S1):928A-929A.

Acknowledgements

We thank Mr Yee-Kit Tse and Ms Mandy Sze-Man Lai for formatting large datasets and performing advanced statistical analyses.

- Sanyal AJ, Van Natta ML, Clark J, et al. Prospective study of outcomes in adults with nonalcoholic fatty liver disease. N Engl J Med 2021;385:1559-69.
- Kanwal F, Shubrook JH, Adams LA, et al. Clinical care pathway for the risk stratification and management of patients with nonalcoholic fatty liver disease. Gastroenterology 2021;161:1657-69.
- Zhang X, Yip TC, Wong GL, et al. Clinical care pathway to detect advanced liver disease in patients with type 2 diabetes through automated fibrosis score calculation and electronic reminder messages: a randomised controlled trial. Gut 2023;72:2364-71.
- Yip TC, Li G, Wong GL, Tse YK, Wong VW. Accuracy of administrative coding for nonalcoholic fatty liver disease and related hepatic complications: a single-center validation study. Hepatology 2021;74(S1):928a-9a.
- Calzadilla-Bertot L, Jeffrey GP, Wang Z, et al. Predicting liver-related events in NAFLD: a predictive model. Hepatology 2023;78:1240-51.

Genetic markers for primary open-angle glaucoma using next-generation sequencing: abridged secondary publication

LJ Chen *, JC Yam, NC Chan, C Huang, M Zhang, B Gong, Z Yang, CP Pang, CC Tham

KEY MESSAGES

- 1. Single-nucleotide polymorphisms in multiple genes/loci—namely AFAP1, CASC20, FNDC3B, FOXC1, LMX1B, GAS7, SPRED2/MIR4778, and TLCD5/ARHGEF12/TMEM136—were associated with primary open-angle glaucoma (POAG), high-tension glaucoma, and/or normaltension glaucoma in Hong Kong Chinese. However, no rare variants were associated with POAG.
- 2. Shared and distinct genes were identified between POAG and primary angle-closure glaucoma.
- 3. The *VAV3* gene was associated with progression of primary angle-closure glaucoma but not POAG.
- 4. Variants *SIX6* and *PAX6*, both POAG genes, were associated with retinal nerve fibre layer thickness

and anisometropia development, respectively, in children but not in adults.

Hong Kong Med J 2025;31(Suppl 7):S9-12 HMRF project number: 07180256

^{1,2,3} LJ Chen, ^{1,2,3} JC Yam, ^{1,2} NC Chan, ⁴ C Huang, ⁴ M Zhang, ⁵ B Gong, ⁵ Z Yang, ^{1,2,3} CP Pang, ^{1,2,3} CC Tham

- Department of Ophthalmology and Visual Sciences, The Chinese University of Hong Kong, Hong Kong SAR, China
- ² Department of Ophthalmology, Prince of Wales Hospital, Hong Kong SAR. China
- ³ Hong Kong Eye Hospital, Hong Kong SAR, China
- ⁴ Joint Shantou International Eye Centre, Shantou, China
- Sichuan Key Laboratory for Disease Gene Study, Sichuan Academy of Medical Sciences & Sichuan Provincial People's Hospital, Chengdu, China
- * Principal applicant and corresponding author: lijia_chen@cuhk.edu.hk

Introduction

Glaucoma is a leading cause of irreversible blindness worldwide. In Hong Kong, approximately 20% of blindness cases are attributed to glaucoma. Most glaucoma cases are primary open-angle glaucoma (POAG), which affects 2% of the global population. Genome-wide association studies (GWAS) have identified common single-nucleotide polymorphisms (SNPs) in more than 30 genes associated with POAG; however, these genes have mainly been identified in Western populations. Primary angle-closure glaucoma (PACG) is another major subtype of glaucoma in Chinese individuals. We previously conducted a systematic review and meta-analysis of PACG and identified 15 SNPs in 13 genes/loci associated with PACG.1 Refractive error is a known risk factor for glaucoma. High myopia is associated with increased risk of POAG, whereas hypermetropia is associated with increased risk of PACG. Therefore, investigation of genes related to refractive errors—including interocular differences (anisometropia)-may provide insights into the genetic architecture of glaucoma. This study aimed to investigate the associations of common and rare variants in multiple genes with POAG and its subtypes, 15 SNPs in 13 genes with PACG, and multiple gene variants with glaucoma-related phenotypes, such as retinal nerve fibre layer thickness, in Chinese individuals. We also evaluated the SNP effects on PACG progression. After identifying an association of *VAV3* with PACG progression, we evaluated its effect on POAG progression.

Methods

Patients with POAG or PACG at the Hong Kong Eye Hospital and Prince of Wales Hospital were recruited for ophthalmological examination and followed up for a minimum of 3 years. Additionally, individuals aged >30 years with normal visual acuity, normal intraocular pressure, and no major ocular disorders were recruited as controls. Schoolchildren were also recruited to investigate the effects of glaucoma genes on glaucoma-related phenotypes such as retinal nerve fibre layer (RNFL) thickness and anisometropia. Datasets of patients with POAG and controls were collected from the Joint Shantou International Eye Centre, Shantou, and the Department of Ophthalmology, Sichuan Provincial People's Hospital, Chengdu.

Candidate genes included: (1) 33 genes identified in previous GWAS of POAG—ABCA1, AFAP1, ANKH, ANKRD55-MAP3K1, ATXN2, BICC1, CADM2, CASC20, CAV1/CAV2, CDKN2B-AS1, DGKG, EXOC2, FMNL2, FNDC3B, FOXC1, GAS7, GMDS, HMGA2, IKZF2, LHPP, LMX1B, LOXL1, MEIS2, PDE7B, PMM2, SIX1/SIX6, SPRED2/MIR4778,

TFAP2B/PKHD1, TGFBR3, TLCD5/ARHGEF12/ TMEM136, TMCO1, TMTC2, and TXNRD2; (2) four disease-causing genes-MYOC, OPTN, WDR36, and *NTF4*; (3) four genes associated with POAG in Hong Kong Chinese—PAX6, TLR4, TNF, and TP53; and (4) the 15 genes associated with PACG.1

Genomic DNA was extracted from whole blood. Targeted candidate genes and variants were analysed by sequencing or genotyping platforms in cases and controls from the Hong Kong cohort using in-house laboratory protocols.

A disease-causing mutation was defined as a coding variant present exclusively in cases, or with a frequency of <1/1000 in controls and showing a significant difference (P<0.05) between cases and controls after multiple corrections. For common (allele frequency >1%) and rare (<0.1%) variants, single-variant association analyses were performed using the Chi-squared test with adjustments for age and sex. Odds ratios (ORs) and 95% confidence intervals were estimated. Genotype-phenotype correlation analyses were conducted using logistic or linear regression.

Results

We identified a SNP, rs2745572, in the FOXC1 gene that was associated with high-tension glaucoma (HTG) [OR=0.73, P<0.001, Table 1]. The protective allele G of rs2745572 was also strongly correlated with lower intraocular pressure in patients with POAG (Beta= -1.43, P<0.001). In the Shantou cohort, SNP rs6596830 in the FOXC1 locus, rather than rs2745572, showed significant associations PACG. When patients whose glaucoma remained

with POAG (OR=0.75, P<0.001) and HTG (OR=0.75, P<0.001), suggesting population-specific effects.²

We also identified multi-gene associated with POAG, including SNP rs4414666 in the SPRED2/MIR4778 locus (OR=1.18, P=0.023), rs62283813 in *FNDC3B* (OR=1.22, P=0.032), rs938604 in AFAP1 (OR=0.74, P=0.004), rs3829849 in LMX1B (OR=0.73, P=0.013), and rs2326788 in CASC20 (OR=1.23, P=0.022) [Table 2].

Relative to normal-tension glaucoma (NTG), HTG was more strongly associated with SNP rs4414666 in SPRED2/MIR4778 (OR=1.28, P=0.004), rs62283813 in *FNDC3B* (OR=1.40, P=0.001), rs938604 in AFAP1 (OR=0.65, P<0.001), rs3829849 in LMX1B (OR=0.68, P=0.011), rs2326788 in CASC20 (OR=1.26, P=0.026), and rs9913911 in GAS7 (OR=0.82, P=0.021) [Table 3]. In contrast, only two variants were associated with NTG: rs2326788 in CASC20 (OR=1.24, P=0.041) and rs1893261 in the TLCD5/ARHGEF12/TMEM136 locus (OR=0.81, P=0.025). No disease-causing mutations or rare variants were significantly associated with POAG in the Hong Kong cohort.

In a meta-analysis of PACG, we identified 15 SNPs in 13 genes/loci associated with the disease, then catalogued rare coding variants in 16 genes/ loci associated with PACG. We demonstrated overlapping genes between PACG and POAGnamely ABCA1, ATOH7, CALCRL, IL6, and VAV3.1 Notably, variants in ABCA1, ATOH7, CALCRL, IL6, and VAV3 were not associated with POAG. Among the 15 SNPs, LOXL1 rs3825942 (G153D, OR=0.65, P=0.0026) showed a significant association with

TABLE 1. Associations of single-nucleotide polymorphisms (SNPs) in FOXC1 with primary open-angle glaucoma (POAG), high-tension glaucoma (HTG), and normal-tension glaucoma (NTG).

SNP	Gene/locus	Minor allele/	POAG		HTG		NTG	
		major allele	Odds ratio (95% confidence interval)	P value	Odds ratio (95% confidence interval)	P value	Odds ratio (95% confidence interval)	P value
rs7750978	AL512329.2	A/C	0.94 (0.81-1.09)	0.41	0.83 (0.69-0.99)	0.041	1.02 (0.86-1.21)	0.81
rs7774792	AL512329.2	A/T	0.90 (0.77-1.06)	0.22	0.92 (0.76-1.12)	0.41	0.87 (0.72-1.05)	0.15
rs6596830	AL512329.2	A/T	1.07 (0.91-1.25)	0.40	1.20 (1.00-1.44)	0.053	0.99 (0.83-1.19)	0.91
rs2745572	50 kb upstream of FOXC1	G/A	0.90 (0.77-1.05)	0.16	0.73 (0.61-0.88)	<0.001	1.06 (0.89-1.26)	0.55
rs56210598	FOXC1	G/C	1.08 (0.93-1.24)	0.31	1.04 (0.88-1.24)	0.64	1.09 (0.92-1.29)	0.30
rs2745596	FOXC1	T/G	0.83 (0.60-1.17)	0.30	0.77 (0.51-1.17)	0.23	0.87 (0.59-1.28)	0.48
rs2235716	FOXC1	T/C	0.95 (0.81-1.11)	0.51	0.97 (0.80-1.18)	0.76	0.90 (0.75-1.09)	0.27
rs2235717	FOXC1	G/C	0.95 (0.80-1.13)	0.57	0.96 (0.78-1.18)	0.68	0.90 (0.73-1.10)	0.31
rs4959583	FOXC1	A/C	1.16 (0.86-1.57)	0.32	1.01 (0.70-1.46)	0.95	1.31 (0.94-1.83)	0.11
rs984253	FOXC1	A/T	0.87 (0.65-1.16)	0.33	0.76 (0.53-1.09)	0.13	0.97 (0.70-1.33)	0.83
rs7763581	FOXC1	T/G	0.91 (0.75-1.11)	0.37	0.85 (0.67-1.09)	0.20	0.97 (0.77-1.21)	0.78
rs2569876	FOXC1	G/A	0.98 (0.84-1.14)	0.78	1.03 (0.86-1.24)	0.75	0.90 (0.75-1.08)	0.26

TABLE 2. Associations of single-nucleotide polymorphisms (SNPs) with candidate genes for primary open-angle glaucoma (POAG).

Chromosome	Nearest gene	SNP	Minor	Major	Minor allele frequency		P value	Odds ratio (95%
			allele	allele	POAG	POAG Controls		confidence interval)
2	SPRED2/MIR4778	rs4414666	G	Т	0.47	0.43	0.023	1.18 (1.02-1.37)
3	FNDC3B	rs62283813	G	Α	0.22	0.19	0.032	1.22 (1.02-1.46)
4	AFAP1	rs938604	Α	G	0.13	0.16	0.0039	0.74 (0.61-0.91)
9	LMX1B	rs3829849	Т	С	0.08	0.11	0.013	0.73 (0.58-1.94)
20	CASC20	rs2326788	G	Α	0.25	0.21	0.022	1.23 (1.03-1.47)

TABLE 3. Associations of single-nucleotide polymorphisms (SNPs) with candidate genes for high-tension glaucoma (HTG) and normal-tension glaucoma (NTG).

Chromosome	Nearest gene	SNP	Minor	Major	Minor	inor allele frequency NTG vs controls HTG vs cont		NTG vs controls		G vs controls	
	allele allele HTG N		NTG	Controls	P value	Odds ratio (95% confidence interval)	P value	Odds ratio (95% confidence interval)			
2	SPRED2/MIR4778	rs4414666	G	Т	0.49	0.45	0.43	0.36	1.08 (0.91-1.28)	0.0039	1.28 (1.08-1.51)
3	FNDC3B	rs62283813	G	Α	0.25	0.20	0.19	0.61	1.06 (0.85-1.31)	0.0011	1.40 (1.14-1.72)
4	AFAP1	rs938604	Α	G	0.13	0.14	0.16	0.16	0.85 (0.67-1.07)	<0.001	0.65 (0.51-0.83)
9	LMX1B	rs3829849	Т	С	0.08	0.09	0.11	0.099	0.79 (0.59-1.05)	0.011	0.68 (0.51-0.92)
11	TLCD5/ARHGEF12/ TMEM136	rs1893261	Α	G	0.32	0.27	0.31	0.025	0.81 (0.67- 0.97)	0.77	1.03 (0.86-1.23)
17	GAS7	rs9913911	G	Α	0.46	0.49	0.51	0.29	1.10 (0.93-1.30)	0.021	0.82 (0.69-0.97)
20	CASC20	rs2326788	G	Α	0.25	0.25	0.21	0.041	1.24 (1.01-1.51)	0.026	1.26 (1.03-1.54)

rs6689476 was associated with PACG progression at not associated with POAG in adults. the 3rd year (OR=2.86, P=0.045), 5th year (OR=2.84, P=0.037), and 10th year (OR=2.74, P=0.030).3 In contrast, these variants were not associated with POAG or its progression, suggesting genetic diversity between POAG and PACG.

We investigated the effects of multiple SNPs in glaucoma-associated genes on glaucoma-related ocular phenotypes, including RNFL thickness. In Hong Kong children, temporal-inferior p-RNFL thickness was associated with SNPs rs33912345 (P=7.7 ×10⁻⁴) and rs10483727 (P=0.0013) after adjustments for age, sex, and axial length.4 In contrast, SIX6 variants were not associated with RNFL thickness in adult patients with POAG.

We also investigated multiple gene variants in refractive error, including anisometropia, in children to determine the roles of certain glaucoma genes (eg, PAX6) in refractive error, given that high myopia is a known risk factor for POAG. At the 3-year follow-up, PAX6 rs644242 was associated with anisometropia in terms of axial length (P=0.0003; OR=1.61) and spherical equivalent (P=0.03) among children.⁵ PAX6 was associated with glaucoma, especially

stable for 10 years were regarded as controls, VAV3 early-onset glaucoma. However, PAX6 variants were

Discussion

We demonstrated an association between rs2745572 in FOXC1 and HTG in Hong Kong Chinese. The OR of the risk allele was comparable to the GWAS results (OR=1.23) in POAG. However, in the Shantou Chinese cohort, SNP rs6596830 in the FOXC1 locus, rather than rs2745572, showed significant associations with POAG and HTG, suggesting population-specific effects.²

We identified SNPs in multiple genes/loci associated with POAG and its subtypes. Notably, rs2326788 in CASC20 was the only variant associated with both HTG and NTG, suggesting that genetic profiles differ between these two subtypes. No significant associations were identified between other genes and POAG (HTG/NTG), suggesting possible ethnic differences in the POAG genetic profiles of Chinese and Western populations. Moreover, we identified no rare variants associated with POAG in the Hong Kong cohort, likely due to the low minor allele frequencies of these variants

(<0.1%), which resulted in insufficient statistical power to detect significant differences.

It has been suggested that the genetic components of PACG and POAG are distinct. However, the identification of overlapping genes suggests that PACG and POAG share certain genetic markers or even biological pathways. Functional characterisation of these overlapping genes may shed new light on the pathogenesis of various glaucoma subtypes.

The association between the missense variant *LOXL1* rs3825942 and PACG indicated that it may serve as a reliable genetic marker for PACG. Tenyear follow-up data suggested that *VAV3* rs6689476 represents a genetic marker for PACG progression.³ In contrast, none of these gene variants was associated with POAG in the Hong Kong cohort, suggesting genetic diversity between PACG and POAG.

SIX6 was associated with p-RNFL thickness in children, suggesting a role for SIX6 in RNFL variation during neural retinal development in childhood. The effect of SIX6 on glaucoma susceptibility might begin during childhood. Timely follow-up of children carrying the risk alleles may help identify those at risk of POAG onset.

We found that *PAX6* rs644242 was associated with anisometropia onset in Hong Kong Chinese children, implying roles in imbalanced refractive change and axial elongation between the eyes. Eyeball elongation in early life may increase the risk of future glaucoma. Accordingly, timely follow-up of children carrying the risk alleles may help identify those at risk of developing POAG later in life.

Conclusion

Common SNPs in multiple genes/loci showed associations with POAG, HTG, and/or NTG in Hong Kong Chinese. In contrast, no rare variants were associated with POAG. Variants in multiple genes may serve as useful genetic biomarkers for glaucoma, endophenotypes, and glaucoma progression in Chinese individuals. Gene variants could represent cost-effective biomarkers for disease risk assessment.

Funding

This study was supported by the Health and Medical Research Fund, Health Bureau, Hong Kong SAR Government (#07180256). The full report is available from the Health and Medical Research Fund website (https://rfs1.healthbureau.gov.hk).

Disclosure

The results of this research have been previously published in:

- 1. Liang YJ, Ling A, Chan PP, et al. Genetic association of primary angle-closure glaucoma and disease progression. Clin Exp Ophthalmol 2025;53:660-7.
- 2. Liang YJ, Wang YY, Rong SS, et al. Genetic associations of primary angle-closure disease: a systematic review and meta-analysis. JAMA Ophthalmol 2024;142:437-44.
- 3. Wang YY, Zhang XJ, Kam KW, et al. Association of polymorphisms in ZFHX1B and PAX6 with anisometropia in Chinese children: The Hong Kong Children Eye Genetics Study. Invest Ophthalmol Vis Sci 2023;64:6.
- 4. Lu SY, Zhang XJ, Wang YM, et al. Association of *SIX1-SIX6* polymorphisms with peripapillary retinal nerve fibre layer thickness in children. Br J Ophthalmol 2023;107:1216-22.

- Liang YJ, Wang YY, Rong SS, et al. Genetic associations of primary angle-closure disease: a systematic review and meta-analysis. JAMA Ophthalmol 2024;142:437-44.
- Wu Z, Huang C, Zheng Y, et al. Primary open-angle glaucoma risk prediction with ABCA1 and LOC102723944 variants and their genotype-phenotype correlations in southern Chinese population. Mol Genet Genomics 2023;298:1343-52.
- 3. Liang YJ, Ling A, Chan PP, et al. Genetic association of primary angle-closure glaucoma and disease progression. Clin Exp Ophthalmol 2025;53:660-7.
- 4. Lu SY, Zhang XJ, Wang YM, et al. Association of *SIX1-SIX6* polymorphisms with peripapillary retinal nerve fibre layer thickness in children. Br J Ophthalmol 2023;107:1216-22.
- Wang YY, Zhang XJ, Kam KW, et al. Association of polymorphisms in ZFHX1B and PAX6 with anisometropia in Chinese children: The Hong Kong Children Eye Genetics Study. Invest Ophthalmol Vis Sci 2023;64:6.

Mate-pair low-pass genome sequencing for prenatal diagnosis of fetuses with ultrasound anomalies: abridged secondary publication

Z Dong *, TY Leung, IFM Lo, YKY Kwok

KEY MESSAGES

- DNA from 400 fetuses with ultrasound anomalies was examined using chromosomal microarray analysis (CMA) and low-pass mate-pair genome sequencing (GS) to identify clinically significant copy-number variants (CNVs), structural variants, and regions with absence of heterozygosity.
- 2. CMA and low-pass mate-pair GS reported diagnostic yields of 8.5% and 10.3%, respectively.
- 3. Low-pass mate-pair GS additionally identified cryptic CNVs (n=4) and mosaic CNVs (n=2), and reclassified 12 (60%) of 20 variants of uncertain significance identified by CMA.
- 4. Low-pass mate-pair GS classified 14 structural variants as variants of uncertain significance due

- to the unavailability of cultured cells for RNA sequencing or inconclusive RNA sequencing results in the submitted samples.
- 5. Low-pass mate-pair GS can serve as an alternative for the confirmation of fetal ultrasound anomalies.

Hong Kong Med J 2025;31(Suppl 7):S13-7 HMRF project number: 08190226

 $^{\rm 1}$ Z Dong, $^{\rm 1}$ TY Leung, $^{\rm 2}$ IFM Lo, $^{\rm 1,2}$ YKY Kwok

- Z Dolly, 11 Leully, IFW LO, 7 TKT KWOK
- Department of Obstetrics and Gynaecology, The Chinese University of Hong Kong, Hong Kong SAR, China
- ² Clinical Genetic Service, Department of Health, Hong Kong SAR, China
- * Principal applicant and corresponding author: elvisdong@cuhk.edu.hk

Introduction

In China, the rate of birth defects is estimated to be 5.6%. Ultrasonography and follow-up invasive prenatal diagnosis can provide prognostic information for the option of termination of pregnancy, as well as planning for future pregnancies including prenatal diagnosis and preimplantation genetic testing.

Next-generation sequencing, including low-pass genome sequencing (GS), has been used for prenatal copy-number variant (CNV) analysis with enhanced detection resolution and improved sensitivity for identifying mosaicism, compared with chromosomal microarray analysis (CMA).¹⁻² Next-generation sequencing is recommended for germline structural variant detection by the American College of Medical Genetics and Genomics.³ In our pilot studies, low-pass mate-pair GS (4-fold) enabled a comprehensive investigation of CNVs, structural variants, and regions with absence of heterozygosity.⁴ We applied this method in a prospective cohort of 400 fetuses with ultrasound anomalies, along with CMA, to evaluate detection performance.

Methods

Pregnant women who underwent invasive genome testing for fetal ultrasound anomalies were recruited. DNA was extracted, and CMA was performed. Additionally, 500 ng of genomic DNA

was fragmented into 3-to-8-kb fragments. Mate-pair library construction was performed and sequenced to >4-fold read depth.⁴ CNVs, structural variants, and regions with absence of heterozygosity were identified using our previously reported method⁵ and then validated by breakpoint-junction-specific polymerase chain reaction and Sanger sequencing, as well as quantitative polymerase chain reaction.

RNA sequencing (RNA-seq) with enrichment of messenger RNA was performed from cultured cells of chorionic villi or amniotic fluid, generating >10 Gb of data per sample. Paired reads were aligned to the human reference genome (hg19) using STAR. Expression levels (in transcripts per million) of candidate genes were compared with those of our in-house gestation-matched controls.

Results

Among 400 fetuses with ultrasound anomalies, CMA yielded a diagnosis in 34 (8.5%) cases with aneuploidies, pathogenic/likely pathogenic CNVs, and suspected parental consanguinity, whereas lowpass mate-pair GS yielded a diagnosis in 41 (10.3%) cases (Table). Both methods consistently identified 14 cases with aneuploidies; however, low-pass matepair GS additionally identified a case (with a negative CMA finding) of mosaic trisomy 12 at a 20% mosaic level, which was confirmed by karyotyping (12/80 cells).

TABLE. Detection yields provided by chromosomal microarray analysis and low-pass mate-pair genome sequencing

Classification	No. of cases detected						
	Chromosomal	Low-pass	Low-pass mate-pair genome sequencing				
	microarray analysis	mate-pair genome sequencing	Copy-number Structural variants / variants aneuploidies		Regions with absence of heterozygosity		
Pathogenic/likely pathogenic	34	41 [†]	37*	5*	3		
Variant of uncertain significance	20	20	6	14	0		

Four cases with pathogenic/likely pathogenic copy-number variants were involved in translocation (n=3) and insertion (n=1).

Both methods consistently identified 17 cases with pathogenic/likely pathogenic CNVs; additionally, low-pass mate-pair GS identified six other cases of pathogenic/likely pathogenic CNVs. Three of the cases were affected by homozygous Southeast Asian-type thalassaemia; a mosaic 9Mb 15q terminal deletion at a 20% level (Fig 1) was detected in a fetus with increased nuchal translucency (NT) and generalised hydrops (22B2742), which had been missed by CMA. Furthermore, in case 22B0083 with a ventricular septal defect, low-pass mate-pair GS identified a 35-kb intragenic deletion involving the second exon of RBFOX2. Given that de novo lossof-function mutations or deletions encompassing RBFOX2 have been found in congenital heart disease probands,6,7 this deletion was considered likely pathogenic. Finally, case 22C1583 was referred (increased NT, positive Down syndrome screening, and left ventriculomegaly) for CMA, which reported a de novo duplication of 3.5 Mb, whereas low-pass GS indicated an ins(2;13)(q14.2;q31.3) insertion involving this duplication (Fig 2). Haploinsufficient GLI2 is located downstream of the insertion site, and an over 2-fold reduction of *GLI2* expression was observed compared with the control.

Low-pass mate-pair GS also identified the exact genomic locations and orientations of pathogenic/likely pathogenic deletions. Three cases with terminal deletions and duplications occurring simultaneously were attributed to translocations. In case 23B0659 with hydrocephaly and a ventricular septal defect, two interstitial deletions in 14q were reported by CMA, but only a smaller deletion was confirmed in the father (Fig. 3). Low-pass mate-pair GS indicated a complex insertion involving chromosomes 1, 14, and 22 in the father, in which chromosome 14 was fragmented into eight segments. Segments 3 and 7 of chromosome 14 were inserted into chromosome 1, whereas segments 2 and 4 were inserted into chromosome 22; segment 6 was lost. The fetus inherited only the derivative chromosome 14, which explained the discrepancies between deletions identified in the fetus and those identified in the father.

CMA reported 15 duplications as variants of uncertain significance in 15 cases due to the involvement of known disease-causing gene(s) through a loss-of-function mechanism at the CNV boundary. Of these, 11 (73.3%) were defined as forward tandem duplications by low-pass mate-pair GS; they were unlikely to lead to disease via a loss-of-function mechanism because genes involved at the CNV boundaries remained intact. Overall, among 20 cases with variants of uncertain significance reported by CMA, 11 were reclassified as likely benign and one as likely pathogenic, resulting in a 60% revision of classification for variants of uncertain significance.

Low-pass mate-pair GS also identified six CNVs as variants of uncertain significance. In case 23C0031 with increased NT and a prenatal skin fold of 4.07 mm, low-pass mate-pair GS identified a 12-kb intragenic heterozygous deletion in *DCBLD2*, the deletion of which causes cardiomyopathy⁸ in an autosomal recessive manner. A reduction of RNA expression and aberrant RNA splicing were observed, warranting investigation. Further studies are needed to determine whether an additional point mutation arose through a compound heterozygosity mechanism.

Low-pass mate-pair GS identified four translocations (one balanced), 28 inversions, and 26 insertions with or without cryptic duplications/ deletions. In case 22C1007 with increased NT and positive Down syndrome screening (CMA negative), a de novo balanced translocation t(3;6)(p14.1;q16.1) was identified and then confirmed by karyotyping; however, RNA-seg could not be performed due to failure of cell re-culture. Concerning inversions, sizes varied from 12 kb to 2.6 Mb. None was classified as pathogenic/likely pathogenic because no haploinsufficient disease-causing gene was directly disrupted or no conclusive evidence from RNA-seq was available. With respect to structural rearrangements, low-pass mate-pair GS identified four cases with pathogenic findings (three unbalanced translocations and one insertion) and 14 cases with variants of uncertain significance.

[†] Seven cases had additional pathogenic findings identified by low-pass mate-pair genome sequencing, including one mosaic aneuploidy, one mosaic deletion, four pathogenic cryptic deletions, and one *de novo* insertion.

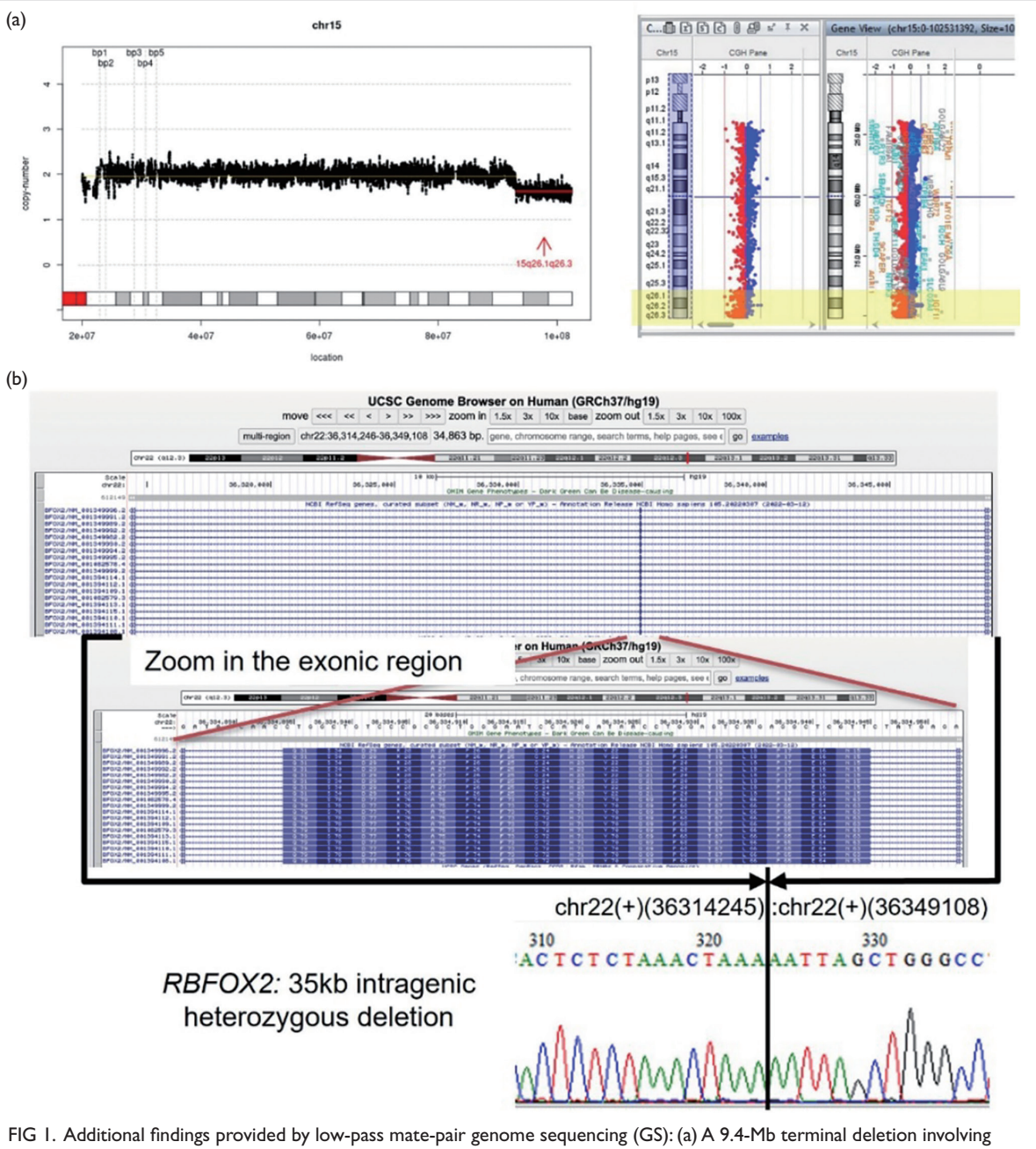


FIG 1. Additional findings provided by low-pass mate-pair genome sequencing (GS): (a) A 9.4-Mb terminal deletion involving 15q26.1q26.3 with 20% mosaicism is identified in case 22B2742 (indicated by a red line), which was missed by routine chromosomal microarray analysis (highlighted in yellow). (b) A 35-kb intragenic heterozygous deletion (involving exon 2 of 14 in all transcripts of *RBFOX2*, in-frame deletion) was detected by low-pass GS. The re-joined sequence after deletion was validated by Sanger sequencing.

Absence of heterozygosity analysis indicated that three (0.8%) cases potentially involved parental consanguinity, warranting further investigation into homozygous point mutations that contributed to the fetal anomalies.

The average turnaround time was 9 days (including 3.5 days for sequencing and automated data analysis without hands-on processing) for low-pass mate-pair GS and 5 days for CMA. The reagent costs were HK\$1700 for low-pass mate-pair GS and HK\$1720 for CMA.

Discussion

We prospectively investigated detection performance of low-pass mate-pair GS and CMA in 400 fetuses with ultrasound anomalies. Low-pass mate-pair GS provided an additional 1.8% diagnostic yield compared with CMA (10.3% vs 8.5%); it also revised CNV classification in 60% (12/20) of cases with variants of uncertain significance identified by CMA.

Low-pass mate-pair GS demonstrated its

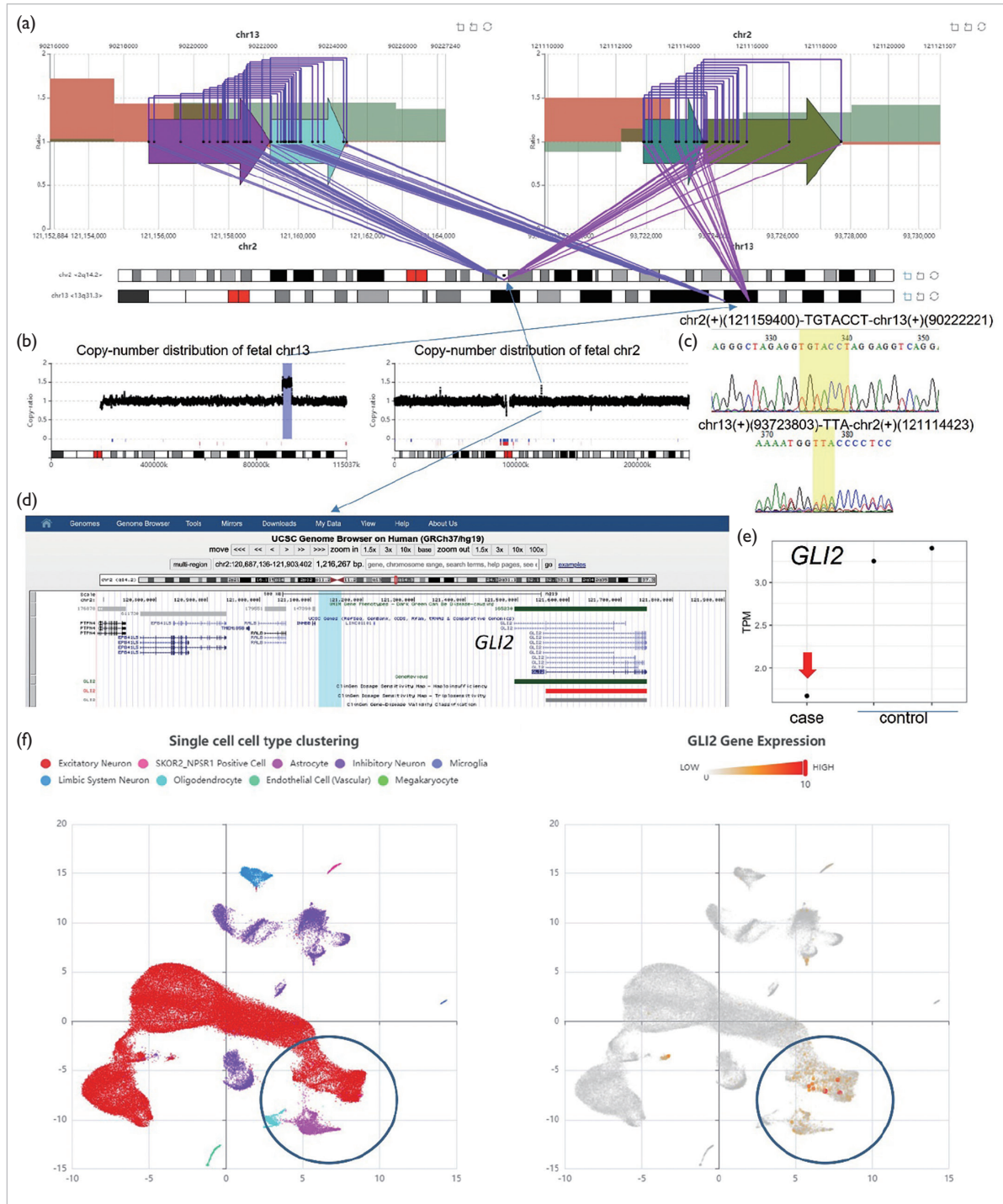


FIG 2. A de novo insertion identified by low-pass mate-pair genome sequencing: (a) and (b) Chimeric read-pair and copy-ratio analysis revealed an insertion ins(2;13)(q14.2;q31.3). (c) Breakpoint-junction-specific polymerase chain reaction and Sanger sequencing confirmed the rearrangement. (d) Haploinsufficient GLI2 is located downstream of the insertion site. (e) An >2-fold reduction of expression in the case compared with gestational-week-matched controls was observed. (f) Single-cell RNA sequencing indicates that GL12 is highly expressed in astrocytes and excitatory neurons.

advantage in detecting small CNVs, balanced changes involving CNVs, such as insertions and detected and delineated the composition of genomic other indications.

translocations, and inversions; it revealed a high complex structural rearrangements, resulting in prevalence of rare CNVs and structural variants revisions to clinical management for families. Our in the population, highlighting the need for a findings suggest that low-pass mate-pair GS can large population-based dataset to aid variant serve as an alternative for the confirmation of fetal interpretation. Additionally, low-pass mate-pair GS ultrasound anomalies, with potential extension to

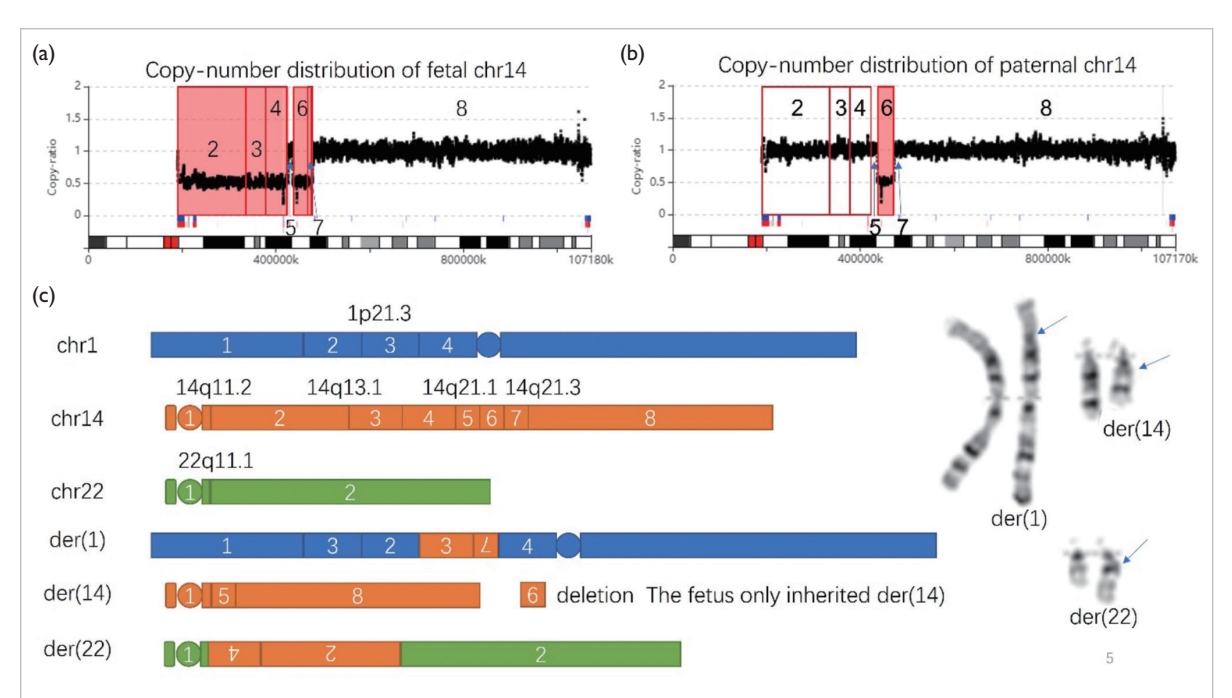


FIG 3. Genomic composition revealed by low-pass mate-pair genome sequencing: Copy-number distribution of chromosome 14 in the (a) fetus (23B0659) and (b) father. Two interstitial heterozygous deletions are identified in the fetus, but only one smaller deletion is identified in the father (segment 6). (c) A complex rearrangement involving chromosomes 1, 14, and 22 is shown in the father, but the fetus inherits only the derivative chromosome 14. (d) Karyotyping analysis of the father confirms the finding. Each arrow indicates the location of abnormalities in the derivative chromosome.

Funding

This study was supported by the Health and Medical Research Fund, Health Bureau, Hong Kong SAR Government (#08190226). The full report is available from the Health and Medical Research Fund website 2. (https://rfs2.healthbureau.gov.hk).

Disclosure

The results of this research have been previously published in:

- 1. Zhou Z, Tan C, Chau MHK, et al. TEDD: a database of temporal gene expression patterns during multiple developmental periods in human and model organisms. Nucleic Acids Res 2023;51:D1168-D1178.
- 2. Li K, Zhao Y, Chau MHK, et al. Low-pass genome sequencing-based detection of paternity: validation in clinical cytogenetics. Genes (Basel) 2023;14:1357.
- 3. Qian J, Wang H, Liang H, et al. Mate-pair sequencing enables identification and delineation of balanced and unbalanced structural variants in prenatal cytogenomic diagnostics. Clin Chem 2025;71:155-68.

Acknowledgements

We thank Prof Choy Kwong Wai, Dr Cao Ye, and Dr Qian Jicheng for their laboratory work.

- Wang H, Dong Z, Zhang R, et al. Low-pass genome sequencing versus chromosomal microarray analysis: implementation in prenatal diagnosis. Genet Med 2020;22:500-10.
- Chaubey A, Shenoy S, Mathur A, et al. Low-pass genome sequencing: validation and diagnostic utility from 409 clinical cases of low-pass genome sequencing for the detection of copy number variants to replace constitutional microarray. J Mol Diagn 2020;22:823-40.
- Raca G, Astbury C, Behlmann A, et al. Points to consider in the detection of germline structural variants using next-generation sequencing: a statement of the American College of Medical Genetics and Genomics (ACMG). Genet Med 2023;25:100316.
- Dong Z, Zhao X, Li Q, et al. Development of coupling controlled polymerizations by adapter-ligation in matepair sequencing for detection of various genomic variants in one single assay. DNA Res 2019;26:313-25.
- Dong Z, Chau MHK, Zhang Y, et al. Deciphering the complexity of simple chromosomal insertions by genome sequencing. Hum Genet 2021;140:361-80.
- Homsy J, Zaidi S, Shen Y, et al. De novo mutations in congenital heart disease with neurodevelopmental and other congenital anomalies. Science 2015;350:1262-6.
- Glessner JT, Bick AG, Ito K, et al. Increased frequency of de novo copy number variants in congenital heart disease by integrative analysis of single nucleotide polymorphism array and exome sequence data. Circ Res 2014;115:884-96.
- 8. Alhamoudi KM, Barhoumi T, Al-Eidi H, et al. A homozygous nonsense mutation in DCBLD2 is a candidate cause of developmental delay, dysmorphic features and restrictive cardiomyopathy. Sci Rep 2021;1:12861.

Molecular stratification of gliomas using nextgeneration sequencing: abridged secondary publication

AKY Chan, DTM Chan, JYT Chan, H Chen, NYF Chung, QJQ Huang, JSH Kwan, KKW Li, WC Li, EM Liu, XZ Liu, HHF Loong, TM Malta, Y Mao, HK Ng *, H Noushmehr, MFM Poon, WS Poon, ZF Shi, WW Wang, ZY Zhang

KEY MESSAGES

- Adult diffuse gliomas are heterogeneous groups of tumours.
- 2. A combination of single-gene biomarkers can be used to stratify adult gliomas into molecular groups. Our proposed molecular grading system is superior to the histological grading system in terms of prognostication for adult gliomas.
- 3. IDH-wildtype, TERTp-wildtype adult glioblastomas clustered into different methylation classes, and CDKN2A/B deletion is an independent prognostic factor in this subset of gliomas.
- 4. Methylation classes, MGMTp methylation, TERTp mutation, and MMR mutation are prognostic biomarkers for IDH-wildtype, H3-

wildtype glioblastomas in adolescents and young adults. These tumours are similar to the above IDH-wildtype, TERTp-wildtype glioblastomas in that they do not frequently exhibit the diagnostic molecular criteria for regular glioblastomas.

Hong Kong Med J 2025;31(Suppl 7):S18-21

HMRF project number: 07180736

AKY Chan, DTM Chan, JYT Chan, H Chen, NYF Chung, QJQ Huang, JSH Kwan, KKW Li, WC Li, EM Liu, XZ Liu, HHF Loong, TM Malta, Y Mao, HK Ng, H Noushmehr, MFM Poon, WS Poon, ZF Shi, WW Wang, ZY Zhang

Department of Anatomical and Cellular Pathology, The Chinese University of Hong Kong, Hong Kong SAR, China

* Principal applicant and corresponding author: hkng@cuhk.edu.hk

Introduction

Diffuse gliomas are the most common primary brain tumours in adults. According to the World Health Organization (WHO), diffuse gliomas can be classified into grades II to IV (glioblastoma). However, this grading system has considerable interobserver variability and weak reproducibility. It does not fully reflect the variable clinical course and biological diversity, even within a single grade group. Molecular studies have identified multiple biomarkers with diagnostic and prognostic implications, including IDH1/2 mutation, TERT promoter (TERTp) mutation, BRAF mutation, 1p19q codeletion, epidermal growth factor receptor (EGFR) amplification, and chromosome 10q deletion.

We developed a molecular grading system for diffuse gliomas in adults using histological data from 1275 patients in the Hospital Authority. Adult gliomas can be stratified into six molecular grades with distinct clinical outcomes using a combination of single-gene molecular biomarkers. We demonstrated that molecular grading is superior to conventional histological grading for prognostication. We then used next-generation sequencing (NGS) and methylation profiling to delineate the molecular landscapes of 72 IDH-wildtype, TERTp-wildtype adult glioblastomas and 50 IDH-wildtype, H3-

wildtype glioblastomas in adolescents and young adults.³ These glioblastomas are heterogeneous groups of tumours. We also identified molecular biomarkers associated with clinical outcomes; they do not frequently display the molecular diagnostic features of regular IDH-wildtype glioblastomas.

Methods

Crude cell lysate was prepared from formalin-fixed paraffin-embedded sections. DNA from the lysate was amplified using forward and reverse primers. Locus-specific probes were denatured, incubated overnight, washed, and visualised. At least 100 non-overlapping signals were counted and analysed in each case. Amplification was considered present when clusters appeared or when >5% of tumour cells displayed a target/reference signal ratio >2. Deletion was considered present when >25% of counted nuclei exhibited one target signal and two reference signals.

In-house glioma-specific target panels were constructed for targeted sequencing. DNA quality and quantity were assessed. Samples that passed quality control underwent library preparation. DNA libraries were further assessed for quality and quantity before sequencing. Paired-end reads were aligned to the human reference genome. Variants were identified and annotated.

generated to detect fusion transcripts of 15 cancerrelated genes. Paired-end reads were aligned to the human genome assembly GRCh37 (hg19); fusion genes were identified. DNA was subjected in 67 cases. Overall, 4.15±6.187 mutations were to bisulphite modification and hybridisation. Background correction, dye-bias global normalisation, and calculation of DNA methylation levels were then performed.

Results

We stratified 1275 cases of adult gliomas into six molecular grades based on IDH mutations, 1p19g codeletion, TERT promoter mutation, BRAF mutation, EGFR amplification, 10q loss, and H3.1 and H3.3 mutations.1 The clinical features of molecular grading were classified into six groups: (1) IDH mutant and 1p19q codeleted; (2) IDH mutant, 1p19q non-codeleted, and TERT mutant; (3) IDH mutant, 1p19q non-codeleted, and TERT wildtype; (4) IDH wildtype and BRAF mutant; (5) IDH wildtype, BRAF wildtype, and without evidence of TERTp mutation, EGFR amplification, 10q loss, or H3 mutation; and (6) IDH wildtype and positive for TERTp mutation, EGFR amplification, 10g loss, or H3 mutations (Table).

Of all cases, 1028 were classified based on sufficient molecular data. Molecular grades were strongly associated with prognosis across the entire cohort (P<0.001, Fig 1). Multivariable analysis showed that molecular groups had independent prognostic value across the cohort after adjustments for age, sex, histological grade, tumour resection, radiotherapy, and chemotherapy.

Molecular grading was superior to conventional histological grading for prognostication. For example, WHO grade III (molecular group 1) tumours had a longer overall survival (OS) than WHO grade II (molecular group 6) tumours (P<0.001), and WHO grade IV (molecular group 4) tumours had a longer OS than WHO grade III (molecular group 6) tumours (P=0.004).

We investigated 72 IDH-wildtype, TERTpwildtype adult glioblastomas.2 Global methylation profiling revealed three methylation subtypes classic-like, mesenchymal-like, and LGm6-GBM-in IDH-wildtype, TERTp-wildtype adult glioblastomas. The LGm6-GBM subtype was the most common (57%). There was, however, no survival difference among epigenetic subtypes.

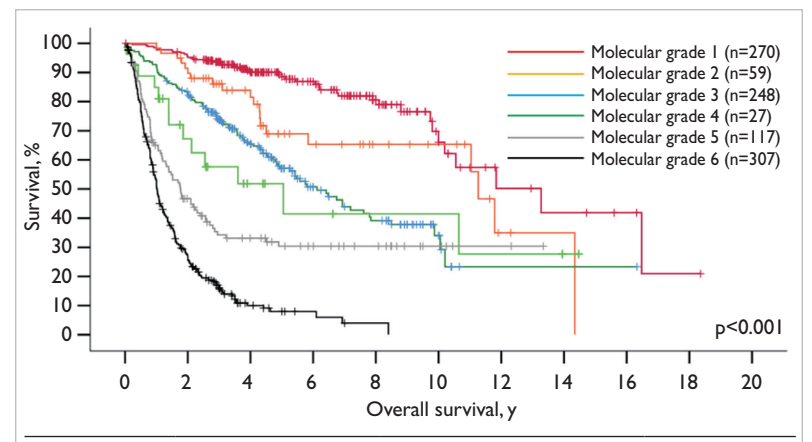
EGFR amplification, TERTp mutation, and combined chromosome 7 gain and chromosome 10 loss (+7/-10) are common molecular features in regular glioblastomas. However, in this cohort, only 34.7% of samples demonstrated EGFR amplification. None showed TERTp mutation or chromosome +7/-10. Additionally, cyclin-dependent kinase (CDK) 4 amplification was detected in nearly 60% of

RNA was extracted, and libraries were samples, and platelet-derived growth factor receptor A (PDGFRA) amplification was observed in 38.9% of the cohort.

> DNA-targeted sequencing was performed detected per sample, with values expressed as mean±standard deviation. Mismatch repair (MMR) gene mutations (MSH2, MSH6, MLH1, and PMS2) were mainly found in LGm6-GBM tumours. As expected, cases exhibiting MMR mutations showed a higher mutation load than those lacking MMR mutations (9.00±11.832 vs 3.49±4.794 mutations

TABLE. Multivariate analysis of clinical and molecular features of IDH-wildtype, TERTp-wildtype glioblastomas.

Variables	Overall surviv	/al	Progression-free	survival
	Hazard ratio (95% confidence interval)	P value	Hazard ratio (95% confidence interval)	P value
Age	1.011 (0.990-1.032)	0.303	0.999 (0.977-1.021)	0.931
Sex				
Male	1	0.697	1.281 (0.698-2.353)	0.424
Female	1.127 (0.617-2.059)			
Location				
Hemisphere	1	0.114	0.974 (0.383-2.477)	0.956
Non-hemisphere	0.447 (0.165-1.214)			
Operation				
Gross total resection	1	0.047	1	0.003
Non-total resection	1.824 (1.007-3.302)		2.598 (1.369-4.931)	
Chemotherapy				
Yes	1	0.003	1	0.003
No	6.644 (1.901- 23.225)		6.711 (1.917- 23.494)	
Radiotherapy				
Yes	1	0.688	1	0.147
No	1.220 (0.462-3.223)		2.095 (0.771-5.692)	
MGMTp				
Unmethylated	1	0.096	1	0.745
Methylated	0.609 (0.340-1.092)		0.908 (0.509-1.622)	
Epidermal growth factor receptor amplification				
No	1	0.456	1	0.627
Yes	1.269 (0.679-2.372)		1.177 (0.610-2.270)	
Platelet-derived growth factor receptor A amplification				
No	1	0.866	1	0.884
Yes	0.947 (0.506-1.775)		0.952 (0.489-1.851)	
CDKN2A/B homozygous deletion				
No	1	0.023	1	0.020
Yes	2.068 (1.107-3.864)		1.996 (1.115-3.572)	



Molecular grade	Median overall survival, y	Hazard ratio (95% confidence interval)	P value
1	13.3	1	<0.001
2	11.3	2.06 (1.21-3.51)	0.008
3	6.1	3.57 (2.51-5.08)	< 0.001
4	5.1	4.26 (2.28-7.95)	< 0.001
5	1.8	7.7 (5.29-11.2)	< 0.001
6	1.0	18.1 (13-25.3)	<0.001

FIG 1. Overall survival curves of adult gliomas according to molecular grading (n=1028).

per sample, P=0.017). ATRX mutation was detected in four (6%) of 67 cases. ATRX-mutated cases had a higher mutation load than those without (22.25±13.022 vs 3.00±3.172 mutations per sample, P<0.001). A possible explanation is a link between ATRX deficiency and impaired non-homologous chromosomal end joining, which renders cells more sensitive to DNA-damaging agents. No prognostic implication of single-gene mutations was detected throughout the cohort.

Cyclin-dependent kinase inhibitor 2A/B (CDKN2A/B) homozygous deletion was associated with shorter OS (P=0.031) and a trend towards worse progression-free survival (P=0.088). Multivariate analysis revealed that CDKN2A/B deletion was an independent prognostic factor (Table).

Global methylation profiling revealed that 50 tumours clustered into the following subgroups: (1) glioblastoma, IDH wildtype, subclass midline (GBM_midline); (2) glioblastoma, IDH wildtype, subclass RTK I/II/III/mesenchymal (GBM_RTK/mesenchymal); (3) anaplastic pleomorphic xanthoastrocytoma (PXA); and (4) low-grade glioma (LGG) classes, including LGG_GG (ganglioglioma), LGG_MYB (MYB/MYBL1), and LGG_SEGA (subependymal giant cell astrocytoma).³

LGG-clustered tumours had significantly longer OS than those clustered with GBM_midline and GBM_RTK/mesenchymal methylation classes (Fig 2). PXA-clustered tumours also showed longer OS than GBM midline-clustered tumours. The

survival difference among methylation groups remained significant in multivariate analysis (P=0.040).

Combined chromosome 7 gain and chromosome 10 loss (+7/-10), TERTp mutation, and EGFR amplification are common in regular glioblastomas. However, only one case showed combined +7/-10, whereas TERTp mutation and EGFR amplification were detected in 20.4% and 14.0% of samples, respectively. The most frequent gene copy number variations and mutations in these glioblastomas were CDKN2A/B deletions (>60%) and TP53 mutation (40.8%), respectively.

Targeted NGS was successfully performed in 49 cases. The most prevalent mutation identified was TP53 (40.8%), followed by KMT2C (38.8%), BRAF (28.6%), NF1 (28.6%), ATRX (24.5%), and SETD2 (20.4%). BRAF mutation was associated with younger age (P=0.034) and was a favourable prognostic factor within the PXA-clustered group (P=0.018). SETD2 mutation was associated with shorter OS in the entire cohort (P<0.001). Additionally, 10 (20.4%) of 49 cases carried either the C228T or C250T hotspot mutation of TERTp, and tumours with TERTp mutation had significantly worse OS (P<0.001).

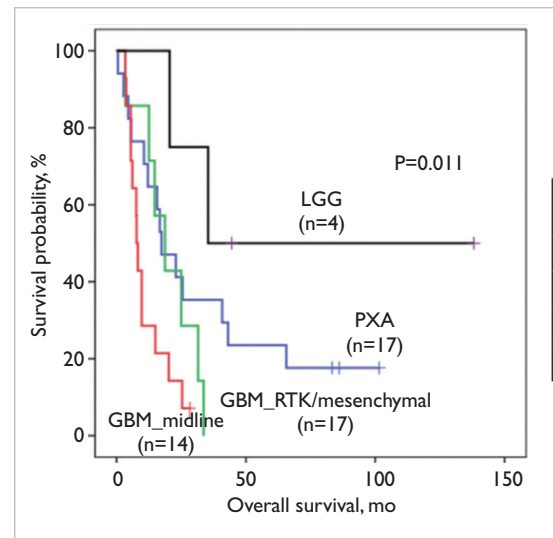
MGMTp methylation was found in 20% of cases and was associated with better OS for the entire cohort (P=0.032), even after adjustment for confounders (P=0.025). Tumours with mutations in any MMR genes (MLH1, MSH2, MSH6, and PMS2) were associated with worse OS (P=0.046); this association remained significant after adjustment for confounders (P=0.002). Tumours with TERTp mutation had worse OS (P<0.001), although significance was lost in multivariate analysis.

Discussion

Molecular criteria were first introduced in the 2016 WHO classification of central nervous system tumours. Many centres now use a combination of histological features, WHO grades, and molecular characteristics for pathological diagnosis. There remains a need to develop a simple molecular grading algorithm for gliomas based on single-gene testing.

Adult gliomas can be categorised into six molecular subgroups based on the biomarkers IDH1/2, TERTp, BRAF, H3.1, H3.3, and chromosome 10q status. The prognostic power of these molecular groups is superior to that of histological grading alone. These molecular biomarkers can be readily assessed in routine pathology laboratories. Accordingly, we established a simple molecular grading system for clinical practice to refine prognostic stratification in adult gliomas.

IDH-wildtype, TERTp-wildtype adult glioblastomas can be divided into three methylation subtypes.² CDKN2A/B deletion was identified as



	P value						
Methylation classes	PXA	GBM_RTK/ mesenchymal	GBM_ midline	LGG-like			
PXA	-	0.345	0.030	0.219			
GBM_RTK/mesenchymal	0.345	-	0.125	0.023			
GBM midline	0.030	0.125	-	0.011			
LGG-like	0.219	0.023	0.011	-			

FIG 2. Kaplan-Meier survival curves for methylation classes of IDH-wildtype, H3-wildtype glioblastomas in adolescents and young adults: low-grade glioma (LGG) clustered tumours show the best survival, followed by anaplastic pleomorphic xanthoastrocytoma (PXA), GBM_RTK/mesenchymal, and GBM_midline tumours.

an independent prognostic factor in this genotype-specific subset of glioblastomas. Only one-third of these glioblastomas exhibited the molecular diagnostic features of regular IDH-wildtype glioblastomas. Tumour grading should be assessed cautiously when evaluating TERTp-wildtype gliomas. PDGFRA alterations should be incorporated into the molecular diagnostic criteria for IDH-wildtype, TERTp-wildtype adult glioblastomas.

We previously characterised 50 IDH-wildtype, H3-wildtype glioblastomas in adolescents and young adults using global methylation profiling and NGS.³ These tumours clustered into four methylation subgroups associated with different clinical outcomes. They did not commonly exhibit the diagnostic molecular criteria of regular glioblastomas, a finding similar to that observed in IDH-wildtype, TERTp-wildtype glioblastomas. Our findings illustrate the heterogeneity among these glioblastomas; careful consideration of patient age is warranted when diagnosing IDH-wildtype, H3-wildtype gliomas in adolescents and young adults who lack the molecular features of adult IDH-wildtype glioblastomas.

Conclusion

We developed a molecular-based grading system for adult gliomas, which has become part of the molecular diagnostic service for CNS tumours at our hospitals. We implemented NGS using our customised panel for selected glioma patients. Our work has advanced the practice of personalised medicine.

Funding

This study was supported by the Health and Medical Research Fund, Health Bureau, Hong Kong SAR Government (#07180736). The full report is available from the Health and Medical Research Fund website (https://rfs1.healthbureau.gov.hk).

Disclosure

The results of this research have been previously published in:

- 1. Chan AK, Shi ZF, Li KK, et al. Combinations of single-gene biomarkers can precisely stratify 1,028 adult gliomas for prognostication. Front Oncol 2022;12:839302.
- 2. Liu EM, Shi ZF, Li KK, et al. Molecular landscape of IDH-wildtype, TERT-wildtype adult glioblastomas. Brain Pathol 2022;32:e13107.
- 3. Shi ZF, Li KK, Huang QJ, et al. Molecular landscape of IDH-wild-type, H3-wild-type glioblastomas of adolescents and young adults. Neuropathol Appl Neurobiol 2022;48:e12802.

- Liu EM, Shi ZF, Li KK, et al. Molecular landscape of IDHwildtype, TERT-wildtype adult glioblastomas. Brain Pathol 2022;32:e13107.
- Chan AK, Shi ZF, Li KK, et al. Combinations of single-gene biomarkers can precisely stratify 1,028 adult gliomas for prognostication. Front Oncol 2022;12:839302.
- Shi ZF, Li KK, Huang QJ, et al. Molecular landscape of IDH-wild-type, H3-wild-type glioblastomas of adolescents and young adults. Neuropathol Appl Neurobiol 2022;48:e12802.

Magnetic resonance imaging-based machine learning to detect mild cognitive impairment associated with Alzheimer's disease: abridged secondary publication

H Ko *, VCT Mok, L Shi, J Abrigo, BYK Lam, ATC Lee

KEY MESSAGES

- 1. The Alzheimer's Disease Resemblance Atrophy Index (AD-RAI) is effective for identifying amyloid-positive and tau-positive pathology in patients with mild cognitive impairment.
- 2. The AD-RAI outperforms other conventional magnetic resonance imaging features (eg, hippocampus volume, hippocampus fraction, and medial temporal lobe atrophy score) in terms of accuracy, sensitivity, and specificity.
- The AD-RAI can serve as a screening tool for the early detection and management of Alzheimer's disease.

Hong Kong Med J 2025;31(Suppl 7):S22-4

HMRF project number: 08190666

- ¹ H Ko, ¹ VCT Mok, ² L Shi, ² J Abrigo, ¹ BYK Lam, ³ ATC Lee
- Department of Medicine and Therapeutics, The Chinese University of Hong Kong, Hong Kong SAR, China
- ² Department of Imaging and Interventional Radiology, The Chinese University of Hong Kong, Hong Kong SAR, China
- ³ Department of Psychiatry, The Chinese University of Hong Kong, Hong Kong SAR, China
- * Principal applicant and corresponding author: ho.ko@cuhk.edu.hk

Introduction

Alzheimer's disease (AD) is the most common form of dementia. In Hong Kong, the prevalence of dementia is projected to triple in two decades, reaching 300 000 cases. Early diagnosis and treatment are crucial. Staging of AD is based on amyloid-beta plagues and tauopathy, facilitating early identification of preclinical and prodromal AD through biomarkers. Individuals with mild cognitive impairment (MCI) who exhibit amyloid-positive and tau-positive (A+T+) pathology (ie, prodromal AD) have a substantially greater risk of experiencing short-term clinical progression.2 The approval of lecanemab and donanemab for early AD treatment underscores the need for precise diagnosis. Standard detection involves cerebrospinal fluid assays and positron emission tomography, which are invasive and costly. Thus, the use of a non-invasive diagnostic method is pivotal for the early diagnosis of AD.

Structural magnetic resonance imaging (MRI) has been used to evaluate cognitive impairments and neurodegeneration through atrophy, which are key AD biomarkers.³ Using advanced machine learning techniques and automated quantification tools for multiple brain regions, we developed an algorithm that produces the Alzheimer's Disease Resemblance Atrophy Index (AD-RAI), which captures the distinct pattern of atrophy across various brain regions associated with AD.⁴ The AD-RAI outperformed hippocampal measures in predicting conversion among cognitively unimpaired individuals and patients with MCI.⁴

This study aimed to investigate the performance of AD-RAI for detecting A+T+ pathology in patients with MCI. The diagnostic performance of AD-RAI was compared with that of conventional AD imaging techniques: hippocampus volume and visual ratings of medial temporal lobe atrophy (MTA).

Methods

Chinese patients with MCI aged 50 to 80 years, whose primary language was Cantonese, were recruited from the community and the Prince of Wales Hospital, Hong Kong. Patients were excluded if they had a diagnosis of non-AD dementia, a history of stroke, parkinsonism, major psychiatric disease, or any significant neurological disease (eg brain tumour), or any contraindication for brain imaging. All patients were examined by an experienced dementia specialist to determine eligibility. Based on brain imaging results, patients were categorised as A+T+ (prodromal AD) or non-A+T+.

MCI was defined using the 2018 National Institute on Aging and Alzheimer's Association research framework. Memory complaints were assessed using the Chinese Abbreviated Memory Inventory; those who responded 'Yes' to any of its five questions were considered to have subjective memory complaints. Participants with an ageadjusted z-score of \leq -1 standard deviation in the Hong Kong List Learning Test trial 4, a score \leq 16th percentile in the Hong Kong version of the Montreal Cognitive Assessment (MoCA), or a Clinical Dementia Rating of \leq 0.5 were considered to have

MCI, regardless of independence in daily activities.

Structural MRI was conducted using 3.0 Tesla Achieva TX scanners (Philips Medical Systems, Best, Netherlands), focusing on the three-dimensional T1-weighted sequence. The AD-RAI was generated by assessing the extent of atrophy in AD-specific brain regions including the hippocampus, ventricles, and various cortical lobes. Diagnostic performance of the AD-RAI was compared with that of conventional atrophy metrics. MTA was rated on coronal images using the Scheltens 5-point scale; a score of ≥ 2 was defined as MTA.

Univariate logistic regression was conducted to assess the relationships between outcomes and various biomarkers. Adjustments were made for age, sex, education level, and baseline MoCA scores in relation to imaging features. A+T+ status was the dependent variable. Receiver operating characteristic curve analysis was used to assess the model's discriminative performance (sensitivity, specificity, and accuracy). Optimal cut-offs were determined using Youden's index: hippocampus volume of 6.07 mL, hippocampus fraction of 0.41%,⁵ and AD-RAI of 0.4.

Results

In total, 26 male and 41 female patients (mean age, 68.8 years) were included in the analysis. Patients with and without A+T+ pathology were comparable in terms of baseline characteristics. However, patients with A+T+ pathology had higher AD-RAI (P<0.001), lower hippocampus volume (P<0.001), lower hippocampus fraction (P<0.001), and greater likelihood of displaying an MTA score \geq 2 (P<0.001) [Table 1].

In the multivariable logistic regression, patients with A+T+ pathology were associated with

higher AD-RAI (adjusted odds ratio [aOR]=101.29, P<0.001), lower hippocampus volume (aOR=11.38, P=0.001), lower hippocampus fraction (aOR=13.32, P=0.001), and greater likelihood of displaying an MTA score ≥ 2 (aOR=10.37, P<0.001), independent of age, sex, education level, and baseline MoCA score (Table 2).

The AD-RAI cut-off value of \geq 0.4 achieved an area under the curve of 83.6%, which was higher than that for hippocampus volume of \leq 6.07 mL (70.1%), hippocampus fraction of \leq 0.41% (69.9%), and MTA score of \geq 2 (71.6%). The AD-RAI cut-off of \geq 0.4 had 81.8% sensitivity, 85.3% specificity, and 83.6% accuracy (Table 3).

Combining the clinical model with the AD-RAI cut-off of \geq 0.4 achieved the highest area under the curve of 90.0%, with 84.9% sensitivity, 85.3% specificity, and 85.1% accuracy (Table 3). Combining the clinical model with other MRI features also led to improvements in performance metrics.

Discussion

The AD-RAI surpassed conventional brain atrophy metrics in identifying A+T+ pathology. This finding is consistent with our previous research, which indicates the superior efficacy of AD-RAI over hippocampus volume and hippocampus fraction in identifying A+T+ pathology among cognitively unimpaired individuals or patients with MCI. Typically, MTA and reductions in hippocampus volume are among the earliest changes detectable on structural MRI, manifesting years prior to the onset of clinical symptoms, and possibly indicative of progression from MCI to AD. However, multiple neuropathological subtypes of AD have been identified. Early-stage structural abnormalities observed on MTA might be minimal to mild, which

TABLE 1. Clinical characteristics of patients with Alzheimer's disease.

Characteristic	Total (n=67)	With amyloid- positive and tau- positive pathology (n=33)	Without amyloid- positive and tau- positive pathology (n=34)	P value
Age, y	68.8±5.1	66.6±7.1	67.8±6.2	0.306
Male sex	26 (38.8)	13 (39.4)	13 (38.2)	0.922
Education level, y	8.2±4.8	8.8±4.8	8.5±4.8	0.905
Hong Kong version of Montreal Cognitive Assessment	20.12±4.67	18.97±4.38	19.55±4.53	0.174
Alzheimer's Disease Resemblance Atrophy Index	0.19±0.24	0.72±0.33	0.45±0.39	<0.001
Hippocampus volume, mL	6.48±0.74	5.58±1.04	6.04±1.00	< 0.001
Hippocampus fraction, %	0.46±0.05	0.4±0.06	0.43±0.06	< 0.001
Intracranial volume, mL	1403.51±116.85	1377.36±119.88	1390.63±118.19	0.286
Medial temporary lobe atrophy score ≥2	32 (47.8)	23 (69.7)	9 (26.5)	<0.001

^{*} Data are presented as mean±standard deviation or No. (%) of participants.

TABLE 2. Associations between biomarkers and amyloid-positive and tau-positive pathology in patients with Alzheimer's disease.

Variable	Univariate logistic re	gression	Multivariable logistic re	gression
	Crude odds ratio (95% confidence interval)	P value	Adjusted odds ratio (95% confidence interval)	P value
Age, y	0.94 (0.87-1.02)	0.152	-	-
Sex	0.95 (0.36-2.55)	0.922	-	-
Education level, y	1.03 (0.93-1.14)	0.596	-	-
Hong Kong version of Montreal Cognitive Assessment	0.94 (0.85-1.05)	0.300	-	-
Alzheimer's Disease Resemblance Atrophy Index ≥0.4	26.10 (7.13-95.52)	<0.001	101.29 (10.81-948.79)	<0.001
Hippocampus volume ≤6.07, mL	5.52 (1.94-15.72)	0.001	11.38 (2.79-46.45)	0.001
Hippocampus fraction ≤0.41, %	7.97 (2.29-27.72)	0.002	13.32 (3.05-58.12)	0.001
Intracranial volume, mL	1.00 (0.99-1.00)	0.365	1.00 (0.99-1.00)	0.213
Medial temporal lobe atrophy score ≥2	6.39 (2.21-18.51)	0.003	10.37 (2.86-37.57)	<0.001

TABLE 3. Performance metrics of prediction models for amyloid-positive and tau-positive pathology in patients with Alzheimer's disease.

Variable	Area under the curve (95% confidence interval)	Sensitivity, %	Specificity,	Accuracy,
Alzheimer's Disease Resemblance Atrophy Index ≥0.4	83.6 (74.6-92.6)	81.8	85.3	83.6
Hippocampus volume ≤6.07, mL	70.1 (59.0-81.3)	69.7	70.6	70.2
Hippocampus fraction ≤0.41, %	69.9 (59.6-80.1)	51.5	88.2	70.2
Medial temporal lobe atrophy score ≥2	71.6 (60.7-82.6)	69.7	73.5	71.6
Clinical model	61.8 (48.0-75.6)	42.4	88.2	65.7
Clinical model + magnetic resonance imaging features				
+ Alzheimer's Disease Resemblance Atrophy Index ≥0.4	90.0 (82.6-97.4)	84.9	85.3	85.1
+ Hippocampus volume ≤6.07, mL	78.7 (67.0-90.5)	87.9	76.5	82.1
+ Hippocampus fraction ≤0.41, %	78.9 (67.6-90.1)	57.6	97.1	77.6
+ Medial temporal lobe atrophy score ≥2	80.0 (69.0-90.9)	72.7	82.4	77.6

is insufficient to predict underlying AD pathology. Our findings suggest that AD-RAI is more effective in detecting A+T+ pathology than localised atrophy measurements.

Funding

This study was supported by the Health and Medical Research Fund, Health Bureau, Hong Kong SAR Government (#08190666). The full report is available from the Health and Medical Research Fund website 3. Frisoni GB, Fox NC, Jack CR Jr, Scheltens P, Thompson PM. (https://rfs2.healthbureau.gov.hk).

Disclosure

The results of this research have been previously published in:

1. Cai Y, Fan X, Zhao L, et al. Comparing machine learning-derived MRI-based and blood-based predicting neurodegeneration biomarkers in syndromal conversion in early AD. Alzheimers

Dement 2023;19:4987-98.

- 1. Jack CR Jr, Bennett DA, Blennow K, et al. NIA-AA Research Framework: toward a biological definition of Alzheimer's disease. Alzheimers Dement 2018;14:535-62.
- Yu JT, Li JQ, Suckling J, et al. Frequency and longitudinal clinical outcomes of Alzheimer's AT(N) biomarker profiles: a longitudinal study. Alzheimers Dement 2019;15:1208-
- The clinical use of structural MRI in Alzheimer disease. Nat Rev Neurol 2010;6:67-77.
- Zhao L, Luo Y, Lew D, et al. Risk estimation before progression to mild cognitive impairment and Alzheimer's disease: an AD resemblance atrophy index. Aging (Albany NY) 2019;11:6217-36.
- 5. Liu W, Au LWC, Abrigo J, et al. MRI-based Alzheimer's disease-resemblance atrophy index in the detection of preclinical and prodromal Alzheimer's disease. Aging (Albany NY) 2021;13:13496-514.

Design, modelling, evaluation, and optimisation of intensive care unit network in Hong Kong: abridged secondary publication

EWM Wong *, G Joynt, K Chan

KEY MESSAGES

- 1. We built a framework involving the design, evaluation, and optimisation of intensive care unit (ICU) networks in Hong Kong, particularly during pandemics and mass casualty events.
- 2. The model for the Hong Kong ICU network enables central management and sharing of ICU beds to improve quality of service metrics without incurring additional expenditure on new resources.
- We analysed real data from hospitals in the New Territories Northeast cluster and identified appropriate arrival process and length of service distributions for different types of patients (internal emergency, external emergency, and elective).
- We applied the International Ethics Standards for Sustainability Assurance framework to evaluate the rejection or deferral rate for each type of patients, with reasonable accuracy.

5. We proposed a heuristic algorithm based on particle swarm optimisation to determine the optimal set of relevant network parameters, and then combined it with the International Ethics Standards for Sustainability Assurance method for evaluating each setting. The combination can effectively reduce computation time by up to two orders of magnitude while obtaining the same optimal solution.

Hong Kong Med J 2025;31(Suppl 7):S25-7

HMRF project number: 16171921

¹ EWM Wong, ² G Joynt, ³ K Chan

- Department of Electrical Engineering, City University of Hong Kong, Hong Kong SAR, China
- ² Department of Anaesthesia and Intensive Care, The Chinese University of Hong Kong, Hong Kong SAR, China
- 3 Department of Intensive Care, Tuen Mun Hospital, Hong Kong SAR, China
- * Principal applicant and corresponding author: e.wong@cityu.edu.hk

Introduction

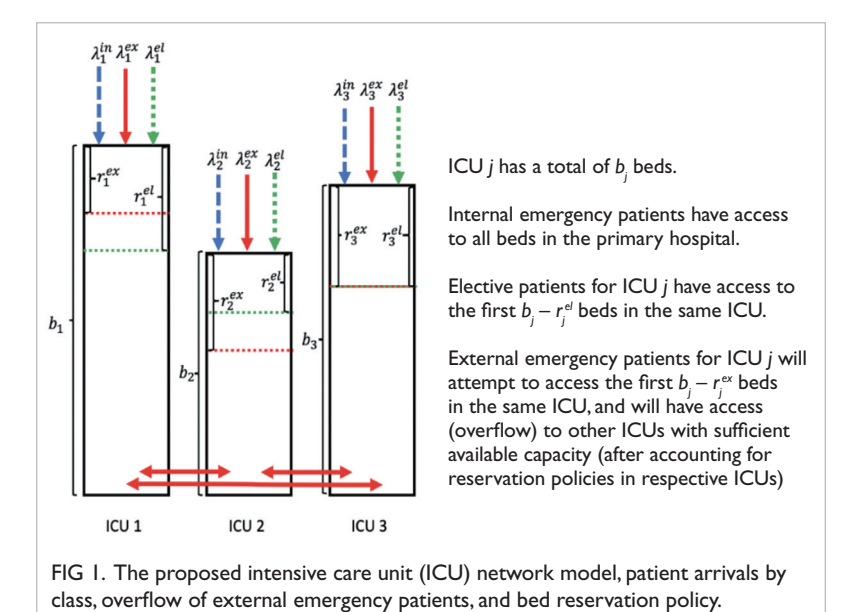
Intensive care units (ICUs) can cost up to six times more per day than general wards.¹ Their demand exceeds supply;² thus, efficient use of ICUs, especially during epidemics and mass casualty events, is crucial. This requires the systematic development of policies for ICU admission. One solution is to group multiple ICUs into a network, allowing some patients to be treated at any ICU within the network.³

We developed analytical models to study hypothetical scenarios, such as short-term increases in admissions caused by epidemics or mass casualty events, and to develop special policies for handling such scenarios. Our models can perform 'what if' analyses on historical events to determine policy effectiveness. This study aimed to demonstrate that (1) an ICU resource-sharing policy increases the proportion of successful admissions, compared with a non-sharing scenario; (2) a framework for evaluating and optimising the control parameters associated with our proposed policies facilitates better management and planning of ICU resources; and (3) newly proposed tools for performance evaluation and optimisation provide significantly enhanced computational efficiency and accuracy comparable to state-of-the-art approaches.

Methods

We constructed a network model comprising multiple ICU hospitals and three classes of patients: internal emergency, external emergency, and elective (Fig 1). Although internal emergency and elective patients must be treated at their original hospital, external emergency patients are flexible and may overflow to any hospital in the network. A reservation threshold was introduced for each class of patients, such that a certain class could not be admitted if the number of available ICU beds at the hospital was below the threshold.

Over 3400 records spanning January 2016 to January 2017 were collected from three ICU hospitals in the New Territories East Cluster (Prince of Wales Hospital, Alice Ho Miu Ling Nethersole Hospital, and North District Hospital). The peakedness (variance-to-mean ratio) of selected patient presentations was high, requiring more general processes than the classical Poisson process used in queuing models. We used two-moment match methodology⁴ to construct an interrupted Poisson process to fit the mean, variance, and peakedness of actual traces of patients by type and hospital. The length of service (LoS) distributions of all types of patients were used because individual



data were unavailable. Exponential and lognormal distributions were utilised to investigate the sensitivity of quality-of-service metrics to the LoS distributions and corresponding parameters.

Although discrete event simulations can accurately evaluate key performance metrics in ICU networks, they are not scalable for optimisation in large-scale systems, in which repeated measurements are needed to verify feasibility and optimality. We used the International Ethics Standards for Sustainability Assurance (IESA) framework, which has demonstrated effectiveness in evaluating blocking probabilities in ICU networks. We applied particle swarm optimisation, a representative heuristic algorithm designed to improve efficiency

over exhaustive search in obtaining optimal solutions to large-scale problems. Specifically, we adopted a variant designed for optimisation problems involving integer decision variables.

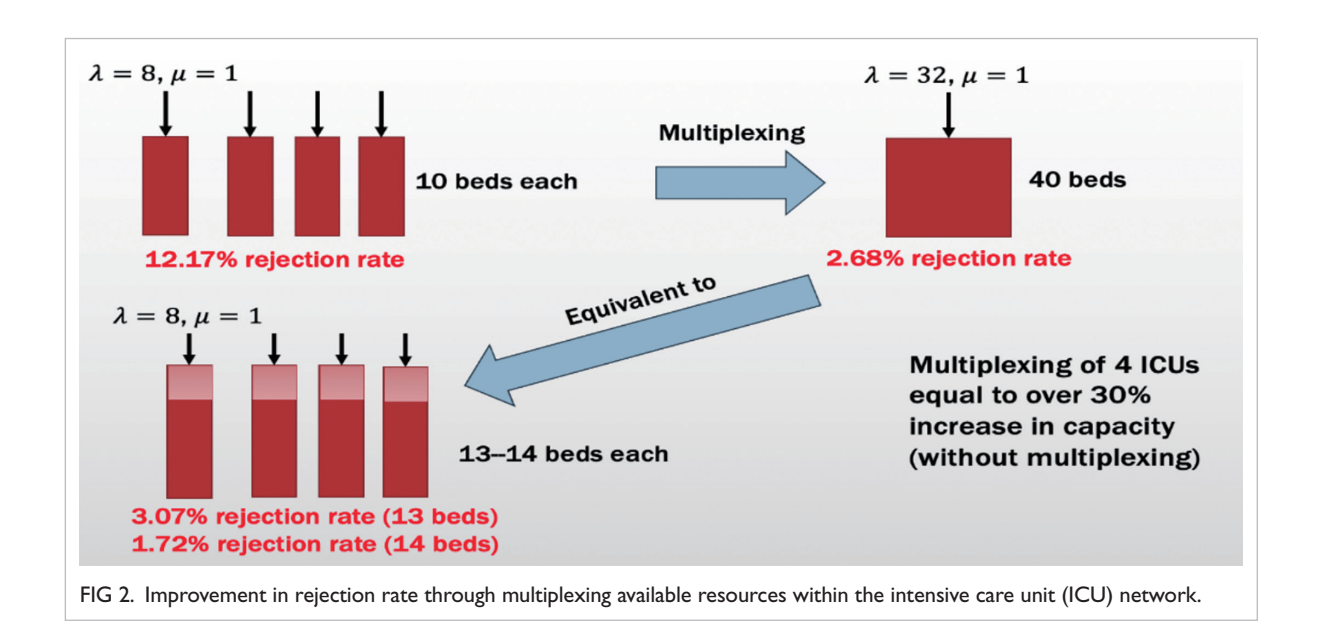
Results

We demonstrated the effect of pooling ICU beds across four hospitals (ie, multiplexing). The overall patient rejection rate was reduced by approximately 78%, compared with the baseline approach, which restricted patients' access to beds outside their original hospital (Fig 2). Although a similar reduction in patient rejection rate could be achieved by increasing the number of beds by 30% to 40%, our multiplexing approach offered a more cost-effective solution without additional expenditure.

Low relative differences in the first three moments were achieved by fitting the interrupted Poisson process to real traces of patient arrival data so that it represented the arrival process for all patient traces in the later stage of the project.

The patient rejection rate, a key quality-of-service metric, was not particularly sensitive to changes in LOS distribution. Given that the IESA framework has shown accuracy across a wide range of scenarios in which assumptions of Poisson arrivals and exponentially distributed LoS values are satisfied, the framework was deemed a valid tool for approximating patient rejection rates in the Hong Kong ICU network.

A weighted sum of rejection rates across patient types was minimised by adjusting bed reservation thresholds for each patient class, while maintaining the rejection rate for each patient class below a predetermined threshold. In ICU networks comprising three to 17 hospitals, results and computation times of three approaches



were compared: (1) discrete event simulation for evaluation and exhaustive search for identifying the optimal solution (baseline approach); (2) IESA for evaluation and exhaustive search for identifying the optimal solution; and (3) IESA for evaluation and particle swarm optimisation for identifying the optimal solution. All three approaches produced the same reservation threshold solution, indicating that IESA accuracy was sufficient for optimisation purposes. In a comparison of computation times, the heuristic particle swarm optimisation + IESA approach reduced the computation time by up to two orders of magnitude, compared with the baseline approach (Fig 3).

Discussion

During pandemics or mass casualty events, it is likely that many infectious cases or casualties will occur at a single location, leading to a surge of patient arrivals requiring ICU care. Our proposed policies for coordinating the response of multiple hospitals through the pooling of available resources can help improve efficiency in handling such incidents.

Hong Kong has a rapidly ageing population; >30% of residents are projected to be aged ≥65 years by 2036. This will increase the burden on the healthcare system, including ICUs. Our proposed models can simulate hypothetical scenarios of increased patient arrivals caused by epidemics, mass casualty events, or population ageing, addressing both short-term and long-term increases in ICU demand.

The substantial enhancement provided by our design, modelling, evaluation, and optimisation tools may prove useful in other applications, particularly those involving multiple ICUs interconnected via patient referrals.³ Future simulations may incorporate additional parameters, such as the number of ICU beds allocated to each hospital and factors related to patient referral policies. Our proposed models may help address questions regarding the balance between efficiency and fairness within a network of ICUs.

Funding

This study was supported by the Health and Medical Research Fund, Health Bureau, Hong Kong SAR Government (#16171921). The full report is available from the Health and Medical Research Fund website (https://rfs1.healthbureau.gov.hk).

Disclosure

The results of this research have been previously published in:

1. Wang J, Chan YC, Niu R, Wong EWM, van Wyk MA. Modeling the impact of vaccination on COVID-19 and its Delta and Omicron variants.

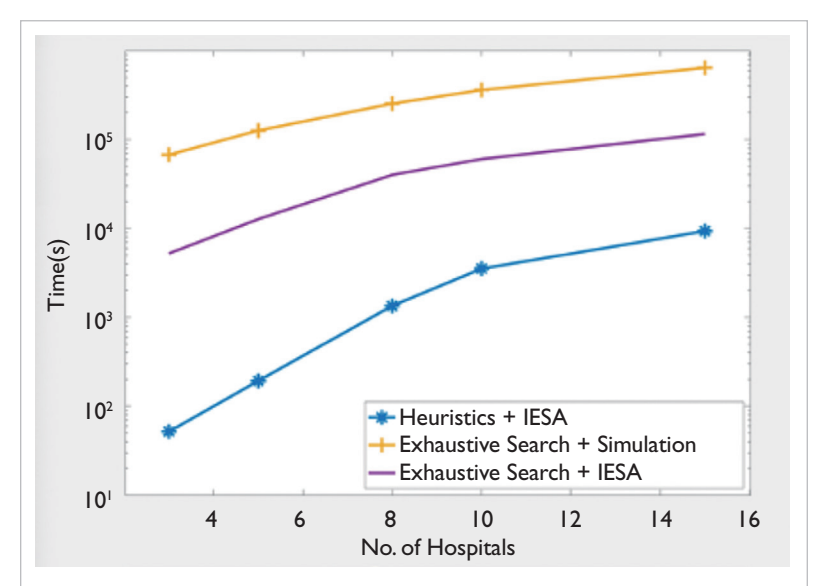


FIG 3. Comparison of computational efficiency across optimisation approaches as the number of intensive care unit (ICU) hospitals in the network increases. Abbreviation: IESA=International Ethics Standards for Sustainability Assurance

Viruses 2022;14:1482.

2. Niu R, Chan YC, Wong EWM, van Wyk MA, Chen G. A stochastic SEIHR model for COVID-19 data fluctuations. Nonlinear Dyn 2021;106:1311-23.

3. Niu R, Wong EWM, Chan YC, Van Wyk MA, Chen G. Modeling the COVID-19 pandemic using an SEIHR model with human migration. IEEE Access 2020;20:195503-14.

4. Chan YC, Wu J, Wong EWM, Leung CS. Integrating teletraffic theory with neural networks for quality-of-service evaluation in mobile networks. Appl Soft Comput 2024;152:111208.

5. Wong EWM, Chan YC. A century-long challenge in teletraffic theory: blocking probability evaluation for overflow loss systems with mutual overflow. IEEE Access 2023;11:61274-88.

- Griffiths JD, Price-Lyold N, Smithies M, Williams JE. Modelling the requirement for supplementary nurses in an intensive care unit. J Oper Res Soc 2005;56:126-33.
- Joynt GM, Gomersall CD, Tan P, Lee A, Cheng CA, Wong EL.
 Prospective evaluation of patients refused admission to an
 intensive care unit: triage, futility, and outcome. Intensive
 Care Med 2001;27:1459-65.
- Litvak N, van Rijsbergen M, Boucherie RJ, van Houdenhoven M. Managing the overflow of intensive care patients. Eur J Oper Res 2008;185:998-1010.
- Jagerman DL. Methods in traffic calculations. AT&T Bell Lab Tech J 1984;63:1283-310.
- Wong EW, Guo J, Moran B, Zukerman M. Information exchange surrogates for approximation of blocking probabilities in overflow loss systems. Proceedings of the 2013 25th International Teletraffic Congress (ITC), Shanghai, China; 2013.

Effectiveness and safety of time-lapse imaging for in vitro fertilisation: abridged secondary publication

DYL Chan *, TC Li, JPW Chung, TL Lee, CC Wang

KEY MESSAGES

- 1. Time-lapse imaging for in vitro fertilisation is claimed to provide an 'undisturbed environment' that could improve clinical outcomes.
- 2. We evaluated 1575 patients who underwent in vitro fertilisation to determine the efficacy of time-lapse imaging.
- 3. Time-lapse imaging did not lead to improved outcomes in terms of live births, clinical

pregnancies, or pregnancy losses.

Hong Kong Med J 2025;31(Suppl 7):S28 HMRF project number: 07180566

- ¹ DYL Chan, ¹ TC Li, ¹ JPW Chung, ² TL Lee, ¹ CC Wang
- Department of Obstetrics and Gynaecology, Prince of Wales Hospital, The Chinese University of Hong Kong, Hong Kong SAR, China
- ² EggLogics, Hong Kong Science Park, Hong Kong SAR, China
- * Principal applicant and corresponding author: drdcyl@gmail.com

Introduction

Subfertility affects approximately one in six adults globally. In vitro fertilisation (IVF) and intracytoplasmic sperm injection (ICSI) are increasingly available, but their success rates have plateaued. Selection of embryos with the highest potential for implantation is essential for success. However, current methods of embryo selection have limitations in predictive accuracy; optimisation of embryo selection techniques is needed. Time-lapse imaging (TLI) has emerged as a promising technology for enhancing embryo selection in IVF.

TLI enables continuous monitoring of embryo development within the incubator, capturing digital images at regular intervals, typically every 5 to 15 minutes, facilitating comprehensive assessment without disturbing the incubation environment (temperature, gas concentrations, pH, and humidity). A stable culture environment may positively influence embryonic development, quality, and ultimately, live birth rates. Nonetheless, evidence regarding TLI's utility remains inconclusive. This study aimed to compare TLI with standard care in terms of live birth rates, clinical pregnancies, and pregnancy losses.

Methods

We enrolled participants undergoing either IVF or ICSI, including women aged 18 to 42 years and men aged >18 years, who received their first, second, or third IVF or ICSI cycle and had at least three 2-pronuclei embryos available. Those concurrently involved in other interventional trials, undergoing treatment with donor gametes, or intending to undergo pre-implantation genetic diagnosis or screening were excluded. Participants were randomly assigned in a 1:1:1 ratio to one of three intervention arms: (1) embryo assessment and selection using morphokinetic parameters and standard morphological embryo scoring in undisturbed culture conditions in TLI incubators, (2) conventional morphological embryo assessment and selection in undisturbed culture conditions in

TLI incubators, and (3) conventional morphological embryo assessment using a light microscope and standard embryo culture in standard incubators (controls). Randomisation was performed using a secure web-based system, stratified by fertility clinic and minimised by the female participant's age (<35 years, 35-40 years, >40 years) and the type of planned first embryo transfer (fresh or frozen).

Results

Of 390 participants, 381 (97.7%) had outcome data available. There were no significant differences among the TLI, undisturbed culture, and control groups in terms of live birth rates (34.4% vs 38.5% vs 37.6%), clinical pregnancy rates (41.4% vs 45.1% vs 40.8%), or pregnancy loss rates (41.4% vs 45.1% vs 40.8%). Three serious adverse events occurred: one in a woman in the TLI group and two in women in the control group; all were unrelated to the trial.

Conclusion

Time-lapse imaging does not lead to improved outcomes in terms of live births, clinical pregnancies, or pregnancy losses.

Funding

This study was supported by the Health and Medical Research Fund, Health Bureau, Hong Kong SAR Government (#07180566). The full report is available from the Health and Medical Research Fund website (https://rfs1.healthbureau.gov.hk).

Disclosure

The results of this research have been previously published in:

1. Bhide P, Chan DYL, Lanz D, et al. Clinical effectiveness and safety of time-lapse imaging systems for embryo incubation and selection in invitro fertilisation treatment (TILT): a multicentre, three-parallel-group, double-blind randomised controlled trial. Lancet 2024;404:256-65.

High-flow nasal cannula therapy for children and adolescents with obstructive sleep apnoea: abridged secondary publication

KCC Chan *, CT Au, KL Kwok, AM Li

KEY MESSAGES

- The efficacies of high-flow nasal cannula (HFNC) and continuous positive airway pressure (CPAP) therapies are similar in reducing disease severity among children and adolescents with moderateto-severe obstructive sleep apnoea.
- 2. Self-reported adherence is higher with CPAP therapy than with HFNC therapy.
- 3. Both HFNC and CPAP therapies significantly improved disease-specific quality-of-life scores, but not behavioural measures.

Hong Kong Med J 2025;31(Suppl 7):S29-31

HMRF project number: 06170456

- ¹ KCC Chan, ^{1,2} CT Au, ³ KL Kwok, ¹ AM Li
- Department of Paediatrics, Faculty of Medicine, The Chinese University of Hong Kong, Hong Kong SAR, China
- ² Translational Medicine, Research Institute, The Hospital for Sick Children, Toronto, Ontario, Canada
- ³ Department of Paediatrics, Kwong Wah Hospital, Hong Kong SAR, China
- * Principal applicant and corresponding author: katechan@cuhk.edu.hk

Introduction

Childhood obstructive sleep apnoea (OSA) is a prevalent sleep-related breathing disorder associated with a variety of morbidities, and timely interventions are essential. Its most common cause is adenotonsillar hypertrophy, and adenotonsillectomy is recommended as the first-line therapy. Continuous positive airway pressure (CPAP) therapy is an alternative for patients with persistent moderate-to-severe OSA (MS-OSA) after adenotonsillectomy, for those without surgically modifiable or correctable causes, and for those with contraindications to surgery. However, low adherence remains a major obstacle in paediatric populations.²

High-flow nasal cannula (HFNC) therapy is a non-invasive respiratory support for acute and chronic respiratory failure. It has been used in CPAP-intolerant children and in those with comorbid obesity and/or medical complexities.³ Its efficacy is comparable to that of CPAP in improving OSA severity among children with MS-OSA.⁴ This study aimed to compare HFNC with CPAP in children and adolescents with MS-OSA in terms of efficacy, treatment adherence, quality of life, and behavioural outcomes.

Methods

Children and adolescents aged 6 to 18 years who were diagnosed with MS-OSA (Obstructive Apnoea Hypopnoea Index [OAHI] ≥5 events/hour) and recommended for CPAP therapy were invited to participate between 2019 and 2023. Participants underwent HFNC and CPAP titration

with polysomnography. If both HFNC and CPAP therapies were efficacious in reducing the OAHI to <5 events/hour, participants were invited for home interventions, with 3 months each of HFNC therapy and CPAP therapy. The sequence was randomly assigned.

HFNC therapy was initiated at a flow of 5 or 15 L/min for paediatric or adult-sized cannulas, respectively, then gradually titrated in 5 or 10 L/min increments, respectively, based on symptoms of snoring, laboured respirations, and oxygen desaturations. The titration lasted 10 to 30 minutes, depending on the participants' tolerance and response to treatment,⁵ until either disordered breathing was normalised or the maximum recommended flow (25 and 50 L/min, respectively) was reached.

CPAP therapy was started at a pressure of 4 cm $\rm H_2O$ and increased in 1 cm $\rm H_2O$ increments as tolerated, up to a maximum of 12 cm $\rm H_2O$, or until all OSAs and hypopnoeas were eliminated, or respiratory event-related arousals and snoring were minimised.

Participants and parents were asked to complete a self-administered questionnaire at baseline and at 3 months regarding OSA-related quality of life (OSA-18), daytime sleepiness (Modified Epworth Sleepiness Scale), quality of life (Paediatric Quality of Life Inventory), and behaviours (Child Behaviour Checklist). Parents or caregivers were also asked to complete daily records of CPAP/HFNC usage for adherence.

Paired t tests and Wilcoxon signed-rank tests were used to compare outcome measures between HFNC and CPAP therapies for parametric and

non-parametric variables, respectively. Adherence, quality of life, and behavioural parameters were analysed using a linear mixed model adjusted for treatment order, age, sex, and maternal education.

Results

In total, 26 male and three female participants (mean±standard deviation age, 12.8±3.0 years) completed the titration. Both HFNC and CPAP

TABLE I. Titration of high-flow nasal cannula (HFNC) and continuous positive airway pressure (CPAP) therapies in children and adolescents with obstructive sleep apnoea (n=29).

Polysomnography		Change	Change in HFNC vs	P value				
parameters	Baseline*	HFNC*	P value	CPAP*	P value	change in CPAP*		
Obstructive Apnoea Hypopnoea Index, events/h	12.60±12.23	-7.16 (-9.23 to -5.09)	<0.001	-9.01 (-12.16 to -5.86)	<0.001	1.85 (-1.60 to 5.30)	0.281	
Obstructive Apnoea Index, events/h	5.37±10.82	-4.16 (-6.96 to -1.35)	0.005	-4.96 (-8.76 to -1.15)	0.013	0.80 (-0.35 to 1.95)	0.167	
Obstructive Hypopnoea Index, events/h	7.22±4.25	-3.95 (-6.08 to -1.82)	0.001	-4.37 (-6.50 to -2.24)	<0.001	0.42 (-1.51 to 2.34)	0.660	
Central Apnoea Hypopnoea Index, events/h	1.89±3.50	1.43 (-0.11 to 2.97)	0.068	1.62 (-1.63 to 4.87)	0.316	-0.19 (-3.99 to 3.61)	0.919	
Oxygen Desaturation Index, events/h	9.83±14.46	-4.56 (-6.33 to -2.78)	<0.001	-5.86 (-9.27 to -2.46)	0.001	1.30 (-2.70 to 5.31)	0.510	
Nadir oxygen saturation, %	88.38±4.78	4.59 (3.29 to 5.88)	<0.001	6.41 (4.78 to 8.05)	<0.001	-1.83 (-3.26 to -0.39)	0.014	
Total Arousal Index, events/h	19.22±11.45	-8.26 (-11.48 to -5.04)	<0.001	-6.43 (-11.10 to -1.76)	0.009	-1.83 (-7.02 to 3.36)	0.476	
Sleep efficiency, %	88.15±7.65	2.36 (-3.00 to 7.73)	0.374	-0.08 (-5.56 to 5.40)	0.976	2.44 (-1.69 to 6.58)	0.236	

^{*} Data are presented as mean±standard deviation or mean (95% confidence interval).

TABLE 2. High-flow nasal cannula (HFNC) therapy versus continuous positive airway pressure (CPAP) therapy among children and adolescents with obstructive sleep apnoea.

Variables	Baseline (n=22)*	HFNC (n=21)*	P value	CPAP (n=21)*	P value	P value (HFNC vs CPAP)
Modified Epworth Sleepiness Scale	7.5 (4.0-11.3)	6.0 (4.0-8.8)	0.271	6.0 (3.0-8.5)	0.132	0.552
Obstructive Sleep Apnoea-18	57.9±15.1	48.7±13.4	0.009	45.2±12.6	<0.001	0.147
Paediatric Quality of Life Inventory						
Child Psychosocial Health Summary	78.5±9.8	81.4±10.7	0.475	78.3±10.3	0.932	0.562
Child Physical Health Summary	83.7±10.4	89.4±9.7	0.101	82.7±15.6	0.829	0.257
Child Paediatric Quality of Life Inventory	80.3±8.8	84.2±9.9	0.203	79.8±10.5	0.952	0.366
Parent Psychosocial Health Summary	71.7±13.9	75.7±13.3	0.189	73.4±13.8	0.311	0.609
Parent Physical Health Summary	78.4±16.1	87.5±9.8	0.005	82.4±16.6	0.244	0.292
Parent Paediatric Quality of Life Inventory	74.0±13.2	79.8±11.4	0.014	76.6±14.3	0.209	0.397
Child Behaviour Checklist						
Anxious/depressed	53.8±5.9	53.7±6.6	0.767	54.8±9.1	0.141	0.833
Withdrawn/depressed	57.6±7.4	56.7±7.7	0.804	57.4±8.5	0.920	0.579
Somatic complaints	59.3±6.7	58.7±7.0	0.565	59.2±7.8	0.855	0.925
Social problems	58.6±8.9	57.8±9.3	0.945	56.5±8.8	0.167	0.317
Thought problems	58.9±7.6	56.6±6.8	0.618	57.3±6.8	0.623	0.536
Attention problems	59.7±6.4	57.9±6.5	0.163	57.6±5.0	0.143	0.240
Rule-breaking behaviours	56.5±6.3	53.9±5.7	0.121	54.1±6.0	0.159	0.636
Aggressive behaviours	58.1±7.9	58.0±8.1	0.863	57.3±8.2	0.607	0.739
Internalising problems	54.1±10.2	53.3±9.8	0.760	53.0±12.6	0.879	0.632
Externalising problems	56.6±8.3	55.1±8.5	0.595	53.0±10.8	0.168	0.306
Total problems	57.2±9.5	56.4±9.2	0.883	54.5±11.6	0.272	0.193

Data are presented as mean±standard deviation or mean (95% confidence interval).

` , ' , ' , ' , ' , ' , ' , ' , ' , ' ,				
Adherence	β (difference between HFNC and CPAP)	Standard error	P value (HFNC vs CPAP)	P value (treatment order)
Self-reported adherence rate (% of nights ≥4 hours use)			
Unadjusted	-17.058	7.013	0.026	0.008
Adjusted for age and sex	-14.929	8.283	0.092	0.009
Adjusted for age, sex, and maternal education	-14.890	8.331	0.095	0.010
Self-reported average number of hours used per night				
Unadjusted	-1.703	0.527	0.005	0.004
Adjusted for age and sex	-1.508	0.639	0.033	0.009

TABLE 3. Comparison of adherence between high-flow nasal cannula (HFNC) therapy and continuous positive airway pressure (CPAP) therapy.

therapies achieved significant improvements in OAHI (-7.16 vs -9.01, P=0.281, Table 1), Obstructive Apnoea Index, Oxygen Desaturation Index, nadir oxygen saturation, and Total Arousal Index.

Adjusted for age, sex, and maternal education

Of the participants, 22 were recruited for home interventions, with 3 months each of HFNC therapy and CPAP therapy. Both HFNC and CPAP therapies achieved significant improvement in the OSA-18 score (P=0.009 and P<0.001, respectively, Table 2), but both therapies were comparable in terms of scores on the Modified Epworth Sleepiness Scale, Paediatric Quality of Life Inventory, and Child Behaviour Checklist.

Self-reported adherence (average number of hours of usage per night) was higher with CPAP than with HFNC (β = -1.505, P=0.034), even after adjustments for age, sex, and maternal education (Table 3). None of the participants reported serious adverse effects.

Discussion

Both HFNC and CPAP therapies were effective in improving most polysomnographic parameters and OSA-18 scores among children and adolescents with MS-OSA. HFNC therapy did not provide additional benefits compared to CPAP therapy. Although HFNC therapy can be an effective alternative to CPAP therapy, its treatment adherence was lower. Given that the benefits of HFNC and CPAP therapies are strongly associated with adherence, additional efforts are needed to improve treatment adherence.

Our study had some limitations. First, treatment efficacy data were collected for only one night in a laboratory environment; thus, the variability of HFNC efficacy over several nights remains unknown. Second, the small sample size did not provide sufficient statistical power for subgroup analyses or identification of factors associated with 5. outcome improvement or adherence. Studies with larger cohorts are needed to validate our findings and explore differences between subgroups.

Conclusion

-1.505

HFNC therapy is an effective alternative to CPAP therapy for children and adolescents with MS-OSA. However, treatment adherence with HFNC therapy is not superior relative to that with CPAP therapy.

0.643

0.034

0.010

Funding

This study was supported by the Health and Medical Research Fund, Health Bureau, Hong Kong SAR Government (#06170456). The full report is available from the Health and Medical Research Fund website (https://rfs1.healthbureau.gov.hk).

Disclosure

The results of this research have been previously published in:

1. Chan KC, Au CT, Kwok KL, et al. Efficacy of highflow nasal cannula therapy and its effectiveness in home settings for paediatric obstructive sleep apnoea. Sleep Med 2025;133:106637.

- Chan KCC, Au CT, Hui LL, Wing YK, Li AM. Childhood OSA is an independent determinant of blood pressure in adulthood: longitudinal follow-up study. Thorax 2020;75:422-31.
- Hawkins SMM, Jensen EL, Simon SL, Friedman NR. Correlates of pediatric CPAP adherence. J Clin Sleep Med 2016;12:879-84.
- Du F, Gu YH, He YC, Deng WF, Liu ZZ. High-flow nasal cannula therapy for pediatric obstructive sleep apnea: a systematic review and meta-analysis. Eur Rev Med Pharmacol Sci 2022;26:4583-91.
- Fishman H, Al-Shamli N, Sunkonkit K, et al. Heated humidified high flow nasal cannula therapy in children with obstructive sleep apnea: a randomized cross-over trial. Sleep Med 2023;107:81-8.
- Hawkins S, Huston S, Campbell K, Halbower A. Highflow, heated, humidified air via nasal cannula treats CPAPintolerant children with obstructive sleep apnea. J Clin Sleep Med 2017;13:981-9.

Diagnostic accuracy of gingival bleeding on brushing, salivary activated MMP-8 and a selfreported questionnaire in early detection of periodontitis: abridged secondary publication

LJ Jin *, G Pelekos, DKL Ho, M Tonetti

KEY MESSAGES

- 1. The modified questionnaire of the Centers for Disease Control and Prevention and the American Academy of Periodontology is useful for self-detecting periodontal diseases, and its integration with demographic/lifestyle variables further improves diagnostic performance.
- 2. The oral rinse activated MMP-8 point-of-care test can identify different severities of periodontitis, and combining it with individual and lifestyle profiles enhances diagnostic performance.
- 3. Self-reported gingival bleeding on brushing is a sign of periodontal diseases, particularly gingival inflammation.
- 4. The haemoglobin levels of saliva/toothpaste slurry could be useful for identifying generalised

severe periodontitis.

5. Salivary biomarkers of certain adipose metabolism—related and ageing-related proteins as well as inflammatory cytokines may potentially identify patients with severe periodontitis.

Hong Kong Med J 2025;31(Suppl 7):S32-5 HMRF project number: 07182796

¹ LJ Jin, ¹ G Pelekos, ¹ DKL Ho, ^{1,2} M Tonetti

- ¹ Faculty of Dentistry, The University of Hong Kong, Hong Kong SAR, China
- ² Shanghai Jiao Tong University School of Medicine, College of Stomatology; National Center of Stomatology; and National Clinical Research Center of Oral Diseases, Shanghai, China
- * Principal applicant and corresponding author: ljjin@hku.hk

Introduction

Periodontal diseases, including gingivitis and periodontitis, are among the most common pathological conditions in humans.1 Periodontitis results from dysbiotic biofilm-induced dysregulated immunoinflammatory responses in susceptible individuals. It is a major cause of severe tooth loss in adults and substantially affects oral health and quality of life. Periodontitis is closely associated with systemic comorbidities such as diabetes mellitus and cardiovascular disease.^{2,3} Periodontal status can reflect host susceptibility to various systemic inflammatory comorbidities.4,5 Gingival bleeding on brushing (GBoB) is a sign of periodontal disease.6 Salivary biomarkers such as salivary activated MMP-8 (aMMP-8), haemoglobin, and proinflammatory cytokines can be used for periodontal assessment and diagnosis.7-9 This study aimed to assess the diagnostic performance of: (1) GBoB as a sentinel sign, (2) salivary aMMP-8 and other oral fluid-based periodontal biomarkers, and (3) a validated questionnaire alone and/or in combination for the early detection of periodontitis.

Methods

The study protocol was approved by the Institutional Review Board of the University of Hong Kong/

Hospital Authority Hong Kong West Cluster (references: UW19-188 and UW22-132). Oral informed consent was obtained from all participants.

In the development cohort, consecutive patients at the Prince Philip Dental Hospital were recruited from July 2019 to August 2020 to undergo three screening tests: (1) a self-administered, eightitem, validated Chinese version of the questionnaire of the US Centers for Disease Control and Prevention (CDC) and the American Academy of Periodontology (AAP), 10,11 (2) an oral rinse aMMP-8 point-of-care test (POCT),7,8 and (3) the GBoB test with subsequent detection of salivary haemoglobin levels in saliva/toothpaste slurry samples (TPS) using ultraviolet-visible spectroscopy. All participants underwent a full-mouth periodontal examination by a single examiner, and periodontal diagnosis was made according to the current classification. 12,13 Oral samples were stored at -80°C for further analysis.

In the external validation cohort, a representative community sample was recruited using random sampling. Individuals with edentulism, pregnancy, periodontal treatment in the previous 12 months, or antibiotic treatment in the last 3 months were excluded. Participants underwent (1) a self-administered and modified 13-item CDC-AAP questionnaire, (2) collection of an unstimulated

whole saliva sample for quantitation of haemoglobin levels using enzyme-linked immunosorbent assay (ELISA) and assessment of a cluster of inflammatory protein biomarkers by Cytokine ELISA Plate Arrays and MILLIPLEX immunoassays, (3) the oral rinse aMMP-8 POCT, (4) the GBoB test with detection of salivary haemoglobin levels in the TPS using ultraviolet-visible spectroscopy and a high-sensitivity ELISA, and (5) full-mouth periodontal and radiographic examinations by two well-calibrated examiners. Periodontal diagnosis was then made following the current classification. ^{12,13} Oral samples were stored at -70°C for further assessment.

All questionnaire responses were dichotomised; missing or unanswered items were excluded from analysis. Periodontal conditions categorised as periodontal health, gingivitis, stages I/II periodontitis, and stages III/IV (severe) periodontitis.¹³ Inter-group differences compared using the Chi-squared test or Fisher's exact test. Univariate associations were examined using binary logistic regression. Logistic regression models were then constructed for identifying periodontal diseases (gingivitis and periodontitis), periodontitis, stages I/II periodontitis, and stages III/IV periodontitis. Variables with P values ≥0.20 were selected for the multivariable models. The backward stepwise selection method was used, and the area under the receiver operating characteristic curve (AUROC), sensitivity, and specificity were calculated. Model 1 included each question from the modified CDC-AAP questionnaire, whereas model 2 consisted of demographic/lifestyle variables (eg, age, sex, tobacco smoking, and diabetes). Model 3 was constructed by integrating models 1 and 2. These models were validated by the algorithms in the development cohort, then used to identify periodontitis and severe periodontitis in the external validation cohort. Discriminative power was evaluated using AUROC, sensitivity, specificity, and positive and negative predictive values.

Results

In the development cohort, 408 individuals (189 men and 219 women) aged 18 to 86 (mean±standard deviation, 41±18) years were included. Of these, 7.8% were current smokers. Overall, 68.6% had periodontitis (15.9% stage I, 15.9% stage II, 29.7% stage III, and 7.1% stage IV), whereas the remaining 31.4% had no periodontitis (16.2% periodontal health and 15.2% gingivitis). The questionnaire exhibited moderate-to-high accuracy for detecting periodontal diseases (gingivitis and periodontitis), periodontitis, and stages III/IV periodontitis, with AUROC of 0.837, 0.803, and 0.870, respectively. Model 3, incorporating the self-reported CDC-AAP questionnaire and demographic/ lifestyle variables, exhibited the highest accuracy

for detecting periodontitis, particularly severe periodontitis (AUROC=0.953, sensitivity=95.7%, and specificity=89.0%).

The results of the aMMP-8 POCT were correlated with periodontal parameters and periodontitis after adjustment for confounders, with 33.2% sensitivity and 93.0% specificity for periodontitis detection (threshold: >10 ng/mL). However, the aMMP-8 POCT was less effective at differentiating among stages of periodontitis or distinguishing periodontal health from gingivitis. The aMMP-8 level adjusted by the number of teeth present improved periodontitis detection, yielding 67.1% sensitivity and 68.8% specificity. It predicted stage IV periodontitis at a threshold of 0.4312 ng/mL (AUROC=0.856, sensitivity=89.7%, and specificity=73.6%). Further integration with age and tobacco smoking enhanced diagnostic performance (AUROC=0.883, sensitivity=82.5%, and specificity=84.4%).

Of the 408 participants, 37.1% reported having GBoB; they exhibited more severe gingival inflammation than those without GBoB (median % of bleeding on probing: 25.0% vs 13.5%; P<0.001). Selfreported GBoB enhanced diagnostic performance for gingival inflammation and periodontal diseases (odds ratios=3-8), but it exhibited relatively low sensitivity for discriminating gingivitis from periodontitis. The haemoglobin level in TPS was positively correlated with the number of bleeding sites (r=0.409 for concentration, r=0.520 for total amount; P<0.001) and the number of periodontal pockets; the strongest correlations were observed with the number of bleeding pockets ≥6 mm (r=0.538, P<0.001), as well as the total amount of haemoglobin and number of bleeding sites (r=0.520, P<0.001). Participants who self-reported having GBoB exhibited higher haemoglobin levels than those without GBoB (205.69 μ g/mL vs 62.98 μ g/mL). A concentration of 90.58 μg/mL of haemoglobin or 0.51 µL of blood volume enabled visual detection of GBoB (AUROC=0.848). Moreover, haemoglobin levels were significantly higher in patients with gingivitis and periodontitis than in individuals with periodontal health. The absence of self-reported GBoB and low haemoglobin levels exhibited high predictive values (93%-98%) for periodontal health.

In the external validation cohort, 384 individuals (146 men and 238 women) aged 18 to 84 (mean±standard deviation, 55.3±16.6) years were included; 89.1% were non-smokers. Of these, 6.3% were periodontally healthy, 19.3% had gingivitis, and 74.4% had periodontitis (4.2% stage I, 21.7% stage II, 59.1% stage III, and 15.0% stage IV). The severity of periodontal diseases significantly increased with age and the prevalences of cardiovascular disease and diabetes.

Overall, there were significant differences in

multiple responses among groups with different periodontal conditions. Most periodontally healthy individuals reported that they had no gum disease and frequently used dental floss. An increased number of individuals experienced chewing difficulty with the onset and progression of gum disease from periodontal health to gingivitis and severe periodontitis. Some questions aimed at identifying periodontal diseases and periodontitis were validated in the external validation cohort, which is representative of the Hong Kong community. The proposed questionnaire-based algorithm for predicting periodontitis achieved higher accuracy in the external validation cohort than in the development cohort.

Increased accuracy was observed for the oral rinse aMMP-8 POCT alone in differentiating among stages of periodontitis. Considering the two thresholds of the aMMP-8 test (10 ng/mL and 20 ng/mL), the external validation data were consistent with the development data. The ratio of aMMP-8 level to the number of teeth present was useful for identifying the patients with severe periodontitis. The aMMP-8 test could differentiate the most susceptible patients at high risk of periodontitis from those at low to moderate risk. Moreover, this test could differentiate localised from generalised form of periodontitis. Integration of demographic/lifestyle factors with the aMMP-8 POCT demonstrated improved diagnostic performance.

The haemoglobin levels in TPS from patients generalised severe periodontitis were significantly higher than those from individuals with localised gingivitis and generalised stages I/II periodontitis. Overall, haemoglobin level was more effective in predicting generalised stage III/IV periodontitis than other stages or extents of periodontitis. Moreover, detectable haemoglobin was present in unstimulated saliva samples mainly from patients with generalised severe periodontitis. Patients with severe periodontitis had significantly increased levels of several salivary biomarkers (eg, adipose metabolism factors). Collectively, these findings highlighted the potential utility of biomarkers in unstimulated saliva and haemoglobin in TPS for assessing periodontal inflammation and disease progression.

Discussion

In the development cohort, the self-reported CDC-AAP questionnaire was useful for detecting periodontitis; combining this questionnaire with demographic/lifestyle variables (eg, smoking) could further enhance the identification of patients with severe periodontitis. The aMMP-8 POCT was also useful for screening to identify periodontitis, particularly when combined with demographic/lifestyle variables such as smoking. Self-reported

GBoB, which can be visually detected after minor blood loss, could serve as a sentinel sign of periodontal diseases, particularly in the presence of gingival inflammation. It may be useful for proactively promoting disease prevention and timely oral/periodontal healthcare.

In the external validation cohort, the modified CDC-AAP questionnaire was useful for identifying periodontitis. It validated several questions for selfdetection of periodontal diseases and periodontitis, such as self-perception of gum disease and selfreported loose teeth. These findings could contribute to public education regarding oral/periodontal health, proactive prevention of periodontal diseases, and the promotion of oral healthcare in clinical practice. The aMMP-8 POCT enabled identifying individuals with and without periodontitis. Its integration with individual and lifestyle profiles further enhanced diagnostic performance in clinical settings. The advanced assays involving the featured panels of biomarkers showed significantly increased levels of certain adipose metabolism-related and ageing-related factors, as well as inflammatory cytokines, in unstimulated saliva from patients with severe periodontitis, compared with individuals without periodontitis. These salivary biomarkers may be useful for evaluating periodontal status and tracking disease progression.

Conclusion

The multi-faceted and integrated approaches of self-reported questionnaires and tests as well as oral fluid-based diagnostic biomarkers may facilitate preventive oral/periodontal healthcare and clinical interventions.

Funding

This study was supported by the Health and Medical Research Fund, Health Bureau, Hong Kong SAR Government (#07182796). The full report is available from the Health and Medical Research Fund website (https://rfs2.healthbureau.gov.hk).

Disclosure

The results of this research have been previously published in:

- 1. Deng K, Pelekos G, Jin L, Tonetti M. Diagnostic accuracy of self-reported measures of periodontal disease: a clinical validation study using the 2017 case definitions. J Clin Periodontol 2021;48:1037-50. 2. Deng K, Pelekos G, Jin L, Tonetti M. Diagnostic accuracy of a point-of-care aMMP-8 test in the discrimination of periodontal health and disease. J
- 3. Deng K, Pelekos G, Jin L, Tonetti M. Authors' response: "Diagnostic accuracy of a point-of-care aMMP-8 test in the discrimination of periodontal

Clin Periodontol 2021;48:1051-65.

health and disease". J Clin Periodontol 2021;48:1499-500.

- 4. Deng K, Pelekos G, Jin L, Tonetti MS. Gingival bleeding on brushing as a sentinel sign of gingival inflammation: a diagnostic accuracy trial for the discrimination of periodontal health and disease. J Clin Periodontol 2021;48:1537-48.
- 5. Li Y, Kung JCK, Shi JY, et al. Diagnostic accuracy of a point-of-care aMMP-8 test for discriminating periodontal health status in adults: validation trials and updated meta-analysis. J Clin Periodontol 2025;52:510-29.

Acknowledgements

We thank Dr Ke Deng, Dr Lut Ting Lam, Dr Choi Ka Kung, Dr Tianfan Cheng, and Ms Tingting Lin for their contributions.

- 1. Guinness World Records. New York: Mint Publishers; 2001: 175.
- Tonetti M, Kornman KS. Periodontitis and systemic diseases – proceedings of a workshop jointly held by the European Federation of Periodontology and American Academy of Periodontology. J Clin Periodontol 2013;40:S1-S209.
- Hajishengallis G, Chavakis T. Local and systemic mechanisms linking periodontal disease and inflammatory comorbidities. Nat Rev Immunol 2021;21:426-40.
- Zhao D, Zhen Z, Pelekos G, Yiu KH, Jin L. Periodontal disease increases the risk for onset of systemic comorbidities in dental hospital attendees: an 18-year retrospective cohort study. J Periodontol 2019;90:225-33.
- 5. Zhao D, Wu MZ, Yu SY, Pelekos G, Yiu KH, Jin LJ.

- Periodontitis links concurrent systemic comorbidities among 'self-perceived health' individuals. J Periodont Res 2022;57:632-43.
- Deng K, Pelekos G, Jin LJ, Tonetti MS. Gingival bleeding on brushing as a sentinel sign of gingival inflammation: a diagnostic accuracy trial for the discrimination of periodontal health and disease. J Clin Periodontol 2021;48:1537-48.
- Deng K, Pelekos G, Jin L, Tonetti MS. Diagnostic accuracy of a point-of-care aMMP-8 test in the discrimination of periodontal health and disease. J Clin Periodontol 2021:48:1051-65
- Sorsa T, Mäntylä P, Rönkä H, et al. Scientific basis of a matrix metalloproteinase-8 specific chair-side test for monitoring periodontal and peri-implant health and disease. Ann N Y Acad Sci 1999;878:130-40.
- Lorenz K, Keller T, Noack B, Freitag A, Netuschil L, Hoffmann T. Evaluation of a novel point-of-care test for active matrix metalloproteinase-8: agreement between qualitative and quantitative measurements and relation to periodontal inflammation. J Periodont Res 2017;52:277-84.
- Eke PI, Dye BA, Wei L, et al. Self-reported measures for surveillance of periodontitis. J Dent Res 2013;92:1041-7.
- Deng K, Pelekos G, Jin L, Tonetti MS. Diagnostic accuracy of self-reported measures of periodontal disease: a clinical validation study using the 2017 case definitions. J Clin Periodontol 2021;48:1037-50.
- Caton JG, Armitage G, Berglundh T, et al. A new classification scheme for periodontal and peri-implant diseases and conditions: introduction and key changes from the 1999 classification. J Clin Periodontol 2018;45(Suppl 20):S1-S8
- Tonetti M, Greenwell H, Kornman KS. Staging and grading of periodontitis: framework and proposal of a new classification and case definition. J Clin Periodontol 2018;45(Suppl 20):S149-S161.

Dance injury and prevention strategies in recreational dancers: abridged secondary publication

AYL Wong *, PSH Yung, D Samartzis, DKC Chan, B Surgenor, C Hiller, C Chan, V Schoeb, D Harbutt

KEY MESSAGES

- 1. Among 1465 dancers, the risk of dance injuries was almost doubled in professional dancers compared with amateur dancers.
- 2. Among 704 teenage dancers, the three most common sites of dance-related injuries were the knee (14.9%), ankle (14.8%), and lower back (10.4%).
- 3. Among teenage recreational dancers, scoliosis was an independent risk factor associated with a higher 12-month prevalence of injuries to the lower back 2 Department of Orthopaedics and Traumatology, The Chinese University (odds ratio=2.7) or knee (odds ratio=2.6).
- 4. Teenage dancers and their parents perceived that dance training increases the risk of dance injuries; dance injuries can cause negative emotions in teenage dancers; and some dancers may ignore injuries and delay post-injury healthcare seeking.
- 5. Both teenage dancers and their parents considered that dance instructors are the first person to provide opinions regarding dance injury management.
- 6. Both online and face-to-face workshops for dance

instructors can improve dance injury prevention knowledge among both instructors and students.

Hong Kong Med J 2025;31(Suppl 7):S36-7 HMRF project number: 01170248

¹ AYL Wong, ² PSH Yung, ³ D Samartzis, ⁴ DKC Chan, ⁵ B Surgenor, ⁶ C Hiller, ⁷ C Chan, ⁸ V Schoeb, ⁹ D Harbutt

- ¹ Department of Rehabilitation Sciences, The Hong Kong Polytechnic University, Hong Kong SAR, China
- of Hong Kong, Hong Kong SAR, China
- Department of Orthopedic Surgery, Rush University Medical Center, Australia
- Department of Early Childhood Education, The Education University of Hong Kong, Hong Kong SAR, China
- ⁵ Victorian College of the Arts, University of Melbourne, Australia
- ⁶ Faculty of Medicine and Health, The University of Sydney, Australia
- Department of Health Sciences, Macquarie University, Australia
- School of Health Sciences, University of Applied Sciences and Arts Western Switzerland, Switzerland
- ⁹ Educational Development Centre, The Hong Kong Polytechnic University, Hong Kong SAR, China
- * Principal applicant and corresponding arnold.wong@polyu.edu.hk

Introduction

Recreational dance is a popular activity among teenagers and young people.1 Dance can impose different levels of physical load/stress on various body parts. For example, jazz and breakdance involve many rapid and explosive movements, whereas ballet and Chinese dance involve more repetitive end-of-range movements. Recreational dancers may not have sufficient knowledge to reduce their risks of dance injuries. An epidemiological study revealed that the rates of dance injury among young dancers are similar to those of young gymnasts.2 Therefore, it is necessary to identify high-risk dancers and adopt effective dance injury prevention strategies. This study aimed to determine the 12-month prevalence of dance injury among recreational dancers in Hong Kong; to explore perceptions, attitudes, and beliefs towards dance injury prevention among dance students, their parents, and dance instructors; and to evaluate the effectiveness of dance injury prevention programmes for dance instructors.

Methods

This epidemiological study was conducted via

online and face-to-face platforms to evaluate the prevalence of dance injury in amateur dancers. A dance injury questionnaire was developed by a panel of multidisciplinary experts in epidemiology, orthopaedics, physiotherapy, exercise science, and dance science. The questionnaire was then distributed to members of the Hong Kong Dance Federation, the Hong Kong Dance Alliance, and students involved in the Schools Dance Festival.

Focus groups and semi-structured interviews were conducted to solicit opinions from adolescent dancers, their parents, and dance instructors regarding dance injury and its prevention.

To evaluate the effectiveness of dance injury prevention programmes, 58 dance instructors were randomly assigned to one of three groups: a 1-day, six-module face-to-face SafeDanceTraining workshop (n=19), self-learning of SafeDanceTraining by watching videos and reading materials on an online platform (n=19), or no intervention until completion of the 6-month follow-up (n=20). All dance instructors were required to recruit eight to 10 students who were followed up for 6 months. Both instructors and students were asked to complete a monthly questionnaire regarding dance injuries.

Results

In total, 1465 dancers completed the questionnaire, and 42% of them reported dance-related injuries. Professional dancers reported an average of 4.4 injuries per year, whereas amateur dancers reported an average of 2.6 injuries per year. In the last 12 months, the three most common injury sites were the knee (16.4%), ankle (15.6%), and lower back (13.3%). A higher prevalence of lower back or knee dance-related injuries was associated with dance instructors (odds ratio [OR]=2.5), a history of previous injuries (OR=2.3), pre-professional dancers (OR=2.2), professional dancers (OR=2.1), and scoliosis (OR=1.9).

Among 704 teenage dancers, the most common injury sites in the last 12 months were the knee (14.9%), ankle (14.8%), and lower back (10.4%). A higher prevalence of lower back or knee injury was associated with scoliosis (OR=2.6-2.7) and older age (OR=2-3). Among 175 children and 118 young Chinese dance practitioners, the 12-month prevalence of dance injury was higher among youth aged 15 to 24 years than among children aged 10 to 14 years (52.5% vs 19.6%; 6.5 vs 4.6 injuries per 1000 dance hours). The most common injury sites in the respective groups were the knee (15.3% vs 7.4%), lower back (9.5% vs 4.6%), and ankle (16.9% vs 5.1%). Each additional year of age was associated with a 1.2to 1.3-fold greater likelihood of sustaining dancerelated injuries to the upper back, lower back, and pelvis/buttocks. Taller Chinese dance practitioners had a higher risk of lower limb injury.

Additionally, 33 teenage dance students, eight parents, and eight dance instructors participated in the focus group interviews. Approximately 90% of the student dancers had a history of dance injury. More dance injuries were associated with dance training; dance injuries caused negative emotions; post-injury healthcare-seeking behaviour was influenced by several factors (eg, the 'no pain, no gain' misconception); there were no recommended pathways to follow after a dance injury; and dancers relied on self-perceived effective injury prevention or management methods. Interviews with dance instructors revealed five themes: insufficient knowledge regarding dance injury prevention, tight class schedules affecting injury prevention, strict dance examination criteria causing students to practise repetitive movements, their own history of dance injuries, and the use of specific teaching methods to prevent dance injury.

In total, 58 dance instructors recruited 440 students. However, only 38 instructors and 291 students completed the 6-month follow-up due to the COVID-19 pandemic. Dance instructors showed significant improvements in average dance injury prevention knowledge immediately after completing the face-to-face or online workshop (by 46.8% to 46.9%). This knowledge was retained at the 6-month follow-up. Similarly, dance students in the face-to-face or online workshop group demonstrated significant improvements in dance injury prevention

knowledge at the 6-month follow-up (by 37.7% to 39.7%). Individuals who received no intervention did not show significant improvements in dance injury prevention knowledge. Nonetheless, all three groups showed a significant reduction in dance injury rates among instructors and students at the 6-month follow-up, partly due to less frequent dance practice during the COVID-19 pandemic.

Discussion

The findings of this study were shared with the public during SMART Fun Day 2019 and 2021. A 1-day symposium (DanceMed 2021) was held to educate healthcare professionals, physiotherapy students, and the public about the prevalence of dance injury, common conservative and surgical management approaches, and preventive methods. Free physical assessments and health consultations were provided for recreational dancers. Pamphlets were distributed to attendees at the symposium and to 30 dance schools.

Dance instructors were able to enhance their dance injury prevention knowledge through face-to-face or online workshop, which in turn improved their students' knowledge and awareness regarding safe dance practice. However, intervention effectiveness remains uncertain due to the high attrition rates of instructors and students during the COVID-19 pandemic. Further large-scale studies should be conducted to validate our findings. This project has laid the foundation for further promotion of safe dance practice in Hong Kong. The Hong Kong Association of Dance Medicine and Science will organise similar *SafeDanceTraining* workshops in the future.

Funding

This study was supported by the Health and Medical Research Fund, Health Bureau, Hong Kong SAR Government (#01170248). The full report is available from the Health and Medical Research Fund website (https://rfs2.healthbureau.gov.hk).

Disclosure

The results of this research have been previously published in:

1. Wong AYL, Chan C, Hiller C, et al. Is scoliosis associated with dance injury in young recreational dancers? A large-scale cross-sectional epidemiological study. J Dance Med Sci 2022;26:41-9.
2. Hung RKH, Yung PSH, Ling SKK, et al. Prevalence of dance-related injury and associated risk factors among children and young Chinese dance practitioners. Medicine (Baltimore) 2023;102:e36052.

- Cahalan R, Bargary N, O'Sullivan K. Pain and injury in elite adolescent Irish dancers: a cross-sectional study. J Dance Med Sci 2018;22:91-9.
- 2. O'Kane JW, Levy MR, Pietila KE, Caine DJ, Schiff MA. Survey of injuries in Seattle area levels 4 to 10 female club gymnasts. Clin J Sport Med 2011;21:486-92.

Prostate Health Index for risk stratification before magnetic resonance imaging: abridged secondary publication

PKF Chiu *, WCW Chu, CMC Cho, YCJ Teoh, CF Ng

KEY MESSAGES

- 1. The use of multiparametric magnetic resonance imaging (MRI) and the Prostate Health Index (PHI) can improve risk stratification for men with elevated prostate-specific antigen levels.
- 2. Selectively avoiding MRI in men with lower PHI scores can reduce costs and unnecessary biopsies, while ensuring timely diagnosis of clinically significant prostate cancer.
- 3. Risk stratification based on PHI can optimise allocation of limited MRI resources and improve the efficiency of prostate cancer screening and

early detection.

Hong Kong Med J 2025;31(Suppl 7):S38-40

HMRF project number: 08191476

- ¹ PKF Chiu, ² WCW Chu, ² CMC Cho, ¹ YCJ Teoh, ¹ CF Ng
- Department of Surgery, The Chinese University of Hong Kong, Hong Kong SAR, China
- ² Department of Imaging and Interventional Radiology, The Chinese University of Hong Kong, Hong Kong SAR, China
- * Principal applicant and corresponding author: peterchiu@surgery.cuhk.edu.hk

Introduction

In Hong Kong public hospitals, the waiting time for magnetic resonance imaging (MRI) in patients with elevated prostate-specific antigen (PSA) levels can exceed 1 year. It is therefore important to allocate MRI resources to patients at higher risk of prostate cancer. The Prostate Health Index (PHI) has been shown to predict clinically significant prostate cancer in patients with a score of 3 or 4 in the Prostate Imaging Reporting and Data System (PI-RADS), but the role of PHI in predicting abnormal prostate MRI results is not well described.

Prostate cancer is the second most common cancer in men globally,¹ and its incidence is rapidly increasing in Asia, particularly in Hong Kong.² Diagnosis typically involves a prostate biopsy for those with high PSA levels, but this can lead to unnecessary biopsies and over-diagnosis.³ In Hong Kong, blood testing for PHI is commonly used to assess those with high PSA levels.³

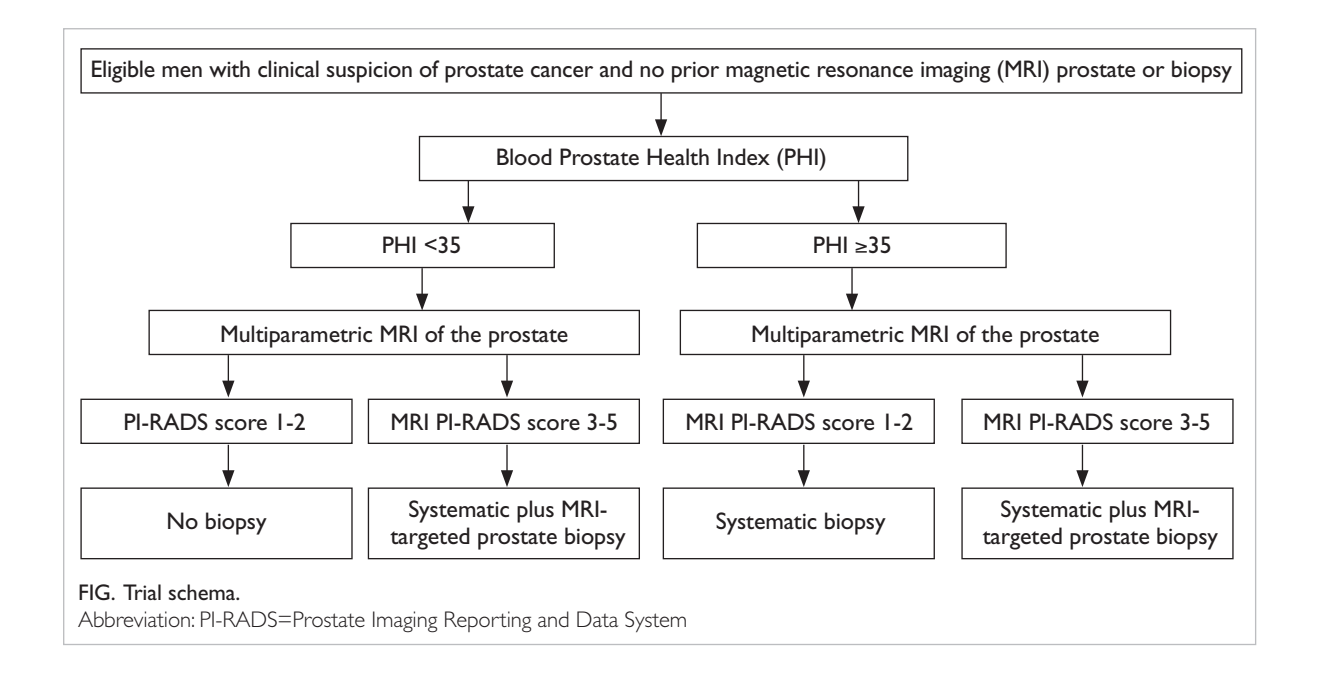
Multiparametric MRI can improve detection of clinically significant prostate cancer. It can guide targeted biopsies and reduce unnecessary ones, as demonstrated by the PROMIS and PRECISION trials. European guidelines recommend MRI before considering a biopsy for those with high PSA levels. However, access to MRI is limited in Hong Kong public hospitals. Thus, it is important to focus resources on patients at higher risk. The role of PHI in predicting abnormal MRI results remains unclear. This study aimed to optimise allocation of MRI resources based on risk stratification in a cohort of Chinese men.

Methods

Consecutive Chinese men aged ≥18 years with PSA levels of 4 to 10 ng/mL, normal prostate findings on digital rectal examination, and a record of blood testing for the PHI were prospectively recruited from Prince of Wales Hospital and North District Hospital, Hong Kong. Participants underwent contrast-enhanced multiparametric MRI of the prostate; results were reported according to PI-RADS v2.1 criteria and scored from 1 to 5. The proportions of abnormal MRI results (PI-RADS 3-5) were compared among PHI ranges. Systematic and MRI-guided biopsies were offered to participants with PHI ≥35; for those with PHI <35, biopsies were offered only if MRI findings were abnormal (Fig)

The proportions of abnormal MRI results were analysed across PHI ranges. Various PHI cut-offs were evaluated for their association with PI-RADS scores of ≥ 3 or ≥ 4 and for the detection of any clinically significant prostate cancer (International Society of Urological Pathology [ISUP] grade ≥ 2 or Gleason score ≥ 7) on prostate biopsy.

Assuming that two-thirds of eligible patients would have PHI <35, and that abnormal MRI results would be observed in 15% of those with PHI <35 and 40% of those with PHI \geq 35, a total of 143 men (95 with PHI <35 and 48 with PHI \geq 35) were required to achieve 90% power and a 5% type I error. A sample size of 159 was targeted to account for an anticipated 10% withdrawal rate. All tests were two-sided; statistical significance was set at 0.05.



Results

In total, 159 men with elevated PSA levels (4-10 ng/mL) were recruited and underwent blood testing for PHI. Six (3.8%) men withdrew from the study before undergoing MRI. Of the 153 patients who completed prostate MRI, 55 had PHI \geq 35 or MRI PI-RADS \geq 3 and underwent prostate biopsy, except for one who declined. Among the 54 men who underwent biopsy, the median age was 69.0 (interquartile range [IQR], 64-73) years, the median PSA level was 5.7 (IQR, 4.8-7.0) ng/mL, the median PHI was 26.3 (IQR, 21.8-31.5), and the median prostate volume was 58.0 (IQR, 42.0-75.5) mL.

MRI findings of PI-RADS \geq 3 were observed in 21.6% (27/125) of men with PHI <35 and 50.0% (14/28) of men with PHI \geq 35 (P=0.002). MRI findings of PI-RADS \geq 4 were observed in 9.6% (12/125) of men with PHI <35 and 35.7% (10/28) of men with PHI \geq 35 (P<0.001) [Tables 1 and 2].

In terms of clinically significant prostate cancer detection, ISUP grade ≥ 2 prostate cancer was diagnosed in 6.4% (8/125) and 46.4% (13/28) of men with PHI <35 and PHI ≥ 35 , respectively (P<0.001). ISUP grade ≥ 3 prostate cancer was diagnosed in 1.6% (2/125) and 25.0% (7/28) of men with PHI <35 and PHI ≥ 35 , respectively (P<0.001). There was a sharp increase in ISUP grade ≥ 2 among those with PHI 30 to 34.9 (18.8%), compared with PHI <30 (4.6%) [Tables 1 and 2].

Among the 54 men who underwent biopsy, 11 (20.4%) experienced biopsy-related adverse events, including seven cases of haematuria, one case of haematospermia, one case of acute urinary retention (which occurred before biopsy), and two cases of post-biopsy urinary tract infection. The latter three events were categorised as severe adverse events.

Discussion

The PHI can be used to identify patients at higher risk of prostate cancer who require prostate MRI. This approach could prevent unnecessary MRI examinations and biopsies, conserving resources and reducing patient anxiety. Men with a PHI score ≥35 had a higher risk of prostate cancer, whereas men with a PHI score <25 had significantly lower rates of abnormal MRI results and prostate cancer. By omitting MRI in men with PHI scores <25, the number of MRI examinations could be reduced by 44.4% to 81.7%. However, men with PHI scores of 30 to 34.9 had a substantially higher risk of prostate cancer than those with scores <30. Thus, a PHI score of 30 may be a more appropriate threshold for determining the need for MRI.

The benefit of additional MRI was mainly observed among men with PSA levels of 4.0 to

TABLE I. Proportions of patients with abnormal Prostate Health Index (PHI) in terms of various Prostate Imaging Reporting and Data System (PI-RADS) scores and International Society of Urological Pathology (ISUP) grades.

Baseline PHI No. (%) of patients (n=153)				(n=153)	
	PI-RADS ≥3	PI-RADS ≥4	Prostate cancer	ISUP grade ≥2 prostate cancer	ISUP grade ≥3 prostate cancer
<25.0 (n=68)	15 (22.1)	8 (11.8)	9 (13.2)	4 (5.9)	0
25.0-29.9 (n=41)	8 (19.5)	2 (4.9)	2 (4.9)	1 (2.4)	1 (2.4)
30.0-34.9 (n=16)	4 (25.0)	2 (12.5)	3 (18.8)	3 (18.8)	1 (6.3)
35.0-44.9 (n=15)	7 (46.7)	5 (33.3)	6 (40.0)	5 (33.3)	4 (26.7)
45.0-54.9 (n=7)	3 (42.9)	1 (14.3)	4 (57.1)	2 (28.6)	0
≥55.0 (n=6)	4 (66.7)	4 (66.7)	6 (100)	6 (100)	3 (50.0)

TABLE 2. Stratification of patients with abnormal Prostate Health Index (PHI) using various PHI cut-offs, compared with various Prostate Imaging Reporting and Data System (PI-RADS) scores and International Society of Urological Pathology (ISUP) grades (n=153).

Stratification	PHI cutoff		P value	PHI cutoff		P value	PHI cutoff		P value
	<35 (n=125)*	≥35 (n=28)*		<30 (n=109)*	≥30 (n=44)*	-	<25 (n=68)*	≥25 (n=85)*	-
PI-RADS ≥3	27 (21.6)	14 (50.0)	0.002	23 (21.1)	18 (40.9)	0.012	15 (22.1)	26 (30.6)	>0.05
PI-RADS ≥4	12 (9.6)	10 (35.7)	< 0.001	10 (9.2)	12 (27.3)	0.004	8 (11.8)	14 (16.5)	>0.05
Prostate cancer	14 (11.2)	16 (57.1)	<0.001	11 (10.1)	19 (43.2)	< 0.001	9 (13.2)	21 (24.7)	>0.05
ISUP grade ≥2 prostate cancer	8 (6.4)	13 (46.4)	< 0.001	5 (4.6)	15 (34.1)	< 0.001	4 (5.9)	17 (20.0)	0.032
ISUP grade ≥3 prostate cancer	2 (1.6)	7 (25.0)	<0.001	1 (0.9%)	8 (18.2)	< 0.001	0	9 (10.6)	0.004

Data are presented as No. (%) of patients.

10.0 ng/mL. The number of MRI examinations required to diagnose one additional case of ISUP grade ≥2 prostate cancer was 20 in men with PHI ≥35 and 94 in men with PHI <35. Among all men with PSA ≥4.0 ng/mL, 45.4% (89/196) avoided unnecessary biopsy through the combined use of PHI and MRI. A screening algorithm incorporating PSA, PHI, and MRI could effectively detect clinically significant prostate cancer while reducing unnecessary biopsies; the PHI served as an important step in risk stratification for prostate cancer screening.⁵

This study had some limitations, including a relatively small sample size and the fact that not all men with PHI <35 and negative MRI findings underwent prostate biopsy.

Conclusions

The PHI can serve as a routine biomarker to stratify the risk of abnormal MRI results and clinically significant prostate cancer in men with elevated PSA levels. Balancing MRI utilisation against the risk of missed diagnoses, MRI can be safely avoided in men with PHI <30.

Funding

This study was supported by the Health and Medical

Research Fund, Health Bureau, Hong Kong SAR Government (#08191476). The full report is available from the Health and Medical Research Fund website (https://rfs1.healthbureau.gov.hk).

Acknowledgements

We thank Ms Cindy Hong and Ms Angel Kong for their assistance with this project, and Dr Xiaobo Wu for help in preparing this report.

- Culp MB, Soerjomataram I, Efstathiou JA, Bray F, Jemal A. Recent global patterns in prostate cancer incidence and mortality rates. Eur Urol 2020;77:38-52.
- Hong Kong Cancer Registry. Accessed 5 August 2025. Available from: https://www3.ha.org.hk/cancereg/allagesresult.asp. 2021.
- Alberts AR, Roobol MJ, Verbeek JFM, et al. Prediction of high-grade prostate cancer following multiparametric magnetic resonance imaging: improving the Rotterdam European Randomized Study of Screening for Prostate Cancer risk calculators. Eur Urol 2019;75:310-8.
- Kasivisvanathan V, Rannikko AS, Borghi M, et al. MRItargeted or standard biopsy for prostate-cancer diagnosis. N Engl J Med 2018;378:1767-77.
- Chiu PK, Lam TY, Ng CF, et al. The combined role of MRI prostate and prostate health index in improving detection of significant prostate cancer in a screening population of Chinese men. Asian J Androl 2023;25:674-9.

Relationships among whole-body sagittal alignment, musculoskeletal parameters, body balance, and health-related quality of life in Hong Kong Chinese adults: abridged secondary publication

GCW Man *, Z Hu, WCW Chu, SW Law, WH Cheung, LCM Lau, PSH Yung, JCY Cheng

KEY MESSAGES

- 1. Health-related quality of life was correlated with all sagittal parameters, particularly sagittal vertical axis, T1 pelvic angle, KneeFlex angle, and AnkleFlex angle. Age was correlated with health-related quality of life and the Oswestry Disability Index.
- Compared with older adults aged ≥50 years, younger adults aged ≤50 years exhibited less deviation in sagittal alignment, including thoracic kyphosis, lumbar lordosis, pelvic incidence, pelvic tilt, sagittal vertical axis, and T1 pelvic angle.
- 3. Women had significantly lower muscle mass, muscle strength, and bone density than men.
- 4. The three-dimensional odontoid-hip axis angle

varied little between younger and older asymptomatic Chinese adults; standard deviations were 2.3° in the sagittal plane and 1.0° in the coronal plane.

Hong Kong Med J 2025;31(Suppl 7):S41-4

HMRF project number: 05190047

- ¹ GCW Man, ¹ Z Hu, ² WCW Chu, ¹ SW Law, ¹ WH Cheung, ³ LCM Lau, ¹ PSH Yung, ¹ JCY Cheng
- Department of Orthopaedics and Traumatology, The Chinese University of Hong Kong, Hong Kong SAR, China
- ² Department of Imaging and Interventional Radiology, The Chinese University of Hong Kong, Hong Kong SAR, China
- ³ Department of Orthopaedics and Traumatology, Prince of Wales Hospital, Hong Kong SAR, China
- * Principal applicant and corresponding author: geneman@cuhk.edu.hk

Introduction

In Hong Kong, 17% of the population is aged ≥ 65 years, and this percentage is projected to increase to 30% by 2050. The provision of preventive and high-quality care for the ageing population is essential to ensure self-reliance and quality of life and to alleviate the associated financial burden.

Skeletal muscles play a crucial role in sagittal alignment changes during ageing. Patients with lumbar degenerative kyphosis exhibit significantly smaller lumbar muscularity and a higher proportion of fat deposits. Alterations in muscle architecture and activity in lower limbs may lead to changes in upright stance. Lower-limb compensations, such as knee flexion, are key mechanisms for maintaining sagittal alignment.¹ Reduced muscularity and increased fatty degeneration increase the risk of proximal junctional kyphosis. Declining muscle mass and functional sarcopenia are closely linked to osteoporosis and fragility fractures in older adults.

In asymptomatic Chinese adults, thoracic kyphosis steadily increases, whereas lumbar lordosis gradually decreases. Pelvic tilt is greater in men than in women across all age groups, with a gradual age-related increase.² Men and women aged 20 to 60 years significantly differ in KneeFlex

and AnkleFlex angles, but these differences are not significant beyond 60 years of age. Ageing affects the compensation mechanism, leading to greater reliance on pelvis and lower limbs in older people.

This study aimed to identify relationships among whole-body sagittal alignment, muscle mass, muscle strength, body balance, and health-related quality of life, as well as bone density, bone quality, and bone strength parameters.

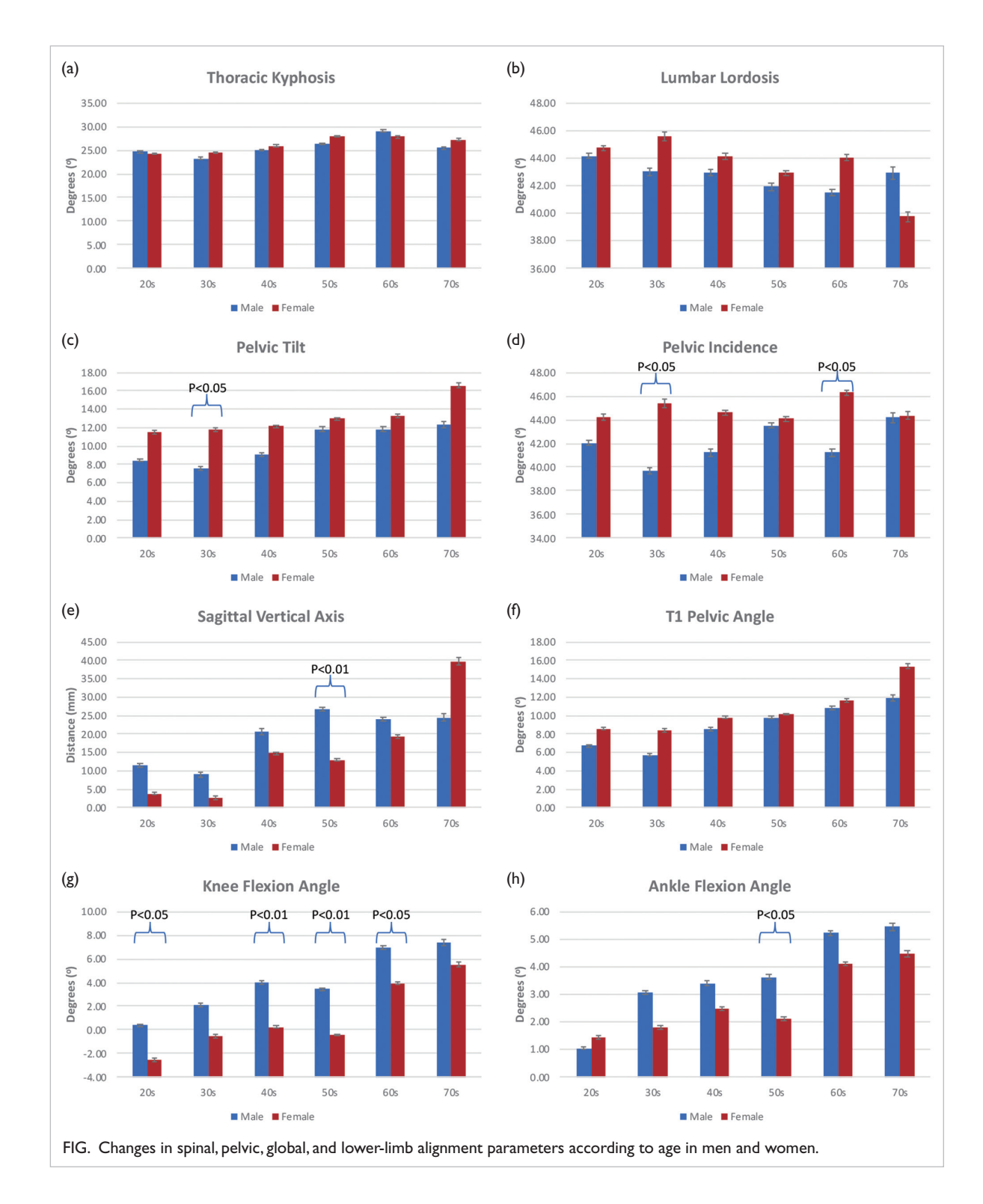
Methods

This was a prospective cross-sectional study. Chinese adults aged 20 to 79 years in Hong Kong were recruited for assessments of sagittal alignment. Whole-body, standing, head-to-toe biplanar low-dose EOS X-ray images (ATEC Spine; Carlsbad [CA], USA) were acquired. The three-dimensional (3D) angle formed by the vertical axis and the line between the odontoid and mid-interacetabular axis (OD-HA angle) was computed and projected onto the sagittal and coronal planes. Bone mineral density, muscle mass, and muscle strength were measured, along with the visual analogue scale score for pain, the Oswestry Disability Index, and the Short Form-36 score.

Results

In total, 467 participants were assessed. Health-related quality of life was correlated with all sagittal parameters, particularly the sagittal vertical axis, T1 pelvic angle, KneeFlex angle, and AnkleFlex angle (Fig). Age was correlated with health-related quality of life and the Oswestry Disability Index. Women

had lower muscle mass, muscle strength—including appendicular skeletal muscle mass (ASMM), ASMM index, and grip strength—and bone mineral density than men. Whole-body sagittal alignment was correlated with health-related quality of life, bone quality, muscle mass, and muscle strength; global spinal parameters exhibited the strongest correlations (Tables 1 and 2). The 3D OD-HA angle



remained quasi-invariant across age groups, varying little between younger and older asymptomatic Chinese adults; standard deviations were 2.5° in the sagittal plane and 1.1° in the coronal plane. These data provide a reference range for head-pelvis balance, which displayed the strongest correlation with musculoskeletal parameters.

Thoracic kyphosis was negatively correlated with grip strength, whereas pelvic incidence, pelvic tilt, and T1 pelvic angle were positively correlated with ASMM and grip strength. The sagittal vertical axis was positively correlated with ASMM index, whereas the KneeFlex angle was positively correlated with ASMM and ASMM index, and the AnkleFlex angle was positively correlated with ASMM index. The 3D OD-HA angle was positively correlated with ASMM, ASMM index, and grip strength; it exhibited stronger correlations with muscle mass and grip strength. Bone mineral densities in the areal femoral neck, areal lumbar spine, and total hip were significantly lower in women.

Discussion

Bone and muscle health play an essential role in maintaining postural balance. Women exhibited significantly lower muscle mass and muscle strength including ASMM, ASMM index, and grip strength. Women also had significantly higher body fat mass, consistent with findings that women are less muscular than men.³ In the Framingham Osteoporosis Study of 800 older adults, the mean 4-year bone losses at the hip, lumbar spine, and radius ranged from 0.2% to 3.6% in men and from 3.4% to 4.8% in women.⁴

Maintenance of global alignment preserves the alignment of all segments above the pelvis and provides optimal posture with minimal energy expenditure. Failure to maintain the centre of gravity within this 'conus of economy' can result in compensatory mechanisms to restore stable global alignment. We have proposed a new 3D index-the OD-HA angle-to quantify 3D headpelvis alignment, which appears quasi-invariant in both younger and older adults.5 The OD-HA angle confirms that the head tends to remain above the pelvis within a small cone of stability. This study provides a reference range for head-pelvis balance across different decades of age and sex. Our findings may facilitate future research concerning spinal deformities, spinopelvic alignment, and global alignment.

Funding

This study was supported by the Health and Medical Research Fund, Health Bureau, Hong Kong SAR Government (#05190047). The full report is available from the Health and Medical Research Fund website (https://rfs2.healthbureau.gov.hk).

remained quasi-invariant across age groups, varying TABLE I. Correlations between sagittal alignment and muscle parameters.

Parameter	Appendicular	Appendicular	Grip strength		
	skeletal skeletal muscle mass muscle mass index		Dominant	Non- dominant	
Thoracic kyphosis	-0.078	-0.045	-0.139*	-0.129*	
Lumbar lordosis	-0.039	-0.054	-0.044	-0.058	
Pelvic tilt	-0.158 [†]	-0.073	-0.190*	-0.177*	
Pelvic incidence	-0.110*	-0.055	-0.126*	-0.129*	
Sagittal vertical axis	0.085	0.164 [†]	0.012	0.040	
T1 pelvic angle	-0.129 [†]	-0.040	-0.158 [†]	-0.141 [†]	
KneeFlex angle	0.139 [†]	0.221†	0.074	0.077	
AnkleFlex angle	0.004	0.096*	-0.035	-0.032	
Odontoid-hip axis angle (sagittal)	0.191†	0.212 [†]	0.157 [†]	0.168 [†]	

^{*} P<0.05

TABLE 2. Correlations between sagittal alignment and bone parameters.

Parameter	Areal femoral neck bone mineral density	Total hip bone mineral density	Areal lumbar spine bone mineral density
Thoracic kyphosis	-0.118*	-0.106	-0.159 [†]
Lumbar lordosis	0.000	-0.027	-0.048
Pelvic tilt	-0.085	-0.073	0.054
Pelvic incidence	-0.049	-0.059	0.010
Sagittal vertical axis	0.011	0.050	0.071
T1 pelvic angle	-0.097	-0.074	0.050
KneeFlex angle	-0.126*	-0.066	0.009
AnkleFlex angle	-0.147*	-0.095	-0.003
Odontoid-hip axis (sagittal)	0.143*	0.212 [†]	0.147 [†]

^{*} P<0.05

Disclosure

The results of this research have been previously published in:

- 1. Ho JS, Ko KS, Law SW, Man GC. The effectiveness of robotic-assisted upper limb rehabilitation to improve upper limb function in patients with cervical spinal cord injuries: a systematic literature review. Front Neurol 2023;14:1126755.
- 2. Hu Z, Vergari C, Gajny L, et al. An analysis on the determinants of head to pelvic balance in a Chinese adult population. Quant Imaging Med Surg 2022;12:2311-20.
- 3. Chau LTC, Hu Z, Ko KSY, et al. Global sagittal alignment of the spine, pelvis, lower limb after vertebral compression fracture and its effect

P<00

[†] P<0.01

on quality of life. BMC Musculoskelet Disord 2021;22:476.

- 1. Zhu F, Bao H, Liu Z, et al. Unanticipated revision surgery in adult spinal deformity: an experience with 815 cases at one institution. Spine (Phila Pa 1976) 2014;39:B36-B44.
- 2. Hu Z, Man GCW, Yeung KH, et al. 2020 Young Investigator 5. Amabile C, Pillet H, Lafage V, Barrey C, Vital JM, Skalli W. Award Winner: Age- and sex-related normative value of whole-body sagittal alignment based on 584 asymptomatic Chinese adult population from age 20 to 89. Spine (Phila Pa
- 1976) 2020;45:79-87.
- 3. Janssen I, Heymsfield SB, Wang ZM, Ross R. Skeletal muscle mass and distribution in 468 men and women aged 18-88 yr. J Appl Physiol (1985) 2000;89:81-8.
- 4. Hannan MT, Felson DT, Dawson-Hughes B, et al. Risk factors for longitudinal bone loss in elderly men and women: the Framingham Osteoporosis Study. J Bone Miner Res 2000;15:710-20.
 - A new quasi-invariant parameter characterizing the postural alignment of young asymptomatic adults. Eur Spine J 2016;25:3666-74.

Registry for congenital upper limb anomalies in Prince of Wales Hospital, Hong Kong: abridged secondary publication

WH Cheung *, PC Ho, WL Tse, MCK Mak, JJSC Koo, JWC Ting, WW Chau, RMY Wong

KEY MESSAGES

- 1. As of July 2023, a total of 1891 records of congenital upper limb anomalies (CULAs) had been collected.
- 2. The first registry of CULAs in Hong Kong can be used for investigating the epidemiology of these anomalies, identifying risk factors, and improving healthcare planning and delivery.
- Existing data regarding general functional and aesthetic outcomes after surgical treatment provide valuable insights into immediate improvements.
- 4. Continued data collection, analysis, and collaboration among stakeholders will enhance our ability to prevent, diagnose, and manage CULAs.

Hong Kong Med J 2025;31(Suppl 7):S45-7

HMRF project number: 17180061

- ¹ WH Cheung, ² PC Ho, ² WL Tse, ² MCK Mak, ³ JJSC Koo, ⁴ JWC Ting, ¹ WW Chau, ¹ RMY Wong
- Department of Orthopaedics and Traumatology, The Chinese University of Hong Kong, Hong Kong SAR, China
- ² Department of Orthopaedics and Traumatology, Prince of Wales Hospital, Hong Kong SAR, China
- ³ Department of Orthopaedics and Traumatology, Alice Ho Miu Ling Nethersole Hospital, Hong Kong SAR, China
- Department of Surgery, Prince of Wales Hospital, Hong Kong SAR, China
- * Principal applicant and corresponding author: louischeung@cuhk.edu.hk

Introduction

Congenital upper limb anomalies physical significantly affect a child's psychological development. More than 100 CULAs have been classified,1 ranging from trigger thumb and simple accessory nubbins to complex syndactyly, hypoplastic thumb, multiple hereditary exostoses, constriction band syndrome, and duplicated thumbs. The incidence and prevalence of CULA conditions vary among ethnicities and geographical regions. We aimed to develop the first CULA registry in Hong Kong, based on patients presenting to Prince of Wales Hospital since 1984.

Methods

The registry was implemented in February 2020; data were collected both prospectively and retrospectively. Exclusion criteria were traumatic injuries or lesions not associated with CULA conditions, pre-existing CULA presented to the orthopaedic or hand clinic for non-CULA conditions, and CULAs lacking assessment or treatment at Prince of Wales Hospital.

Data collected included patient demographics, diagnosis, laterality of upper limb involvement, hand dominance, family history, associated non-upper limb anomalies, and occupational therapy assessment records, as well as radiographic findings, operations, and surgical treatment details. Patients were classified according to three systems: (1) the International Federation of Societies for Surgery of

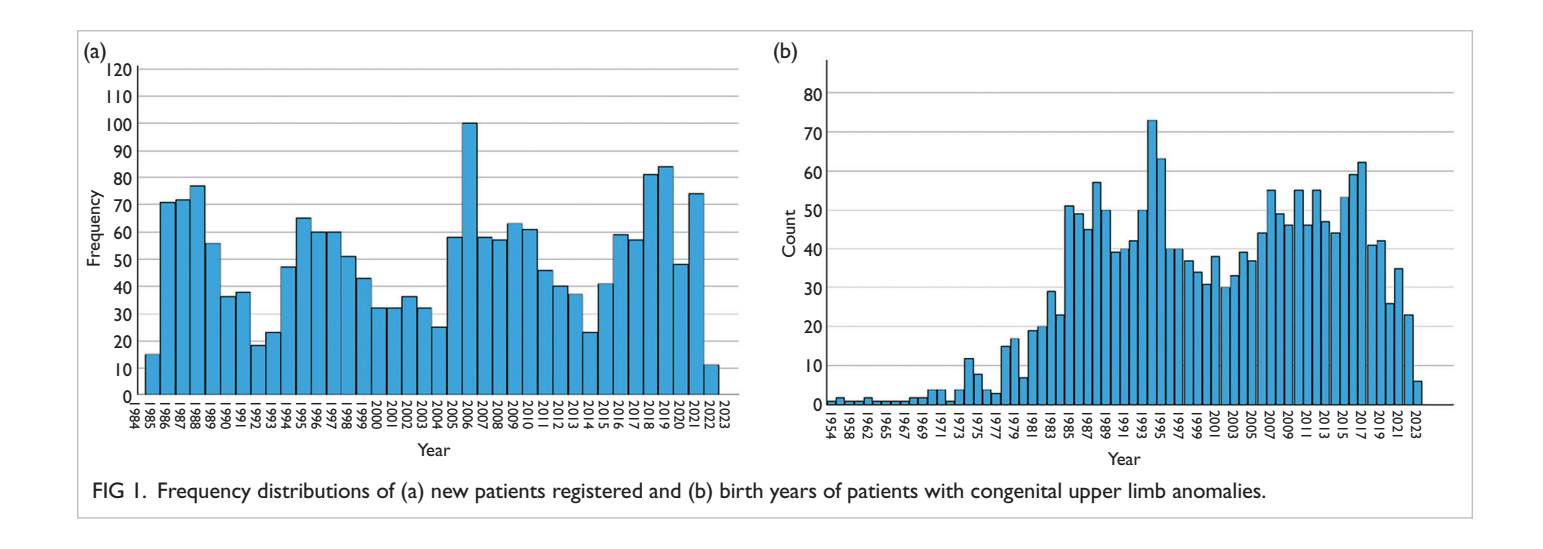
the Hand, (2) the Japanese Society for Surgery of the Hand, and (3) the Oberg, Manske, and Tonkin classification. The registry system was developed and maintained by a professional information technology service using MSSQL, .NET Core, and Vue.js.

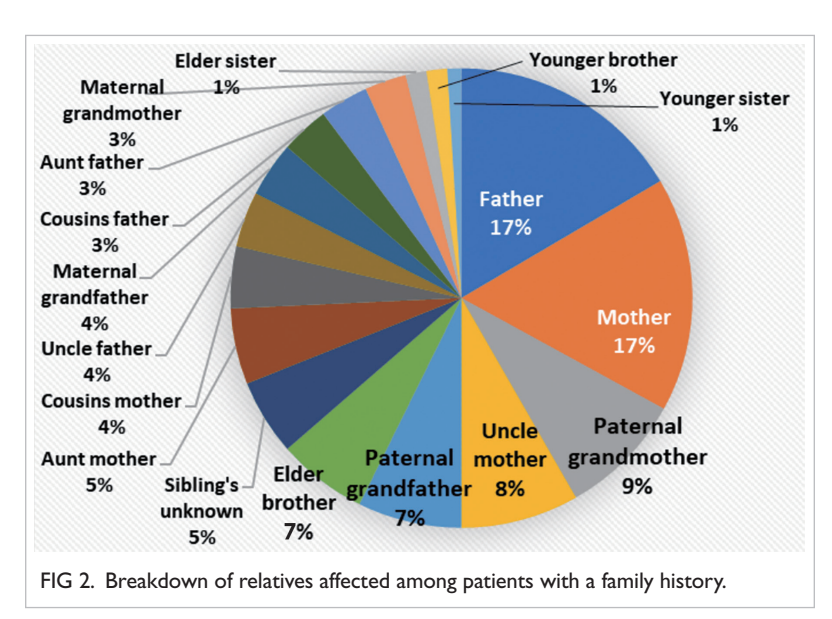
Results

As of June 2023, 2332 patients had presented to the CULA clinic. Of these, 1891 (81.1%) were congenital cases and thus included; the remaining 441 (18.9%) presented with injuries or lesions not associated with CULA (ie, non-congenital) and were thus excluded.

Of the 1891 CULA records, 1070 (56.6%) involved male patients and 821 (43.4%) involved female patients. The registry was designed to capture up to three upper limb anomalies per patient. Among these, 194 (10.3%) patients had two anomalies and 26 (1.4%) had three anomalies.

The highest number of new CULA patients presenting to the clinic was 100 in 2006, followed by 84 in 2019 and 81 in 2018 (Fig 1). The three most frequently documented birth years were 1994 (n=73), 1995 (n=63), and 2017 (n=62) [Fig 1]. The age at first visit was most frequently within the first 2 years of life; 1068 (56.5%) patients presented before 1 year of age, whereas 231 (12.2%) presented between 1 and 2 years of age. The mean±standard deviation age at first presentation was 4.5±6.8 (range, 0.1-60.1) years. At the last follow-up,





among 1522 patients, 117 (7.7%) were aged 0 to 1 year, 761 (50.0%) were aged 1 to 10 years, 466 (30.6%) were aged 10 to 20 years, and 178 (11.7%) were aged >20 years. The mean \pm standard deviation age was 9.5 \pm 8.8 (range, 0.1-61.35) years.

In total, 146 (7.7%) patients reported a family history of CULA, involving 212 affected relatives, including the father (17.0%, n=36), mother (16.5%, n=35), paternal grandmother (8.5%, n=18), uncle's mother (8.0%, n=17), and elder brother (6.6%, n=14) [Fig 2].

The three most common presentations were duplicated thumb (n=1128-1138), trigger thumb (n=456-511), and clasped thumb (n=212-213), depending on the classification system used. Among patients with a second anomaly, the most frequent conditions were clinodactyly (n=54-55), syndactyly (n=34-40), and hypoplastic thumb (n=13).

Discussion

We developed the first CULA registry in Hong Kong, based on patients who presented to the Prince of Wales Hospital between 1984 and 2023. As of June 2023, 1891 patients with CULA were included. Our registry spans almost 40 years, exceeding the 18-year duration of the New York Congenital Malformations Registry.² In comparison, a Korean registry included >10 000 patients aged >9 years,³ but data were recorded for only four CULA conditions. In contrast, our registry comprehensively documents all CULA conditions using three classification systems. Additionally, it includes multimedia records such as photographs, videos, and radiological images.

Although the mean age at first presentation was 4.6 years, almost half of the patients were examined within their first year of life. The birth years of patients peaked in 1994 and 1995 and then declined in 1999 and the following few years, as well as in more recent years. These trends may correspond to reductions in birth rates during the same periods in Hong Kong. The subsequent rise in presentations around 2008 may reflect an increase in birth rates associated with a higher number of pregnant women arriving from Mainland China, many of whom had little or no prenatal screening. There appears to be a steady incidence of congenital anomalies; no major events (eg, introduction of new teratogens) have been identified over the past four decades. There was also no evidence of increased referrals from other districts or across the border.

The three most common conditions were duplicated thumb, trigger thumb, and clasped thumb. Almost all patients with duplicated thumbs underwent early surgery. Many required additional procedures as they grew, owing to subsequent joint laxity, deformity, or stiffness. Patients with trigger or clasped thumbs underwent fewer operations but often required intensive allied health support,

including mobilisation exercises and splinting. The Disclosure health burden varied among patients.

Conclusion

The establishment of the first CULA registry in Hong Kong facilitates investigation of the epidemiology of these conditions, identification of risk factors, and healthcare planning and delivery. It also provides a foundation for future research, multidisciplinary collaboration, policy development, and patient empowerment.

Funding

This study was supported by the Health and Medical Research Fund, Health Bureau, Hong Kong SAR Government (#17180061). The full report is available from the Health and Medical Research Fund website (https://rfs1.healthbureau.gov.hk).

The results of this research have been previously published in:

1. An educational booklet titled Congenital Upper Limb Anomalies/Differences and website covering the major CULA is designed and distributed to the patients and their parents.

- 1. Swanson AB. A classification for congenital limb malformations. J Hand Surg Am 1976;1:8-22.
- 2. Goldfarb CA, Shaw N, Steffen JA, Wall LB. The prevalence of congenital hand and upper extremity anomalies based upon the New York Congenital Malformations Registry. J Pediatr Orthop 2017;37:144-8.
- Shin YH, Baek GH, Kim YJ, Kim MJ, Kim JK. Epidemiology of congenital upper limb anomalies in Korea: a nationwide population-based study. PLoS One 2021;16:e0248105.

AUTHOR INDEX

Abrigo J	22	Li TC	28
Chan AKY	18	Li WC	18
Chan C	36	Liu EM	18
Chan DKC	36	Liu XZ	18
Chan DTM	18	Lo IFM	13
Chan DYL	28	Loong HHF	18
Chan HLY	4	Mak MCK	45
Chan JYT	18	Malta TM	18
Chan K	25	Man GCW	41
Chan KCC	29	Mao Y	18
Chan NC	9	Mok VCT	22
Chau WW	45	Ng CF	38
Chen H	18	Ng HK	18
Chen LJ	9	Noushmehr H	18
Cheng JCY	41	Pang CP	9
Cheung WH	41, 45	Pelekos G	32
Chiu PKF	38	Poon MFM	18
Cho CMC	38	Poon WS	18
Chu WCW	38, 41	Samartzis D	36
Chung JPW	28	Schoeb V	36
Chung NYF	18	Shi L	22
Dong Z	13	Shi ZF	18
Gong B	9	Surgenor B	36
Harbutt D	36	Tan QX	4
Hiller C	36	Teoh YCJ	38
Ho DKL	32	Tham CC	9
Ho PC	45	Ting JWC	45
Hu Z	41	Tonetti M	32
Huang C	9	Tse WL	45
Huang QJQ	18	Tse YK	4
Jin LJ	32	Wang CC	28
Joynt G	25	Wang WW	18
КоН	22	Wong AYL	36
Koo JJSC	45	Wong EWM	25
Kwan JSH	18	Wong GLH	4
Kwok KL	29	Wong RMY	45
Kwok YKY	13	Wong VWS	4
Lam BYK	22	Yam JC	9
Lau LCM	41	Yang Z	9
Law SW	41	Yip TCF	4
Lee ATC	22	Yuen PC	4
Lee TL	28	Yung PSH	36, 41
Leung TY	13	Zhang M	9
Li AM	29	Zhang ZY	18
Li KKW	18	<i>U</i> =	

Disclaimer

The reports contained in this publication are for reference only and should not be regarded as a substitute for professional advice. The Government shall not be liable for any loss or damage, howsoever caused, arising from any information contained in these reports. The Government shall not be liable for any inaccuracies, incompleteness, omissions, mistakes or errors in these reports, or for any loss or damage arising from information presented herein. The opinions, findings, conclusions and recommendations expressed in this publication are those of the authors of the reports, and do not necessarily reflect the views of the Government. Nothing herein shall affect the copyright and other intellectual property rights in the information and material contained in these reports. All intellectual property rights and any other rights, if any, in relation to the contents of these reports are hereby reserved. The material herein may be reproduced for personal use but may not be reproduced or distributed for commercial purposes or any other exploitation without the prior written consent of the Government. Nothing contained in these reports shall constitute any of the authors of these reports an employer, employee, servant, agent or partner of the Government.

Published by the Hong Kong Academy of Medicine Press for the Government of the Hong Kong Special Administrative Region. The opinions expressed in the *Hong Kong Medical Journal* and its supplements are those of the authors and do not reflect the official policies of the Hong Kong Academy of Medicine, the Hong Kong Medical Association, the institutions to which the authors are affiliated, or those of the publisher.